

April 2013

# Optimizing Novel ECG Electrodes

Hailey Jacqueline DiSpirito  
*Worcester Polytechnic Institute*

Jerone Tedroy Mitchell  
*Worcester Polytechnic Institute*

Peter Michael Vardakas  
*Worcester Polytechnic Institute*

Syed Athar Bin Amir  
*Worcester Polytechnic Institute*

Follow this and additional works at: <https://digitalcommons.wpi.edu/mqp-all>

---

## Repository Citation

DiSpirito, H. J., Mitchell, J. T., Vardakas, P. M., & Bin Amir, S. A. (2013). *Optimizing Novel ECG Electrodes*. Retrieved from <https://digitalcommons.wpi.edu/mqp-all/758>

This Unrestricted is brought to you for free and open access by the Major Qualifying Projects at Digital WPI. It has been accepted for inclusion in Major Qualifying Projects (All Years) by an authorized administrator of Digital WPI. For more information, please contact [digitalwpi@wpi.edu](mailto:digitalwpi@wpi.edu).



# WPI

## Optimizing Novel ECG Electrodes

---

*A Major Qualifying Project submitted to the Faculty of Worcester Polytechnic Institute in partial fulfillment of the requirements for the Degree in Bachelor of Science*

---

*Syed Athar Bin Amir*

---

*Hailey DiSpirito*

---

*Peter Vardakas*

---

*Jerone Mitchell*

25<sup>th</sup> April, 2013

---

Professor Ki Chon

Sponsored by



**FLEXCON**

**Abstract**

FLEXcon has developed novel electrocardiogram electrodes that use a dry interface that does not dehydrate over time, in contrast to the current industry standard Ag/AgCl hydrogel electrodes which require dehydration barriers in packaging and dry out over a few days. The optimized carbon to pressure sensitive adhesive concentration for the minimum material impedance is 10% carbon to 90% PSA. The carbon based dry electrodes require activation to lower their impedance below the AAMI defibrillation overload standards. Using a defibrillation overload circuit, which applies electrophoresis to the electrodes, the parameters which give the lowest impedance are 200 V, 100 mA, and a 100 ms discharge time across the electrode. Acquiring electrocardiogram signals from ten subjects, using the FLEXcon electrodes and hydrogel electrodes simultaneously, resulted in 66 minutes of data for analysis. Signal processing of this data showed that, from three FLEXcon electrodes of different sizes, the large electrode had the greatest signal fidelity when compared to the hydrogel electrodes. This study concludes that the 10% carbon concentration electrodes, at the largest size given by FLEXcon for testing, are able to substitute the hydrogel Ag/AgCl electrodes in a clinical setting.

### **Authorship**

**Abstract:** Hailey, Syed, Peter

**Executive Summary:** Syed, Hailey, Jerone, Peter

**Introduction:** Syed

**Literature Review:**

Electrocardiogram: Syed

QRS wave detection: Syed

History of Electrocardiogram: Hailey

Biopotential Electrodes: Jerone

Silver chloride Electrodes used in traditional ECG: Jerone

Hook Effect Artifact: Syed

Novel Dry ECG Electrodes: Hailey

CNT/PDMS Electrodes: Peter

Pressure Sensitive Adhesive by FLEXcon: Jerone

ECG correlated with different skin types: Jerone

Biomedical Signal Processing: Hailey

Electrophoresis: Peter

Properties of Carbon: Peter

**Materials & Methods:** Hailey, Peter

**Results:** Syed, Peter

**Conclusion:** Hailey, Jerone

The entire group contributed to editing each other's work, to the fabrication and testing of the electrodes, and to the acquisition and analysis of the ECG waveforms.

### **Acknowledgments**

The group would like to thank their advisor, Professor Ki Chon, for his gracious assistance for this project so far. The group would also like to thank Mr. Ken Burnham, Mr. John Forster, and Mr. John Pennance of FLEXcon for their help in teaching the group on how to create and test the electrodes for impedance. Finally, the group would like to thank Ms. Lisa Wall for her assistance.

## Table of Contents

Abstract.....	i
Authorship .....	ii
Acknowledgments .....	iv
List of Figures.....	vi
List of Tables.....	vii
Executive Summary .....	viii
1. Introduction.....	1
2. Client Statement.....	3
3. Literature Review.....	5
Electrocardiogram.....	5
QRS wave detection .....	6
History of Electrocardiogram .....	9
Biopotential Electrodes.....	11
Silver chloride electrodes used in traditional ECG .....	12
Hook Effect Artifact .....	15
Novel Dry ECG Electrodes.....	17
CNT/PDMS Electrodes.....	18
Pressure Sensitive Adhesive by FLEXcon.....	20
ECG Correlated with Different Skin Types .....	21
Biomedical Signal Processing.....	22
Electrophoresis .....	24
Properties of Carbon .....	26
4. Materials & Methods.....	28
Materials for Electrode Design .....	28
Methods for Electrode Design .....	28
Materials for Activation Device Design .....	29
Methods for Activation Device Design.....	30
5. Results.....	34
Stage 1 .....	34
Stage 2 .....	43
Signal Processing and Peak Detection Algorithm.....	55
Import Raw Data, Sampling Frequency, time vector .....	55
Detrending Solution, Correction for DC noise.....	56
Bandpass Filtering .....	57
Derivative Filtering, Squaring .....	58
Moving Average Filtering.....	59
Thresholding, peak indices search .....	59
Stage 3 .....	60
FLEXcon and Ag/AgCl Comparison Metrics.....	62
6. Conclusion .....	67
References .....	68
Appendix A.....	71
THINflex® PP 075 H CLEAR A-208 TRACrite™ 100 Technical Data.....	71
Appendix B.....	72
Precision LC Meter 7600 Plus®, IET Labs Inc.™ Performance Sheet.....	72
Appendix C .....	73
Appendix D.....	74
MATLAB Statistical Analysis .....	74
MATLAB Mean Impedance vs. Power Plots.....	77
MATLAB ECG and FFT Waveform Plots .....	78
MATLAB Impedance vs. Frequency Sweep Plots .....	79
Peak Detection Algorithm.....	80
RMSSD Analysis Algorithm .....	84
Appendix E.....	86
Glossary of Statistical Terms and Tests .....	86
Appendix F .....	87
Participant Consent Form .....	87
Appendix G.....	89
Stage 1 Data Set.....	89
Stage 3 Data Set.....	93

## List of Figures

Fig. 1: An electrocardiograph .....	6
Fig. 2: QRS detection algorithm processing steps .....	8
Fig. 3: Einthoven's "string galvanometer" used for his electrocardiogram work .....	9
Fig. 4: Einthoven's Triangle, which uses three leads to form a triangle .....	10
Fig. 5: Equivalent circuit of the Ag-AgCl interface .....	14
Fig. 6: Equivalent circuit model of an ECG lead .....	14
Fig. 7: equivalent circuit model for hook effect observation .....	15
Fig. 8: Cross section of Epidermis .....	22
Fig. 9: Different types of Butterworth filters .....	23
Fig. 10: Impedance spectra of the composites .....	27
Fig. 11. Activation Circuit Block Diagram .....	30
Fig. 12. Activation device with variable parameters. ....	32
Fig. 13. Housing for the activation device. ....	32
Fig. 14. Gaussian distribution plot for 8% carbon load.....	36
Fig. 15. Gaussian distribution plot for 10% Carbon load.....	36
Fig. 16. Gaussian distribution for 12% carbon.....	37
Fig. 17. 0.1 uF Post-Activation Mean Impedances .....	39
Fig. 18. 1.0 uF Post-Activation Mean Impedances .....	40
Fig. 19. 10.0 uF Post-Activation Mean Impedances .....	40
Fig. 20. 100.0 uF Post-Activation Mean Impedances .....	41
Fig. 21: Properly mixed PSA+Carbon Post Impedance Gaussian Curve .....	43
Fig. 22. Impedance vs. Frequency sweep for Ag-AgCl electrodes. ....	44
Fig. 23. Impedance vs. Frequency sweep for small FLEXcon electrodes. ....	44
Fig. 24. Impedance vs. Frequency sweep for medium FLEXcon electrodes. ....	45
Fig. 25. Impedance vs. Frequency sweep for large FLEXcon electrodes. ....	45
Fig. 26. Ag-AgCl resting ECG waveform for 2 second period.....	46
Fig. 27. FFT of resting Ag-AgCl ECG waveform. ....	47
Fig. 28. Movement ECG waveform for Ag-AgCl electrodes.....	47
Fig. 29. FFT of movement Ag-AgCl ECG waveform.....	48
Fig. 30. Resting ECG waveform for small FLEXcon electrodes. ....	49
Fig. 31. FFT of resting small FLEXcon ECG waveform. ....	49
Fig. 32. Movement ECG waveform for small FLEXcon electrodes. ....	50
Fig. 33. FFT of movement small FLEXcon ECG waveform. ....	50
Fig. 34. Resting ECG waveform for medium FLEXcon electrodes.....	51
Fig. 35. FFT of resting medium FLEXcon ECG waveform.....	51
Fig. 36. Movement ECG waveform for medium FLEXcon electrodes.....	52
Fig. 37. FFT of movement medium FLEXcon ECG waveform.....	52
Fig. 38. Resting ECG waveform for large FLEXcon electrodes.....	53
Fig. 39. FFT of resting large FLEXcon ECG waveform.....	53
Fig. 40. Movement ECG waveform for large FLEXcon electrodes.....	54
Fig. 41. FFT of movement large FLEXcon ECG waveform.....	54
Fig. 42. Raw ECG after detrending and DC correction .....	57
Fig. 43. Peak locations for FLEXcon electrodes.....	61
Fig. 44. Peak locations for silver/silver chloride electrodes.....	61
Fig. 45. Representative heart rate time interval series.....	62
Fig. 46. Representation of the Welch power spectral density .....	63
Fig. 47. RMSSD regression for small FLEXcon electrode and Ag/AgCl.....	65
Fig. 48. RMSSD regression for medium FLEXcon electrode and Ag/AgCl .....	65
Figure 49. RMSSD regression for large FLEXcon electrode and Ag/AgCl.....	66
Fig. 50. THINflex® PP 075 H CLEAR A-208 TRACrite™ 100 Table.....	71
Fig. 51. Precision LCR Meter 7600 Plus by IET Labs, Inc.....	72
Fig. 52. Hioki IM 3570 Impedance Analyzer Data Sheet .....	73



**List of Tables**

Table 1: Properties of Carbon-12.....	26
Table 2: List of parts needed to build the activation circuit.....	29
Table 3: Variable parameters for electrode activation.....	30
Table 4 Impedance test results for different carbon levels (STAGE 1).....	34
Table 5 Impedance Test Results, STAGE 1.....	35
Table 6 One sample t-test results.....	38
Table 7 Two sample t-test results.....	38
Table 8 Optimum Parameters for Activation.....	41
Table 9 Settled Carbon and PSA Mixed Impedance Values.....	42
Table 10 Mean and Standard Deviation of Heart Rate Interval Time Series.....	64
Table 11 Complete Mean & STD Table for Stage 3 Impedance Data Set.....	89
Table 12 ECG Statistical Data from Holter Monitor Study.....	93

### **Executive Summary**

The company FLEXcon has designed novel alternative signal receptive media (SRM) electrodes to record ECG signals. The standard electrodes currently available on the market are Silver/Silver Chloride (Ag/AgCl). The overall goal of this project was to optimize FLEXcon's electrodes and compare the signal quality to that of Ag/AgCl electrodes. Lowering post activation impedance of the electrodes was also a key goal of this project. A lower impedance results in higher signal strength in the recording of the ECG signal. The team had four objectives in order to achieve the project goal.

The first objective was to find the optimum mixture for the electrodes. To do this, the team needed to find the optimal percentage of carbon in the carbon-PSA mixture by changing the percentage of carbon from 2-12% in increments of two, and determine which mixture resulted in the lowest post-activation impedance. Second, the investigators had to determine the optimal electrode activation parameters. An activation circuit with variable parameters was built based on industry standards set by the Association for the Advancement of Medical Instrumentation (AAMI), and used a capacitive discharge to cause electrophoresis to occur in these dry carbon based electrodes. The third objective was to simultaneously record ECG using FLEXcon's electrodes as well as Ag/AgCl electrodes on human subjects by using multichannel Holter monitors that are capable of recording ECG from two sets of electrodes. The final objective was processing the signals acquired from the human subjects using MATLAB. This analysis allowed for the comparison of FLEXcon's novel electrodes to the conventional Ag/AgCl electrodes.

After fabricating and testing electrodes of varying carbon concentrations, it was determined that the best mixture for electrodes was 10% carbon and 90% pressure sensitive adhesive (PSA). This type of electrode was fabricated and used for the rest of the project. To satisfy the second objective presented to the group, a defibrillation overload circuit was designed

and implemented to test for various activation parameters. It was found that an activation voltage of 200 V along with activation amperage of 100 mA with a 100 ms capacitor discharge time optimized the post-activation impedance. These parameters resulted in a mean post-activation impedance of 875  $\Omega$  with a standard deviation of 657  $\Omega$ . The AAMI requirement is that the mean post-activation impedance be less than 2 k $\Omega$  with no single electrode impedance exceeding 3 k $\Omega$ .

To compare the signal quality of FLEXcon and Ag/AgCl electrodes, both electrodes were used to record ECG simultaneously in 10 human subjects, with six minutes of data collected per subject. Three different sizes of FLEXcon electrodes were fabricated and compared against the industry gold standard to determine the optimal electrode size. Both time and frequency domain analyses were performed on the collected data. A bandpass filter between 5-11 Hz was used to clean the data collected from both electrode channels, and using MATLAB, the team scripted a peak detection algorithm to locate the R segment of the QRS complex of the ECG waveform. Further analysis included heart rate calculation (beats per minute), RMSSD comparison for electrode variability, RMSSD t-tests, and power spectral density plots. The peak detection graphs from both FLEXcon and Ag/AgCl electrodes showed negligible morphological differences.

Data analysis showed that FLEXcon's large electrode size (5 cm X 4 cm) was by far the most comparable to Ag/AgCl electrodes. The mean heart rate from all the subjects in the Holter monitor study was  $73.9 \pm 9.60$  bpm for the large electrodes, and the mean of the corresponding Ag/AgCl electrodes was  $73.9 \pm 9.77$  bpm. Paired sample t-tests were performed to contrast between the two electrodes, and no statistically significant differences were discovered between FLEXcon's electrodes and the industry standard Ag/AgCl electrodes.

In conclusion, this project verified that the novel Signal Receptive Media (SRM) invented at FLEXcon can be used to fabricate dry ECG electrodes. These electrodes require to be activated by a capacitive discharge, but a key strength they possess in comparison to the industry gold standard is that they do not require special packaging to prevent dehydration. Moreover, they have a significantly longer shelf life, and can be produced at a cheaper cost than Ag/AgCl electrodes. As a result, since the Holter Monitor study proved that the signal acquired by these novel electrodes are morphologically and statistically similar to the signal obtained by Ag/AgCl electrodes, they can potentially replace them as the industry gold standard in the future.

## 1. Introduction

Electrocardiography (ECG) is a graphical interpretation of the electrical activity of the heart, and to properly monitor the cardiac health of a patient, it is crucial to obtain an ECG signal with a low Signal-to-Noise Ratio (SNR). In a typical ECG setup, depending on the particular application, three to twelve signal receptive electrodes are attached to the patient's body. These electrodes are able to pick up the minute changes in potential that occur as a consequence of the propagation of the cardiac vector during the timeframe of a single heartbeat, thus rendering it possible to produce the characteristic ECG waveform that can then be used for diagnostic purposes. To ensure optimal signal strength, it is prudent to minimize the impedance of the skin-electrode interface by lowering the impedance of the electrode used. High impedance levels at the skin-electrode interface can result in significant losses in signal strength and low SNR, which can render the obtained signal difficult to process.

The current industry gold standard for ECG electrodes is the Silver/Silver Chloride hydrogel electrodes. These electrodes consist of a layer of silver chloride, often in the form of a paste-like hydrogel surrounding a silver disc. While the hydrogel layer significantly improves the signal quality by effectively lowering the impedance that exists at the skin-electrode interface, it is also the principal reason behind the relatively short shelf life of these electrodes. The hydrogel layer that exists in the skin-electrode interface diminishes with time as it dehydrates. This leads to a loss of signal quality and an increased incidence of motion artifacts in the ECG. Moreover, this also means that the electrodes need to be carefully packaged to ensure optimal retention of the hydrogel layer.

FLEXcon USA© has attempted to address the issue of dehydration that is prevalent in the current industry gold standard electrodes by designing a novel signal receptive media that does

not require a hydrogel layer. These electrodes are designed by combining a patented Pressure Sensitive Adhesive (PSA) with carbon black. After the electrodes are fabricated, the electrodes need to be activated by electrophoresis to ensure that they meet the Association for the Advancement of Medical Instrumentation (AAMI) requirement for defibrillation overload. AAMI states that for dry, non-hydrogel based electrodes such as FLEXcon electrodes, the average post-activation impedance must remain below 2 k $\Omega$ , and no single electrode could have impedance equal to or greater than 3 k $\Omega$  after activation.

To ensure that FLEXcon electrodes met the AAMI standard for dry electrodes, the group designed and implemented an activation circuit which was capable of providing various levels of activation voltage, amperage with varying discharge times. This allowed the group to obtain the best parameters required for the activation. The group also needed to discern the optimal concentration of carbon in the electrodes, as well as the optimal size of the electrodes. Once the activation parameters as well as the concentration of carbon were determined, the group moved on to a Holter monitor study contrasting the FLEXcon electrodes with the industry gold standard to ascertain if FLEXcon's design could potentially be as receptive to ECG signals as Ag/AgCl electrodes. Simultaneous acquisition of ECG was done using the two electrode types on 10 subjects, and six minutes of data was collected from each subject.

After data collection, the team used the algorithm outlined in "A Real-Time QRS Detection Algorithm" by Pan and Tomkins and implemented it in MATLAB to perform peak detection on data collected from Ag/AgCl electrodes as well as FLEXcon electrodes. This was followed by various statistical analysis steps to contrast between the two types of electrodes. It was discovered that FLEXcon's novel ECG electrodes were directly comparable to the industry gold standard pending further development.

## 2. Client Statement

The following "Client Statement" was proposed by the FLEXcon MQP group on October 2nd, 2012:

*"FLEXcon has patented an alternative Signal Receptive Media (SRM) to the hydrogel currently used in electrocardiogram (ECG) electrodes for heart monitoring. During the MQP, students will develop a test method, design of experiments (DOE) and evaluate the resultant SRM."*

FLEXcon shared its proposal with the FLEXcon MQP group on August 27<sup>th</sup> 2012, identifying three stages with a total of six deliverables.

**Stage 1:** Design an experiment (DOE) with the following input variables:

- a. % carbon loading (or blend if two carbon dispersions are available)
- b. PSA (V-95 vs. V-95 with low crosslinker)
- c. Activation Voltage
- d. Activation Amperage
- e. Activation Time\*

The response variable for both experiments will be Impedance as measured by a test method designed by the students. These results are to be reported directly to FLEXcon.

\*Note: Activation time should be fixed for the initial DOE. Once an optimized formula is identified, design and conduct a second experiment with variable activation duration. Target will be less than 0.5 sec to allow efficient manufacturing.

**Stage 2:** Develop a test protocol to compare signal quality of optimized SRM to Hydrogel. This should include consideration for resistance to noise and interference (e.g. 60Hz, muscle artifacts, etc.).

**Stage 3:** Evaluate the top 2 or 3 SRM designs compared to industry leading hydrogel electrodes using the test method from Stage 2.



### 3. Literature Review

#### Electrocardiogram

The Electrocardiogram, commonly known as ECG or EKG, is a graphical representation of the electrical activity of the heart. Currently, it is usually recorded via Silver-Silver Chloride (Ag-AgCl) electrodes that require a hydrostatic gel to adhere to the patient's chest. Typically, three or more electrodes are used to record various waves that are generated as a result of the heart's electrical activity. The ECG can then be utilized by medical professionals to compute the heart rate and assess the overall health of the heart.

The term Electrocardiogram was first coined by the Dutch physiologist Willem Einthoven (Einthoven, 1893). Using an improved electrometer and a correction formula he developed, Einthoven distinguished the five waves P, Q, R, S and T in the ECG. The first string galvanometer which was designed by Einthoven to record ECG weighed an incredible 600 pounds (Brief history of electrocardiography, 2009).

The sinoatrial node within the heart, also known as the SA node or the heart's natural pacemaker, is located in the right atrium of the heart and initiates the electrical impulse that leads to the generation of the normal sinus rhythm. This leads to a rapid depolarization of the right atrium, which is picked up as the first half of the P-wave in the ECG. This wave of depolarization then spreads to the left atrium of the heart, and is subsequently recorded as the second half of the P-wave. The QRS complex follows the P wave, generated from the depolarization of the ventricles. The T wave is produced by the repolarization of the ventricles. The U wave occasionally follows the T wave as a result of the repolarization of the Bundle of His-Purkinje cells. An image of a healthy ECG signal is provided in Fig. 1.

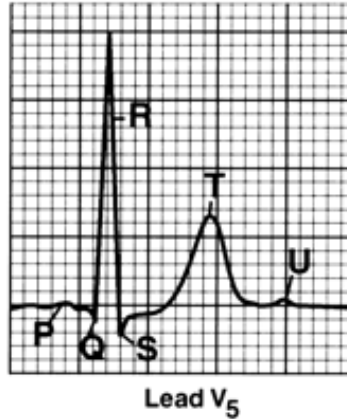


Fig. 1: An electrocardiograph (Hurst, 1998)

The R-R interval between successive ECG signals is used to calculate the heart rate of the patient based on the equation 1.

$$\text{Eqn. 1: Heart Rate} = \frac{1}{R - R \text{ interval duration}}$$

### QRS wave detection

One of the most vital components of an ECG is the QRS complex, characterized by a sharply rising peak during ventricular contraction, which corresponds to the depolarization of the right and left ventricles of the heart. On the electrocardiogram, the Q wave is a short downward deflection from the baseline. It is rapidly followed by a sharp rising peak during the R wave. The S wave is characterized as the downward deflection that follows the R wave. For signal analysis purposes, the QRS complex is treated as a single component of the ECG and usually lasts as long as 60 ms to 100 ms in healthy human adults (Klabunde, 2007).

In the absence of any signal processing, the QRS complex may be very difficult to detect. Even if the physiological variability in each individual QRS complex in a patient is forgone, the presence of numerous noise sources alone can make it challenging for the complex to be detected. Some of the common noise sources in QRS detection include muscle noise, electrode motion, 60Hz interference from power lines, and baseline wander. Occasionally, T waves with

high frequency characteristics can be mistaken for a QRS complex (Pan, 1985). Although the QRS complex contains several high frequency components, for peak detection purposes they are not as relevant as the frequency band between 5Hz and 11Hz (Pan, 1985).

Before any digital signal processing is done, the ECG signal has to pass through an analog lowpass filter (LPF) which bandlimits the ECG to under 50Hz (Pan, 1985). This analog signal is then sampled and quantized to bring the data into the digital domain. Once that has been done, a digital bandpass filter (BPF) begins the signal processing by passing the signal between 5Hz to 15Hz and attenuating every other frequency bands. It is important to note that for real time applications the bandpass filter should be designed with integer coefficients to minimize processing time. What this method accomplishes is minimization of DC noise, 60Hz power line interference, baseline wander, muscle noise and T wave interference. Due to the relatively low amplitude of the QRS complex, which is about 0.7 mV in healthy adults, compared to the power line interference, which is a 60Hz signal at 110V, it may be a good idea for some signal processing applications to implement a notch filter at 60Hz to further attenuate that noise. However, it needs to be noted that any additional signal processing steps add to the computation time of the ECG and thus increases the delay, so there is a tradeoff involved regarding signal integrity and implementation in real time.

The output of the bandpass filter contains less noise, and at this stage the signal is differentiated to provide the QRS complex slope information (Pan, 1985). This process must be done after the bandpass filter, regardless of the particular application, since taking the derivative is often detrimental to the signal-to-noise ratio of the ECG. Once the differentiation has completed, the output is squared point by point. This does two things to the signal; (i) it makes

all data points in the QRS complex to be analyzed positive numbers, and (ii) it provides a way to amplify the output of the derivative in a nonlinear fashion (Pan, 1985).

Once the output of the derivative has been squared, it is passed through a moving window integrator. Conceptually, what a moving window integrator does is act like a lowpass filter. The window takes an empirically determined  $N$  samples and averages their values. Ideally, the window should be as wide as the largest possible QRS period in the set (Pan, 1985). By doing this, the errors introduced by baseline wander in the data can be reduced. The effect of baseline wander can be reduced even further by setting two adjustable thresholds that detect a QRS complex peak and updates based on the past values of the samples periodically. Fig. 2. demonstrates the output from each of these signal processing steps.

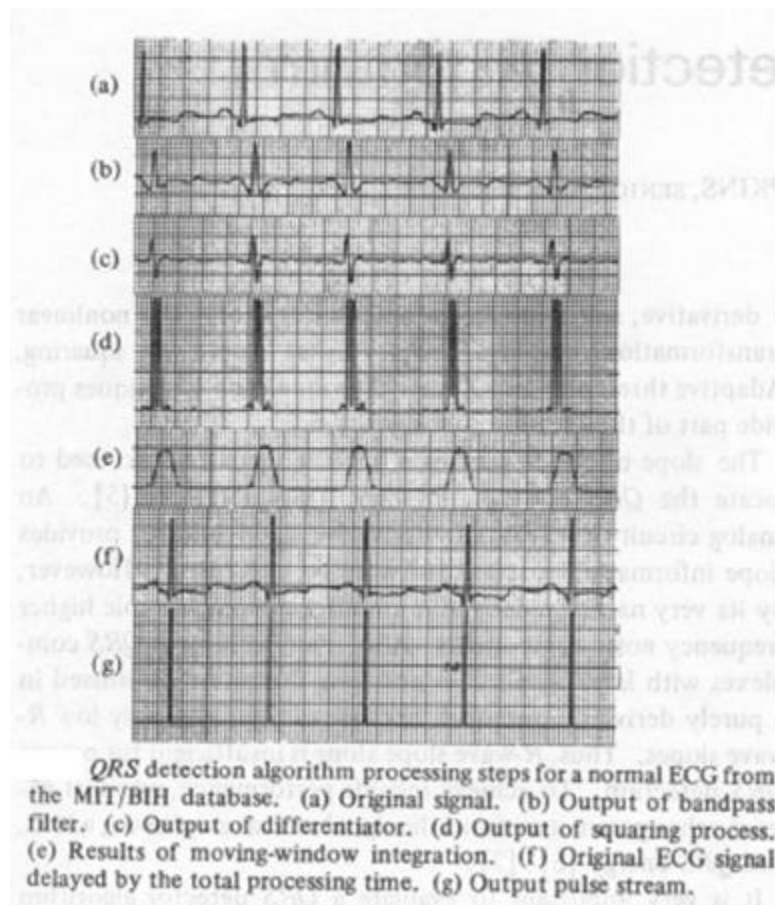


Fig. 2: QRS detection algorithm processing steps

## History of Electrocardiogram

The origin of the ECG, an important diagnostic medical tool, dates back to the late nineteenth century. In 1869, Alexander Muirhead, an electrical engineer who did not publish his studies, attached an ink siphon to a moving coil galvanometer. This sprayed ink onto a moving piece of paper. The first record of a clinical electrocardiogram is from 1887, when Augustus Desire Waller was able to continuously record on photosensitive paper. He did this using a capillary electrometer. He found that the position changes of the meniscus in the capillary electrometer paralleled current changes, and was able to demonstrate this using his dog as a specimen. Willem Einthoven, a respiratory physiology researcher, saw this demonstration and continued Waller's work. He wanted more accurate measurements, so he improved the resolution and modified Waller's technology to produce higher quality readings (Ball, Mar 2010.).

Einthoven used a string galvanometer for his work, shown in Fig. 3. This system contained a quartz filament that passed between two electromagnets. Any current that went through the filament resulted in the movement that was projected and recorded, corresponding to the current changes. In order to improve the response time and sensitivity of the recording, Einthoven used fine quartz string filament, and published his first electrocardiogram in 1902 (Ball, Mar 2010.).



Fig. 3: Einthoven's "string galvanometer" used for his electrocardiogram work (Ball, 2010)

Einthoven continued his work by applying a correction formula to the readings so that they were more accurate, and named the waves in the recording the P, Q, R, S, and T waves. In 1912, Einthoven introduced what is now referred to as “Einthoven’s Triangle,” or vector electrocardiography using three leads to form an equilateral triangle. The term “lead” is used to represent a pair of reference electrodes which together gives a trace of the potential difference between the said electrode pair. In order to record the patient’s ECG, the arms and one leg of the subject were immersed in saline solution (Ball, Mar 2010.). Einthoven’s Triangle can be seen in Fig. 4.

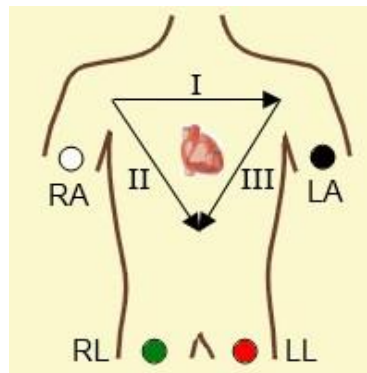


Fig. 4: Einthoven's Triangle, which uses three leads to form a triangle (Normal Vectors)

Due to the large size of the galvanometer that Einthoven was using for his work, the size of the device needed to be reduced before it could be used on a regular basis in a clinical setting (Ball, Mar 2010.). In 1934, Frank Wilson discovered that he could join the lead wires from the arms and leg with a  $5k\Omega$  resistor, resulting in a combined lead which he attached to the negative ECG terminal. Then, he could connect an electrode to the positive terminal, and because of the other connection to the negative terminal, this electrode would be unipolar. Thus, it could be placed anywhere on the body (Jenkins, 2009.).

Further progression of the ECG took place in 1938, when the American Heart Association, along with the Cardiac Society of Great Britain, defined the standard positioning and wiring of

the six chest leads used for the ECG. In 1942, Emanuel Goldberger experimented with the voltage that Wilson's unipolar electrode used, and increased it by 50%. This resulted in the creation of the augmented limb leads, aVR, aVL, and aVF, which, combined with Einthoven's triangle and the six chest leads, result in the 12-lead ECG that is currently used (Kilpatrick, 1994).

### **Biopotential Electrodes**

Biopotential recordings can come in the form of ECG, Electroencephalography (EEG), Electrooculography (EOG) and Electromyography (EMG), which are vital for detection and treatment in patients; they can also provide research opportunities. There has been an increase in interest in wireless mobile systems based on the healthcare industry. A key area is developing alternative biopotential electrodes for patient physiological monitoring. Currently there exist two types, which are in trial. One electrode is a conventional wet adhesive Ag-AgCl, which provides an excellent signal, however is irritating and bulky for mobile uses. The other type of electrode comes in two forms, which are dry and non-contact. They operate without the need for a wet gel adhesive; however they have not gained acceptance for medical uses from the FDA at the present time.

Dry electrodes address the comfort issues that patients frequently mention, but are more difficult to secure on the patient, which makes them less likely to replace the standard ECG and EEG wet gel electrodes used in hospitals. They lack the advantage of a conductive gel, which are more sensitive to the condition of the skin and are highly susceptible to motion artifacts. Because they are dry, the method of sufficient adhesion to the skin is contributed by sweat, which counteracts the increased skin-electrode impedance and makes it almost comparable to that of wet electrodes after a few minutes of sweat build up.

Non-contact electrodes on the other hand require no resistive connection to the body; they have the advantage of being insensitive to skin conditions and can be embedded within clothes for monitoring of patients, while at home or other locations outside the medical setting.

Clinical trials have shown that even though there was a sufficient deal of noise in the signal picked up from non-contact electrodes, due to impedance from cotton which was the medium used for testing, the increased noise did not prevent the detection of an acceptable ECG measurement. The dry electrodes performed equally as well. With this capability of being able to continuously record an biopotential signal without direct contact with the skin opens the doors to the future, because as stated this enable long term clinical home diagnosis and care applications.

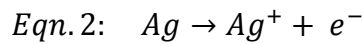
### **Silver chloride electrodes used in traditional ECG**

An ECG electrode is commonly composed of a small metal plate surrounded by an adhesive pad, which is coated with a conducting gel to aid transmission of the signal. The novel ECG electrodes developed at FLEXcon are quite different from these traditional electrodes. The Pressure Sensitive Adhesive (PSA) used in the novel ECG electrodes results in a more durable electrode. In traditional electrodes, the durability is severely limited due to the electrolytic gel drying up too fast. The novel ECG electrodes use activated carbon as a method of transferring electrical impulses in place of the gel, which leads to a greater lifetime. This difference in longevity between the two electrodes can be confirmed as part of this Major Qualifying Project.

The silver chloride reference electrode is widely used in various industrial applications such as the process of recording ECG. It is inexpensive and non-toxic. These qualities therefore make silver chloride electrodes a decent choice of electrodes to be used in a medical setting. A silver chloride electrode consists of a hollow plastic tube electrode body. The conducting part of



the electrode is made of a silver wire which is usually coated with a thin layer of silver chloride. A porous plug on one end maintains contact with the surface of the patient's skin, and the silver conductor is bathed in a chloride solution (Sief Otten, 1998). Silver chloride has a very low solubility in water and forms a white precipitate (AUS-e-TUTE). Due to this, a separate conductive gel is also applied between the silver plate end of the electrode and the patient's skin to maintain a pathway for current to pass through (Townsend, 2001). Usually, the solution consists of a dissolved chloride salt such as potassium chloride in strong concentrations to avoid disintegrating the silver chloride from the silver wire (Roberge, 2012). Some of the silver from the wire may dissolve into the gel to produce silver ions and electrons as shown in equation 2:



Once attached with a combination of saturated potassium chloride solution, the electrode develops a potential of 199mV against the standard hydrogen electrode (Roberge, 2012). At equilibrium, this phase boundary potential depends on the chloride ion activity of the electrolyte; maintaining a constant chloride ion activity is essential in keeping this potential at a constant level. One of the disadvantages of the silver chloride electrode is that silver ions may form precipitates such as silver sulfide and silver nitrate and clog the liquid junction of the electrode (Webster, 1998).

A double layer of  $Ag^+$  and  $Cl^-$  ions build up when the electric field set up by the dissolving ions is balanced by the concentration gradient (Townsend, 2001). This double layer is referred to as the electrode double layer and this can be put in an equivalent circuit model to estimate what the electrical behavior of the body-electrode interface will be like. The equivalent circuit model of the body-electrode interface is provided in Fig. 5. The values of the various

components of the equivalent circuit model depend on the area of the electrode, surface condition, current density and the type and concentration of the conductive gel.

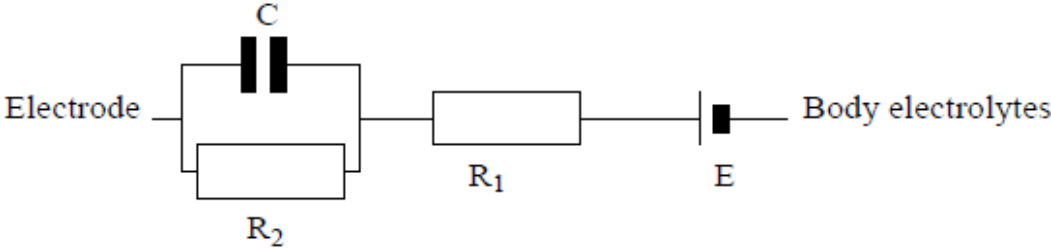


Fig. 5: Equivalent circuit of the Ag-AgCl interface (Townsend, 2001)

One of the major issues faced with silver chloride electrodes is that they easily introduce motion artifacts in the ECG. If the patient is in motion, the distribution of charge at the interface can be mechanically disturbed. This leads to the half-cell potential of the body-electrode interface to change momentarily until the motion is halted and the Nernst equilibrium is re-established. If one of the electrodes in a lead experiences motion while the other stays still, an unwanted potential difference appears in the lead which may cause severe interference in the measurement of ECG (Townsend, 2001). The overall equivalent circuit for a lead is provided in Fig. 6.

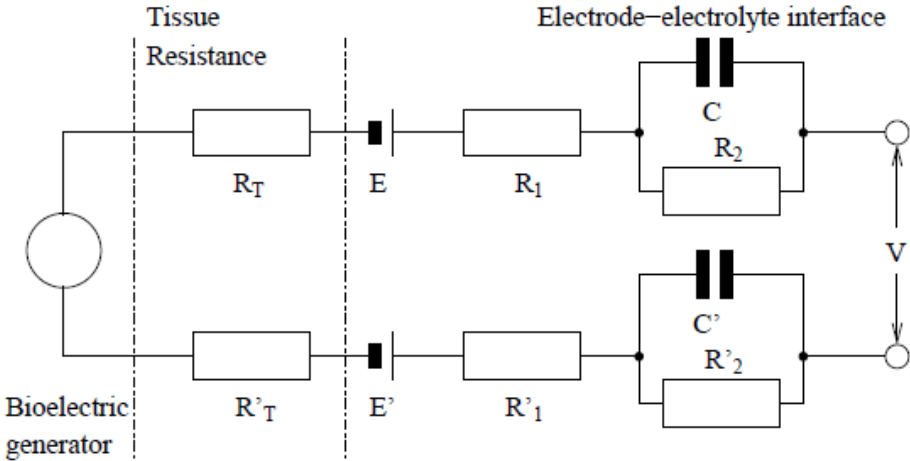


Fig. 6: Equivalent circuit model of an ECG lead (Townsend, 2001)

## Hook Effect Artifact

In Electrical Bio-Impedance (EBI) spectroscopy measurements, the presence of parasitic capacitances creates a measurement error commonly known as the Hook Effect (Buendia, 2010). It is named as such because of its characteristic hook-like shape on an impedance plot against frequency. At higher frequencies, it is observed that the measured impedance appears to increase when it should actually be decreasing at higher frequencies. The hook effect comes into play in impedance measurements at high frequencies, because of the lower impedance that appears from the parasitic capacitance. This drives away current from the true impedance of the component and as a result, the measured impedance is much more than what it is in reality.

Figure 7. shows the equivalent circuit model that can be used to understand the Hook Effect. The presence of the stray capacitance  $C_{PAR}$  causes a portion of the current supplied by the LCR meter to leak through the stray capacitance. This leads to less current flowing through the impedance block that is being analyzed and gives a larger value for the impedance as a result. Although the Hook Effect is not as prominent in low frequencies as it is in high frequencies, the phenomenon is still observable.

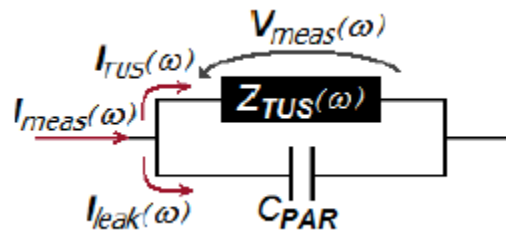


Fig. 7: equivalent circuit model for hook effect observation (Buendia, 2010)

Traditionally, the Hook Effect was corrected by the Td compensation method. This method involves taking the measured impedance and multiplying it with a complex exponential in the form  $e^{j\omega T_d}$ , where  $\omega$  is the frequency in radians and  $T_d$  is a scalar factor. There were a few problems in using this method. Firstly, since the factor Td is a real, scalar number, raising it in a

complex exponential and multiplying the measured impedance with it only changes the phase of the measured impedance and not its amplitude. Secondly, this can only be used to fix the measured impedance for one particular frequency depending on the value of  $\omega$  that is selected (Buendia, 2010).

In a new approach to removing the Hook Effect, Buendia replaced the scalar factor Td with a corrective logarithmic complex function. The function is provided in equation 3.

$$Eqn. 3: F_{CORR}(\omega) = -j \frac{\log[1 - j\omega C_{PAR} Z_{meas}(\omega)]}{\omega}$$

This corrective function depends on the natural frequency  $\omega$ , the parasitic capacitance CPAR and the measured impedance  $Z_{meas}(\omega)$ , and is plugged into the original equation for Td compensation, which is given in equation 4.

$$Eqn. 4: Z_{TUS}(\omega) = Z_{meas}(\omega) * e^{j\omega F_{CORR}(\omega)}$$

The basic idea behind estimating the value of the parasitic capacitance ( $C_{PAR}$ ) is that the susceptance S, which is the complex component of admittance (Y), and where admittance is equal to the conductance summed with  $j$ \*susceptance, of the parasitic capacitance increases in a linear manner with an increase in frequency. On the other hand, the susceptance of the impedance block that is being measured stays constant. So at high frequencies, it can be estimated that most of the susceptance of the measured admittance is provided by the parasitic capacitance (Buendia, 2010).

As a result of this approach, the Hook Effect can be completely removed from the reactance spectrum of the measured impedance. Although this method is extremely effective, it is fairly difficult to estimate the parasitic capacitance as ideally measurements need to be taken at very high frequencies (Buendia, 2010).

### **Novel Dry ECG Electrodes**

Gel electrodes used currently for recording ECGs pose several problems including long-time stability, reduced contact impedance, and reduced motion artifacts. Doctors want the ability to record over a much longer period of time. However, due to shelf life and electrode dehydration, gel electrodes can only be used to record signals for a few days at maximum. Dehydration of the electrode causes noise in the recorded signal. Motion artifacts, another issue encountered when using gel electrodes, are a result of patient movement, electrode placement, breathing, or stretching of the skin under the electrode. These signals can be mistaken as extra systolic measurement from the heart, resulting in an inaccurate ECG (Gruetzmann, 2007).

Dry electrodes also present a few problems. They are composed of metal plates, and shift when the patient moves. The resulting recording is incorrect because of this shifting. The skin is sometimes punctured in order to use the dry electrodes. This method does not allow for long term recording either, because scar tissue grows around the electrode and isolates it. The issue of impedance is somewhat addressed with dry electrodes, because if the electrode has a tight connection with the skin, the skin will moisturize and the impedance will drop (Gruetzmann, 2007).

In order to address the problems faced when using dry electrodes and gel electrodes, a novel electrode was designed. This new technology was a soft, dry foam electrode. The material allows it to adapt to the contact area, including any curves of the skin and hair. It also has an increased contact area with the skin. Unlike the dry electrodes, the foam electrode remains in contact with the skin during movement. The foam makes it so that a charge is not induced when the electrode rubs on the skin. Due to the flexibility of the material, the electrode works on hairy skin, whereas previous rigid dry electrodes do not (Gruetzmann, 2007).

After testing these electrodes, the author found that the foam electrode impedance on hairy skin is about the same as the impedance of the dry electrodes on hairless skin. This demonstrates that it would not be necessary to shave the contact area of skin when using the foam electrodes. The foam electrodes also reduce motion artifacts because they have the most intimate contact with the skin, and adapt to any movements made by the patient. No gel is necessary with the foam electrodes, so the author believes that they will have a longer stability, and be able to be used for recording for longer periods of time than gel electrodes. The problems of the foam electrodes are that they need an improved adhesion layer, and the foam needs to be stabilized. The author proposed that the stabilization can be done by using a cup-like packaging, similar to that of gel electrodes (Gruetzmann, 2007).

### **CNT/PDMS Electrodes**

Carbon nanotubes (CNT) are becoming ubiquitous in the medical market for several applications. In the domain of electrocardiography CNTs can be used as a replacement medium for silver chloride gels. The dry contact offered by CNT electrodes reduces the impedance, increases bio-compatibility and allows many physical forms to be fabricated (Jung, 2012). These electrodes also allow long term potentiation for bio-electric signals, whereas previous gel based electrodes increase in impedance as the gel dehydrates (Jung, 2012).

Initial fabrication techniques for CNT based electrodes use a polydimethylsiloxane (PDMS) dispersion material. Chemical vapor deposition of the CNT and PDMS allowed purity concentrations greater than 90% (Jung, 2012). To reduce aggregates, which impede signal potentiation, a hydrodynamic dispersion was applied through mechanical force to the CNT/PDMS mixture. The machine applied the mechanical dispersion force by dispersing small amounts of solid material onto any liquid materials through a chrome plated hardened steel roller

(EXAKT 50, EXAKT Technologies Inc., Oklahoma City, OK). The CNT dispersion was then placed into a shear flow system between five and fifteen hours. The CNT then homogeneously dispersed in PDMS (Jung, 2012).

Using a master mold which combined a petri dish, an acrylic layer and a snap, the PDMS precursor of liquid pre-polymer and a crosslinking agent was poured into the master mold. This mold was then cured at 80° C for two hours (Jung, 2012). The PDMS master mold was separated from the petri dish and the acrylic layer was removed from the mold. The CNT/PDMS composite was then poured into the PDMS master mold and again thermally cured at 80° C for two hours. PDMS was separated from the CNT/PDMS electrode using methanol (Jung, 2012). After separation the electrodes were connected to an impedance analyzer which modulated with a 50 mV excitation in the range between 10 and 100 kHz. The CNT/PDMS electrodes were bent to measure strain impedance and mechanical stress-strain curves were derived from the results generated by a universal testing machine (Jung, 2012). A BIOPAC ECG amplifier generated the ECG signals from the electrodes placed at the forearms and left leg of several persons. These electrodes were measured under dry conditions and motion artifacts were measured while the ECG subject was walking at a 3 to 5 km/h rate. Cytotoxicity and skin compatibility tests were committed by growing cell cultures onto the electrodes and measuring cell growth rates; the skin compatibility tests were performed by measuring ECG signals from the forearm for seven days with clinical tape.

Nine electrodes each having increased thickness and diameter were used for signal testing, and four groups of nine with different percent weights were allocated. Impedance decreases with increasing signal frequency and diameter. For each case of percent weight [1%, 1.5%, 2%, 4.5%] CNT/PDMS ratio and diameter [2cm, 3cm & 4cm] electrodes the dry contact

impedance was over  $10^6$  Ohms at frequencies less than 102 Hz, and around  $10^3$  Ohms at frequencies greater than 105 Hz with a linear curve between (Jung, 2012). These impedances do not pass the AAMI EC12-2000-4.2.2.4 impedance requirement. Strain deviated the electrical conductivity by about a single order of magnitude while the stress-strain curves had larger Young's Modulus for greater percent weight ratios. For signal quality the signal amplitude vastly increased with higher percent CNT/PDMS ratios. Sweat conditions did not reduce signal quality and slight noise was observed for motion testing at normal walking rates (Jung, 2012). Skin compatibility tests under the seven day wearing condition showed no itching or erythema. The cellular biocompatibility tests showed normal cellular growth within cultures that were directly exposed to the CNT/PDMS medium. Viability of cells on all electrodes was over 95%, giving highly significant reason for the researchers to state that "CNT/PDMS composite did not affect cell growth" (Jung, 2012).

The CNT/PDMS electrodes show quality signals, biocompatibility, ease of fabrication and long term potentiation of bio signals which gel ECG mediums do not exhibit. The CNT/PDMS electrodes are easy to clean with an alcohol solution, with no expected signal loss occurring. This result allows reusability of the CNT/PDMS electrodes where current AgCl electrodes are usually short term and one time use materials.

### **Pressure Sensitive Adhesive by FLEXcon**

FLEXcon has a wide range of PSA products with several applications. One product they have is the THINflex CLEAR Pressure Sensitive Adhesive which offers resistance in shrinking and can be used in ice chest, pasteurization, moisture and humidity products. It has a good acrylic adhesive bond on glass and high surface energy products which will be resistant to lifting, tunneling and flagging over time. Some of its properties are listed in Appendix A, Fig. 50.



Properties include the materials ability to have strong adhesive bonds on various metals, polymers and ceramics, making it extremely universal. The adhesive is available in various forms such as a tape or roll (FLEXcon).

### **ECG Correlated with Different Skin Types**

Since skin is a poor conductor of electricity due to its density and other factors, it has the potential to distort an ECG signal being picked up from within the body. The outer layer of the skin, known as the epidermis, is mainly the problem layer because it has a frequency and amplitude higher than the actual ECG signal. It is also difficult to filter electronically. This type of distortion coupled with 60Hz interference from power lines can result in complicated signals that are not easy understand even after filtering. Research from the National Teaching Institute & Critical Care Exposition(AACN NTI) have shown that the skin-electrode interface in many healthcare establishments are overlooked and a simple change, such as in prepping the patients skin properly greatly increase the quality of the ECG signal (Philips, 2008).

The type of skin a person has plays a key role in improving the overall efficiency of acquiring a quality ECG signal. Patients with dry or dead epidermal layers of skin should have it removed before having electrodes placed on to them, because this type of skin increases the impedance. Natural oils and dirt should also be removed as they too can create resistance to signal quality and prevent electrical flow. Studies by 3M have shown that after using their prep pads, the new measured skin resistance was 20 k $\Omega$ , compared to the average impedance of skin which is a about 345k $\Omega$  (3M, 2009).

Many common procedures are followed in preparing the skin of the patient before the placement of electrodes. The area of the patient's skin where the electrode will be placed needs to be shaved because hair prevents good electrode-skin contact. Soap and water, a non-alcoholic

wipe or a small piece of abrasive ECG skin prep paper can be used in order to improve the conductivity of the skin. Alcohol dries the skin out so it is not advised to be used for cleaning, as it diminishes electrical flow. The site of placement should also be dried in order to increase the capillary blood flow into tissue. Figure 8. depicts the layers of the epidermis on which the electrode would rest.

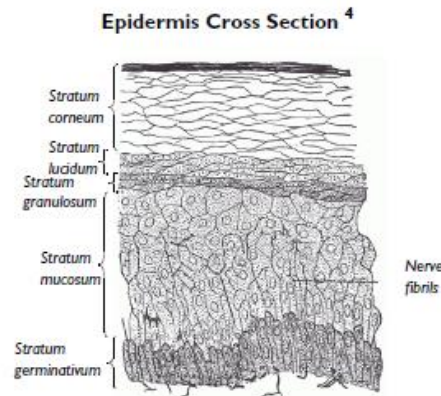


Fig. 8: Cross section of Epidermis

## Biomedical Signal Processing

Biomedical signals are classified as the outputs of a sensing device. In order to read and analyze the signals as accurately as possible, it is necessary to process the recordings. Signal processing plays a key role in understanding recorded signals. It can either be used to extract parts of the signal, or to represent the signal in an alternate way (Luo, 2010.). Signal processing is important for recording ECGs because it allows doctors to eliminate noise to better classify and detect the recordings. It also allows for the most accurate interpretations of the recordings, and allows doctors to focus on specific waves of the heartbeat (Aston, 1990).

Filters are a key tool for signal processing. There are several different types of filters used to attenuate unwanted frequencies, such as noise, from the input signal. A common type of filter used for signal processing is the Butterworth filter, which provides a flat passband. This classification of filters includes low pass, high pass, band pass, and band stop filters, all of which

can be seen below in Error! Reference source not found.9. These all pass signals that have frequencies in the passband, and reject signals in the stopband. Low pass filters pass signals that are below a certain cutoff frequency. High pass filters pass signals with frequencies above the cutoff. Band pass filters only pass frequencies within a certain range, and band stop filters pass all frequencies except those in a certain band.

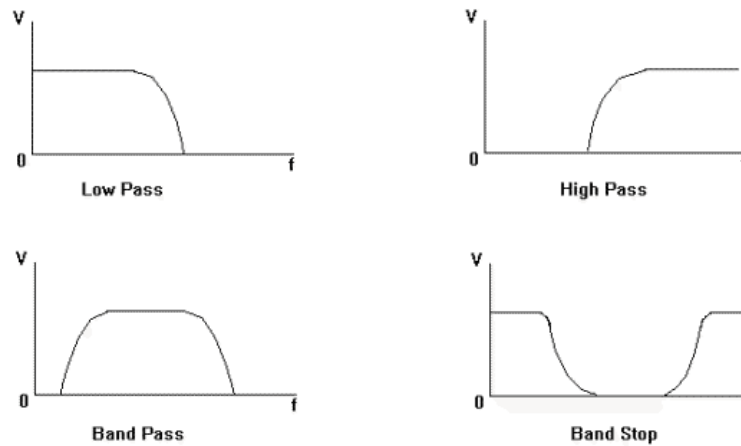


Fig. 9: Different types of Butterworth filters (Filter image)

Filtering a signal sometimes causes problems, such as magnitude distortion. This occurs when the frequency of the unwanted signal overlaps that of the desired signal. When the noise is attenuated, the magnitude of the signal is distorted as well. In order to record an accurate ECG, a technique called oversampling is used. This means that the ECG sampling rate is orders of magnitudes larger than the desired sampling rate, to allow for filtering of the recorded signal. The signal is processed using a low pass filter to avoid noise, and then down-sampled to the desired sampling rate so that it is not aliased (Luo, 2010.). Aliasing occurs when the analog signal picked up from the electrodes is sampled at a frequency lower than twice the bandwidth of the signal.

Line-frequency filters (LFF) are used when filtering ECG recordings. They get rid of 50-60Hz power line interference noise, which is encountered in a clinical setting. The LLF is a

band stop filter that is activated constantly during the recording. This means that it passes most frequencies, and only attenuates those within the specified range. The specified range of signals to attenuate is narrow, and only includes the frequency of the power line noise.

A novel idea for filtering is to integrate the filter into the electrode set up (Gruetzmann, 2007). This would eliminate motion artifacts caused by movements and breathing, because it would remove the unwanted signals starting at their origin. The setup for this filtering technique is putting a high pass filter at the origin of the signal.

### **Electrophoresis**

Electrophoresis is defined as “a technique used for the separation of biological molecules based on their movement due to the influence of a direct electric current” (Lerner, 2008). The technique was first used by Arne Tiselius, a Swedish chemist, which won him a Nobel Prize in 1948 (Berger, 2001). In electrophoresis charged biomolecules, such as carbon structures, are placed within a medium. Electrodes are placed on two sides of the medium and a current is applied. When the current is applied to the medium, the positively charged particles move towards the anode, and the negatively charged particles move towards the cathode (Lerner, 2008). In gel electrophoresis, the medium used has adjustable density and pore size of the gel matrix which allows filtering based on molecular size of the particles (Lerner, 2008).

General media to apply electrophoretic techniques on include: (i) paper, (ii) thin-layer plates and (iii) gels (Berger, 2001). One important aspect of particle behaviors in electrophoretic fields is their isoelectric points. When migrating under the field, displacement is greatest when the difference between the isoelectric point and the pH are greatest. For an equivalent pH and isoelectric point, the particle has zero force and displacement ends within the medium (Berger, 2001).

When a strong electric field in the hundreds of volts per centimeter range is applied, a non-linear electrophoretic effect is detected (Barany, 2009). The first non-linear effect is encapsulated between the outer field and the field-induced ionic charges in the electric double layer. The second non-linear effect is due to the concentration polarization (Barany, 2009). The classical theory of electrophoresis can be described by equation 5:

$$Eqn. 5: \quad v_{eph} = \frac{\epsilon \zeta E}{4\pi n}$$

$V_{eph}$  is the velocity of electrophoresis,  $\epsilon$  is the permittivity of the medium,  $\zeta$  is the electrokinetic potential,  $E$  is the external field gradient, and  $n$  is the viscosity of the medium. When the velocity of the electrophoretic movement of particles is proportional to the strength of the applied field then the electrophoresis is linear. However, when the strong electric field is applied the dependence of  $V_{eph}$  becomes nonlinear with respect to  $E$ . The first non-linear theory of electrophoresis can then be described by equation 6:

$$Eqn. 6: \quad v_{eph} = \mu E + (\mu E)^3$$

$\mu$  describes the cubic electrophoretic effect for spherical particles (Barany, 2009). The net force a particle experiences can then be described in terms of the surface conductivity and the conductivity of the medium, with particle radius  $a$ , as described in equation 7:

$$Eqn. 7: \quad D_u = \frac{K\sigma}{Km * a}$$

For the second non-linearity, described as superfast electrophoresis, the conditions which promote this behavior are the existence of current within the particle, unipolar conductivity of the particle's material, higher conductivity of particles with respect to the medium conductivity, and large electric field gradients (Barany, 2009).

## Properties of Carbon

To describe the electronegativity of Carbon in the normal state the following parabolic Hamiltonian is applied to the Schrodinger differential:

$$\hat{H} = \sum_{pq} h_{pq} \hat{a}_p^\dagger \hat{a}_q + \frac{1}{2} \sum_{pqrs} g_{pq,rs} \hat{a}_p^\dagger \hat{a}_r^\dagger \hat{a}_q \hat{a}_s$$

The energy states of Carbon can then be solved explicitly as shown in equation 8 (Putz, 2011):

$$\text{Eqn. 8: } \langle E_{\lambda \in R}^{I \leftrightarrow A} \rangle = \frac{E_0(1 + \lambda)}{1 + \lambda p_0}$$

$E_0$  is the ground state energy level,  $\lambda$  is the de Broglie wavelength and  $p_0$  is the density of the atomic structure. To approximate the electronegativity of Carbon the frontier orbital must be defined. This orbital is the barrier between occupied and unoccupied orbitals (Ahn, 2007). Since the majority of electromagnetic interactions happen at this barrier the frontier orbital electronegativity can be approximated as shown in equation 9, (Putz, 2011):

$$\text{Eqn. 9: } \chi = -\frac{E_0}{p_0} = -\mu_0 = \infty \text{ for } p_0 \rightarrow 0, \& -E_0 \text{ for } p_0 \rightarrow 1$$

Several features of carbon are listed in Table 1.

Table 1: Properties of Carbon-12

Property	Value	Reference
Ground State Configuration	3P <sub>0</sub>	(Johansson, 1966)
Ionization Energy	11.2603 eV	(Johansson, 1966)
Atomic Mass	12.0000 u	(Krane, 1988)
Abundance	98.89%	(Krane, 1988)
Atomic Radius	76.7 pm	(Alcock, 2007)

Carbon black is defined as “any of a group of intensely black, finely divided forms of amorphous carbon, usually obtained as soot from partial combustion of hydrocarbons...”

(Britannica, 2012). Carbon black atoms are spherical in shape and changes into graphite at 3000°C. Doping of ceramic materials with carbon black causes several changes in the piezoelectric properties of the material. Doping cement with 0.3% carbon black increases the piezoelectric strain by a factor of 1.5 relative to 100% and 0% doping (Shifeng Huang, 2009). Figure 10. illustrates the relative impedance by percent weight of carbon black and applied frequencies in the material:

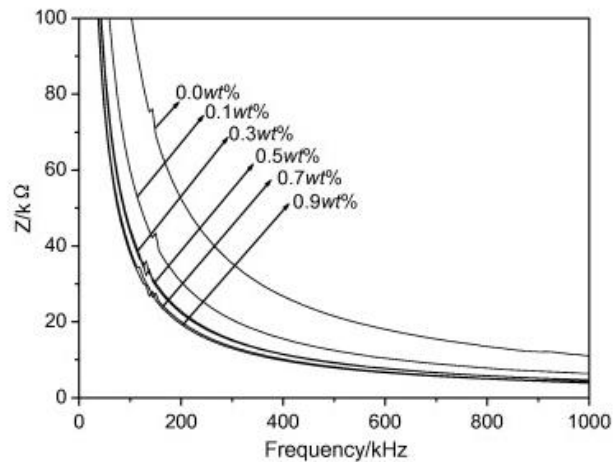


Fig. 10: Impedance spectra of the composites with different carbon black content (Shifeng Huang, 2009)

## 4. Materials & Methods

### Materials for Electrode Design

The materials used for the fabrication of the electrodes consist of the following:

- Pressure sensitive adhesive: V-95
- Dopant: carbon dispersion
- Liner 1: 200 Poly SC-6
- Liner 2: 100 Poly H-9
- Film: PM200W TC-200 EXV-215
- Magnetic mixer
- Beaker
- Pipette
- 12mil spreading tool

### Methods for Electrode Design

In order to create a 30g mixture to make electrodes, the dopant and the PSA are added to a beaker using two pipettes taped together. The amount of carbon added is the percent to be tested out of 30g. The rest of the mixture is composed of PSA. Once the 30g mixture is created, a magnetic mixer is used for about 40 minutes to stir the PSA and dopant. Next, this mixture is spread onto a liner using the 12mil spreading tool. The liner is then placed in a 160° F oven for 10 minutes. After this drying process, the liner is cut into 1" pieces in order to make the electrodes. The film is cut into 1.5" pieces, and the liner is removed from the adhesive. The adhesive is placed onto the film, leaving a small amount of adhesive exposed, in order to prevent the electrode from shorting.

Activation was obtained by applying electrophoresis across the X-Y plane of each electrode. Defibrillation charge testing, based on the AAMI EC12-2000-5.2.2.4 overload circuit diagram, applied the electrophoresis to the electrode films. Carbon columns formed to indicate activation was successful. A voltage meter applied across the activation capacitor checked to see if the electrode was shorted during application of two electrode adhesives. If the voltage slowly



decayed from 200 V the electrode was shorted, otherwise upon activation this voltage was reduced to micro-volts. The electrodes were then removed and two impedance testing clips were attached to the activation points of the material. A 10 Hz signal from the impedance testing device was generated and the impedance was measured.

### Materials for Activation Device Design

Table 2: List of parts needed to build the activation circuit.

Part	Quantity
PC BOARD CEM1 EPOXYGLASS	1
SWITCH DIP PIANO SEALED 10POS	3
DIODE GP 1A 800V DO41	8
SW TOGGLE SPST ON-OFF SOLDER LUG	2
BOX FIBER 13.8X11.9X6.47" GREY	1
BOX NEMA ECONOMY 5.9X5.9X3.54	1
<b>Resistors</b>	
RES 1.00K OHM 1W 5% AXIAL	3
RES 2K OHM 1W 5% METAL OXIDE	3
RES 4.0K OHM 5% WW AXIAL	3
RES 6.0K OHM 5% WW AXIAL	3
RES 8.0K OHM 5% WW AXIAL	3
RES 10.0K OHM 1W 5% AXIAL	3
RES 5W 10K OHM 5% WIREWOUND	3
RES 12K OHM 1W 5% METAL OXIDE	3
RES 14.0K OHM 1/2W 1% AXIAL	3
RES 18K OHM 1W 5% METAL OXIDE	3
RES 20K OHM 1W 5% METAL OXIDE	3
RES 22K OHM 1W 5% METAL OXIDE	3
RES 26K OHM 1/2W 0.1% AXIAL	3
RES 30K OHM 1W 5% METAL OXIDE	21
RES 34.0K OHM METAL FILM .60W 1%	3
RES 38K OHM 1/2W 0.1% AXIAL	3
RES 40K OHM 1/2W 0.1% AXIAL	3
RES 50K OHM 1/2W 1% AXIAL	3
RES 60K OHM 1/2W 0.1% AXIAL	3
RES 70K OHM 1/2W 1% AXIAL	3
RES 80K OHM 1/2W 1% AXIAL	3
RES 90K OHM 1/2W 0.1% AXIAL	3
RES 100K OHM 1W 5% METAL FILM	15
RES 110K OHM 1W 5% METAL OXIDE	3
RES 130K OHM 1W 5% METAL OXIDE	3
RES 150K OHM 1W 5% METAL FILM	3
RES 210K OHM 1/2W 0.1% AXIAL	3
<b>Capacitors</b>	
CAP 0.1UF 400W AXIAL	3
CAP 1.0UF 400W AXIAL	3
CAP 10.0UF 400W AXIAL	3
CAP 100.0UF 400W AXIAL	3

## Methods for Activation Device Design

An activation device with variable parameters was designed and built. The parameters required by FLEXcon are listed in Table 3. Each parameter value was permuted with the other parameters in order to determine the optimum activation of electrodes, using the electrodes with 10% carbon doping.

Table 3: Variable parameters for electrode activation.

Parameter:	Values	Units
Voltage	5, 20, 45, 75, 120, 200	V
Current	1, 2, 5, 10, 20, 50, 100	mA
Frequency	DC, 60, 1000	Hz
Time	1, 10, 100, 1000	ms

The circuit layout was determined based on the AAMI standard defibrillation overload circuit. In order to vary parameters, dip switches were used to change values of resistors and capacitors. Once the values of these parts were determined, the circuit was simulated using Multisim. The power supply used provides an AC voltage from 0-240 Volts, but the circuit based on the AAMI standards is typically used with a DC voltage. In order to address this, a diode rectifier was designed at the input to the circuit to convert the voltage from AC to DC. Figure 11. depicts the block diagram of the activation circuit.

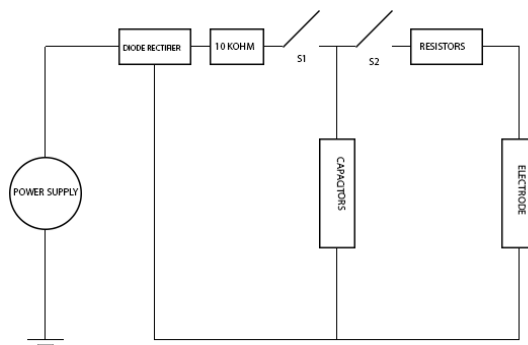


Fig. 11. Activation Circuit Block Diagram

For switches S1 and S2 there are two possible events that occur within the circuit. When S1 is on, and S2 is off, the voltage of the capacitor at steady state can be described as follows.

$$\text{Eqn. 10: } V_C \approx \frac{V_S}{2.5} - V_{10k}$$

Where  $V_C$  is the capacitor voltage and  $V_S$  is the power supply voltage. When S1 is off, and S2 is on, the electrode voltage and current can be approximated, with the electrode impedance ignored, and is shown in equations 11, and 12.

$$\text{Eqn. 11: } V_E = V_C - V_R$$

$$\text{Eqn. 12: } i \approx \frac{V_C}{R}$$

Where  $V_E$  is the electrode voltage and  $V_R$  is the voltage across the variable resistors and  $R$  is the resistance value.

To physically build the circuit, wires that support high power wattage were obtained from the Electrical and Computer Engineering (ECE) Shop, and all other parts listed in the materials section were ordered through the shop. The parts were soldered onto the board based on the schematic. The final board is shown below in Fig. 12, and the housing for the activation device can be seen in Fig. 13. Once this was complete, the different sections of the board were tested using a digital multimeter to make sure everything was functioning properly. After determining that the board was working correctly, the team assembled 840 electrodes, following the procedure laid out in the previous section, “Materials for Electrode Design.”

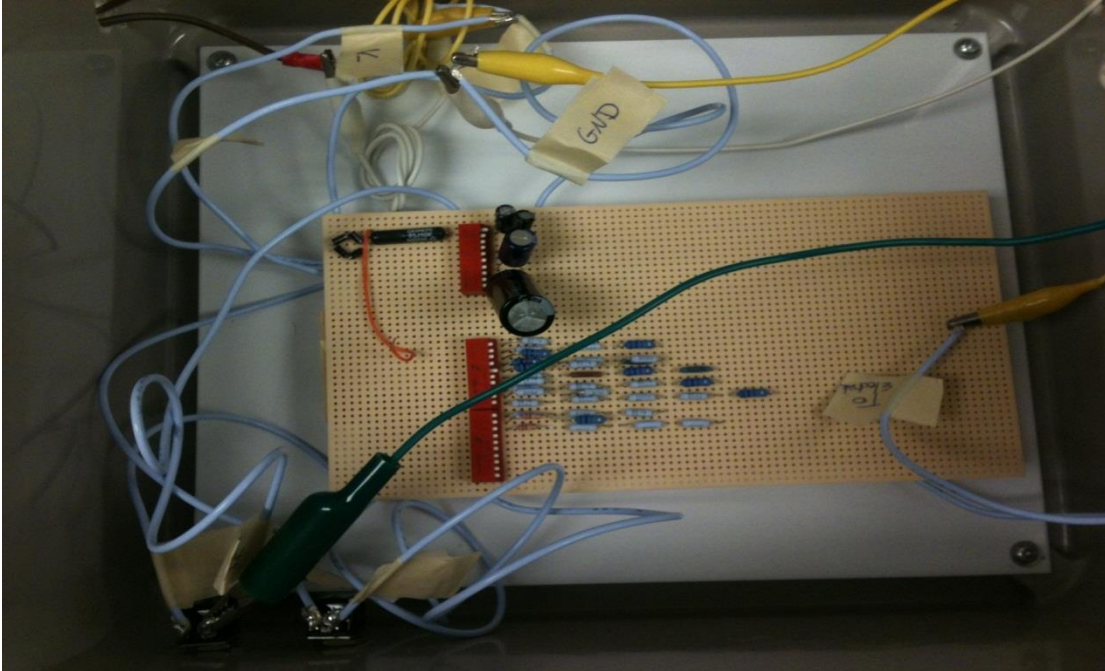


Fig. 12. Activation device with variable parameters.



Fig. 13. Housing for the activation device.

At first, an LCR meter from the Biomedical Engineering Lab in Goddard Hall was used for testing. This meter was old and gave extremely variable impedance values; therefore it was

determined to be unreliable. In order to address this issue, the Hiroki IM 3570 was rented in order to measure the impedances of the electrodes. All pre-activation impedances of the electrodes were measured using this device at a frequency of 10 Hz and voltage of 1 V. Once impedance measurements were taken, a sample size of N=5 electrodes were activated for each combination of the parameters listed in Table 3. The post-activation impedance measurements were taken for each electrode using the LCR meter.

During this portion of the project, the group encountered several setbacks that were addressed. Ordering parts through the ECE shop took an unnecessary amount of time because parts were out of stock, so a new part list needed to be created from a different supplier. Also, finding an LCR meter that had the necessary functionality to measure impedances up to MΩs at a frequency of 10Hz was a problem. Renting an LCR meter allow the large impedances to be recorded. Finally, the variable power transformer used to activate the electrodes shorted a diode in the rectifier more than once and also melted a wire, which was determined by trouble shooting the activation device board.

## 5. Results

### Stage 1

One of the primary deliverables of this qualifying project was to design an experiment which determines the ideal concentration of carbon dispersions in the novel ECG electrode which minimizes post activation impedance. Ideally, a minimal amount of carbon would be used. To narrow down on this, the group designed an initial experiment which tested electrodes created with varying concentrations of carbon [ranging from 2% to 12% carbon loading levels by increments of 2] and measured pre-activation and post-activation impedance. The results from the initial experiment are provided in Table 4.

Table 4 Impedance test results for different carbon levels (STAGE 1)

Carbon Load	Mean Pre-activation Impedance & Standard Deviation (M $\Omega$ )	Mean Post-activation Impedance & Standard Deviation ( $\Omega$ )
2%	10.8 $\pm$ 7.3	2,400,000 $\pm$ 3,240,000
4%	7.5 $\pm$ 10.4	4960 $\pm$ 5400
6%	5.6 $\pm$ 5.0	2900 $\pm$ 3000
8%	6.9 $\pm$ 3.8	273 $\pm$ 35.4
10%	3.3 $\pm$ 5.0	222 $\pm$ 24.6
12%	1.99 $\pm$ 0.77	307 $\pm$ 35.2

For each carbon load level, 5 sample electrodes were used in this initial experiment. From Table 4 it can be observed that the most consistent results were obtained for carbon loads at 8%, 10% and 12%. According to AAMI standards, the mean post activation impedance is required to be under 2K $\Omega$ . Based on that criterion, the group proceeded to the next stage of the experiment by gathering more data on impedance levels for 8%, 10% and 12% carbon levels.

For this part of the project, the group gathered 30 samples of each carbon load levels and performed a similar experiment on the pre-activation and post-activation impedance levels of the electrodes. There were a few outliers in the data that was collected. It is usually challenging to

define a data point as an outlier as no official statistical definition exists for it. For the purposes of this experiment, the group evaluated the first quartile Q1 [25<sup>th</sup> percentile], the third quartile Q3 [75<sup>th</sup> percentile] and the interquartile range IQR [Q3-Q1]. A factor of 1.5 was then multiplied to the IQR and subsequently added to Q3 and subtracted from Q1. Any data point that fell outside of this range was then considered an outlier. A MATLAB script was written to evaluate each data point and discern whether or not it was a valid data point that can be used for analysis. This script has been included in Appendix B. The data for central tendency in these samples is provided in Table 5.

Table 5 Impedance Test Results, STAGE 1

<b>Carbon Load</b>	<b>Mean Pre-activation Impedance &amp; Standard Deviation (M<math>\Omega</math>)</b>	<b>Mean Post-activation Impedance &amp; Standard Deviation (<math>\Omega</math>)</b>
8% Carbon	10.5 $\pm$ 6.01	1170 $\pm$ 1170
10% Carbon	2.09 $\pm$ 2.79	256 $\pm$ 51.4
12% Carbon	3.96 $\pm$ 2.39	286 $\pm$ 56.5

After the removal of outliers, the remaining data was used to plot the Gaussian distribution for the samples. The MATLAB script for this has been included in Appendix B.

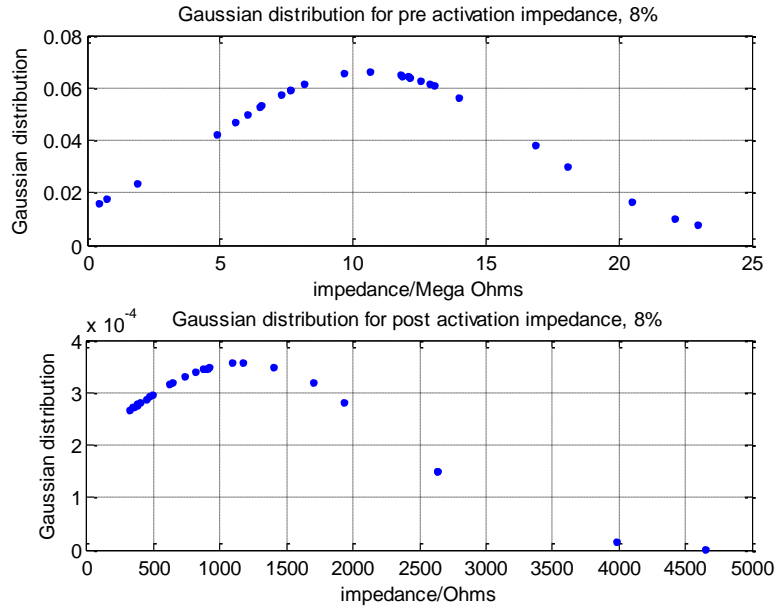


Fig. 14. Gaussian distribution plot for 8% carbon load

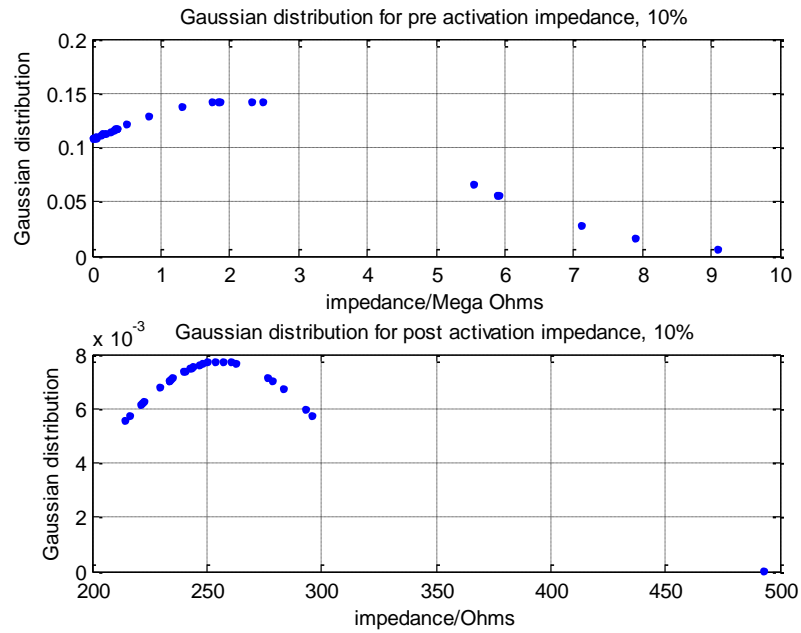


Fig. 15. Gaussian distribution plot for 10% Carbon load



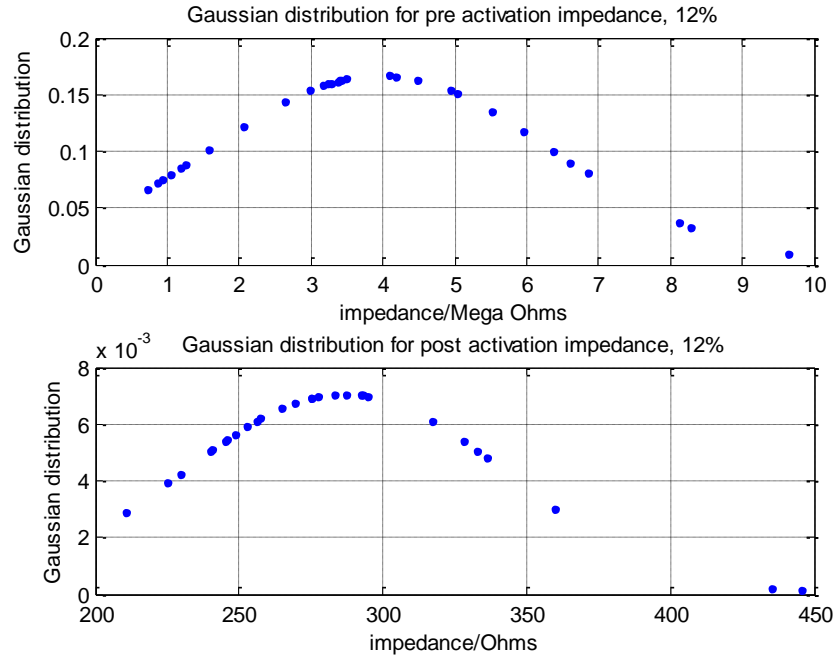


Fig. 16. Gaussian distribution for 12% carbon

In order to verify that the data gathered for pre-activation and post-activation impedances are not from a random sample, two-tailed t-tests were performed in MATLAB. The t-tests were done with a set null hypothesis that at a significance level of 95%, the data in the given vector are a random sample from a normal distribution with a mean of zero and unknown variance. The following results were obtained and have been provided in Table 6. It should be noted that the p-value returned from the t test provides the probability of obtaining a result more extreme than the test statistic. At a significance level of 95%, the p value tells us what the chances of obtaining a result that is more extreme than this confidence interval.

Table 6 One sample t-test results

Sample	Rejection of Null hypothesis	p-value
8%, pre activation	Yes	$1.5*10^{-9}$
8%, post activation	Yes	$1.1*10^{-5}$
10%, pre activation	Yes	$7.8*10^{-4}$
10%, post activation	Yes	$8.5*10^{-21}$
12%, pre activation	Yes	$7.5*10^{-10}$
12%, post activation	Yes	$5.3*10^{-21}$

Following this, two sample t-tests were done to observe whether the data gathered from 8%, 10% and 12% were inherently collected from separate populations or not. The null hypothesis was that the two datasets had equal population means and equal but unknown variances. The results are given in Table 7.

Table 7 Two sample t-test results

Samples	Rejection of Null hypothesis	p-value
10% and 8%, pre activation	Yes	$2.0*10^{-8}$
10% and 8%, post activation	Yes	$7.0*10^{-5}$
12% and 10%, pre activation	Yes	0.0086
12% and 10%, post activation	Yes	0.0396
8% and 12%, pre activation	Yes	$9.5*10^{-7}$
8% and 12%, post activation	Yes	$1.1*10^{-4}$

As expected, the p-value for the 12% and 10% distribution was higher than the rest. This is because the sample means for both of these datasets are comparable to each other. However, the post activation p-value was still lower than 0.05, which means that they can be recognized as two independent populations. It is preferred to limit the amount of carbon black in the PSA-carbon mixture. Therefore, the group has decided to use 10% carbon in the future electrodes to be designed, due to the consistency in post activation impedance in 10% carbon.

Pre-activation and post-activation impedances were recorded for 840 electrodes. The parameters were varied and the complete mean and standard deviation results are included in Appendix E. The following code listing was used to derive the mean and standard deviation from the list of measurements.

```

clc; clear all; close all;

data=xlsread('Impedance Measurements 12-13.xlsx');
n=1;
for i=1:5:840
    for j=1:1:5
        if i==1
            read(j)=data(j,2)*10^(data(j,3));
        else
            read(j)=data(i+j,2)*10^(data(i+j,3));
        end
    end
    mean_data(n)=mean(read);
    std_data(n)=std(read);
    n=n+1;
end

mean_data=mean_data';
std_data=std_data';

```

Figures 17- 20. show the variation of power across the electrode for a 0.1 uF, 1.0 uF, 10.0 uF, and 100.0 uF capacitor respectively, and the resulting averaged impedances for each activation power.

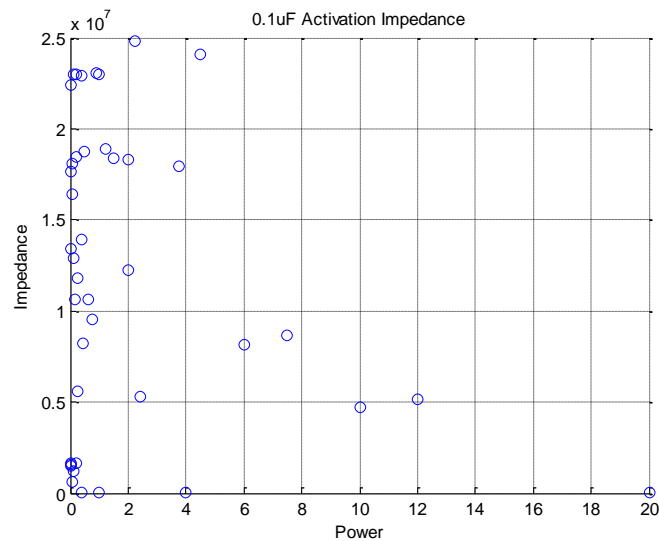


Fig. 17. 0.1 uF Post-Activation Mean Impedances

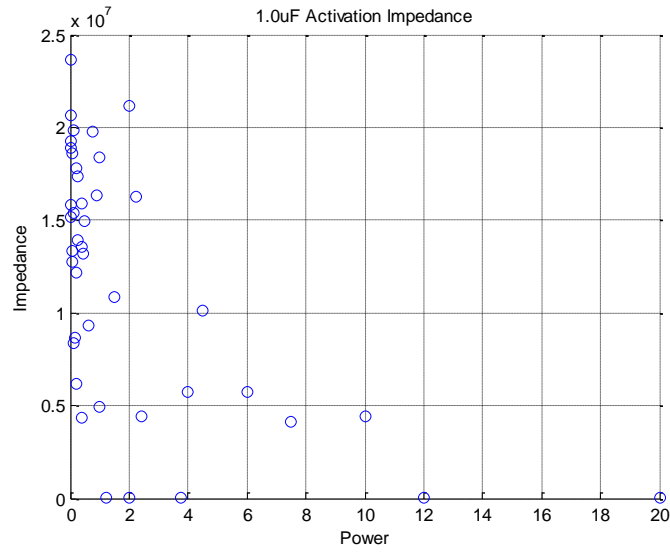


Fig. 18. 1.0 uF Post-Activation Mean Impedances

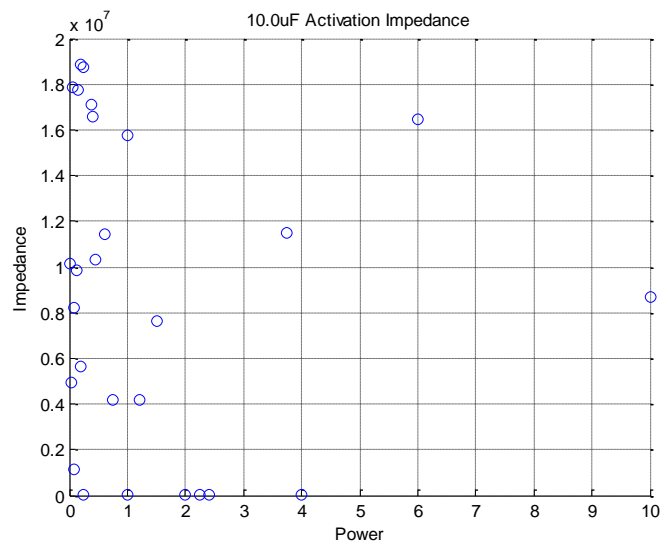


Fig. 19. 10.0 uF Post-Activation Mean Impedances

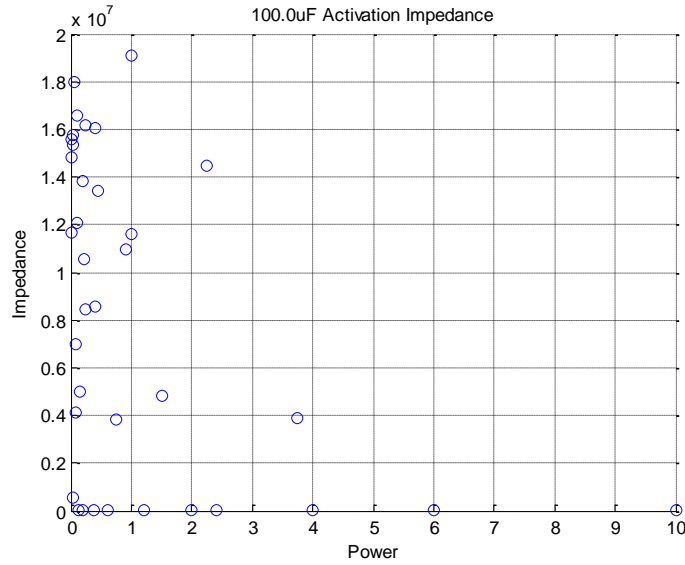


Fig. 20. 100.0 uF Post-Activation Mean Impedances

The mean post-impedance trend implies that for higher activation powers the impedance tends to drop exponentially, with a greater rate of decrease for larger capacitor values. Using larger capacitors causes the activation time to increase and can be correlated with the drop in impedance.

Table 8 details the specific mean and standard deviation values for low post-activation impedances. These values correspond to the optimum activation parameters for the current data set.

Table 8 Optimum Parameters for Activation

Parameters			Pre-Activation [ $\Omega$ ]		Post-Activation [ $\Omega$ ]	
<i>Voltage</i>	<i>Capacitance</i>	<i>Current</i>	<i>MEAN</i>	<i>STD</i>	<i>MEAN</i>	<i>STD</i>
200V	.1 $\mu$ F	20mA	18835105	3706363	3678.83	1875.343
200V	.1 $\mu$ F	100mA	17177040	8404301	6040.96	6671.187
200V	1 $\mu$ F	10mA	20869620	2340181	2412.112	1342.27
120V	1 $\mu$ F	10mA	7827510	9834031	1247.771	262.3298
200V	1 $\mu$ F	100mA	20716840	2772424	443.5232	189.509
120V	1 $\mu$ F	100mA	20636080	3326407	829.6632	296.6535
200V	10 $\mu$ F	10mA	21570320	3224722	1673.75	494.7733
200V	10 $\mu$ F	20mA	15640541	8898123	1195.448	2161.881
120V	10 $\mu$ F	20mA	21097100	1966878	1048.699	1506.763

From Table 8 the optimum activation parameters are 1  $\mu\text{F}$ , 200 V and 100 mA of current. However, using the 100 mA current results in carbon columns that expand until they burst, resulting in smoke. Therefore the 50 mA current may be the optimum current for activation.

Extra electrode testing was conducted over the Winter break. However, the data derived was from a carbon and PSA mix that settled over a month and generated very large impedances. These impedance values are found in Table 9.

Table 9 Settled Carbon and PSA Mixed Impedance Values

Voltage [V]	Capacitance [ $\mu\text{F}$ ]	Current [mA]	Post Impedance [Z]
120	1	10	3421039.54500000
200	1	100	2043.68715000000
120	1	100	20805957.5070000
200	10	10	5459910.94300000
200	10	20	34753.8865000000
120	10	20	14812342.5075000
200	10	50	3615684.59400000
200	100	10	2311178.29550000
200	100	20	2830.16400000000
200	100	50	1452770.11895000

Since the 200 V, 100 mA, 1  $\mu\text{F}$  activation parameter generated the lowest impedance, this activation parameter was retested with a properly mixed solution. Figure 21. depicts the Gaussian distribution of post-activation impedances.

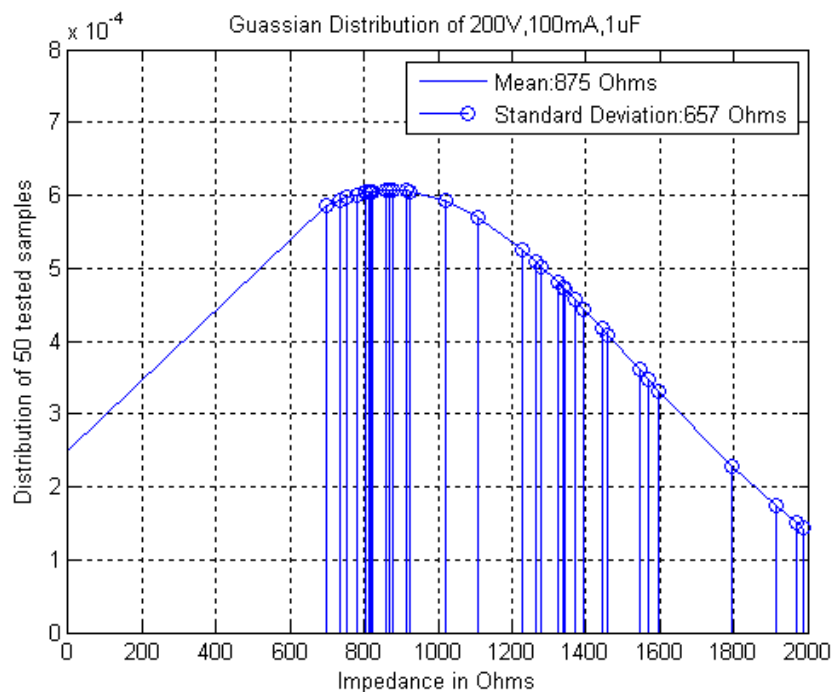


Fig. 21: Properly mixed PSA+Carbon Post Impedance Gaussian Curve

The mean of 43 activation electrode impedances is 875  $\Omega$ , and the standard deviation is 657  $\Omega$ . These values are under the AAMI requirements of 2 k $\Omega$  mean and no single activation impedance exceeding 3 k $\Omega$ . Due to the AAMI requirements being met for the 10% doped carbon and PSA mix, activated at 200 V, 100 mA, with a 1  $\mu$ F capacitor, these electrodes meet all requirements for the next stage of the project.

## Stage 2

Four electrode types are tested for their impedance vs. frequency characteristics. Three FLEXcon electrodes of sizes [Width x Height]: 3.5 cm x 2.5 cm, 4 cm x 3 cm, and 5 cm x 4 cm. The fourth electrode is the standard tab Ag-AgCl electrode for comparison testing, and is approximately the same size as the smallest FLEXcon electrode. Two electrodes were mounted on the right forearm, one by the palm side of the wrist, and the second was 5 cm away towards the elbow. These electrodes were connected to the Hioki IM3570 impedance analyzer. Figure 22.

depicts the impedance vs. frequency sweep of the Ag-AgCl electrodes. Figures 23- 25. depict the impedance vs. frequency sweeps for small, medium, and the largest FLEXcon electrodes respectively.

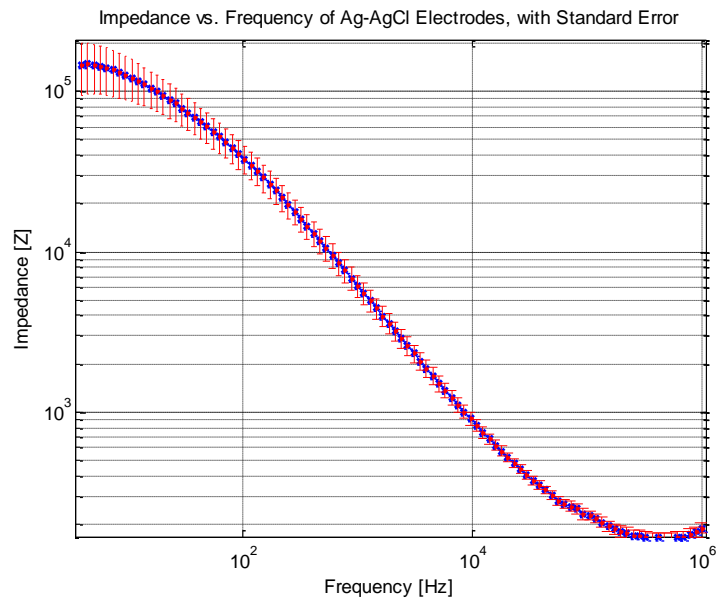


Fig. 22. Impedance vs. Frequency sweep for Ag-AgCl electrodes.

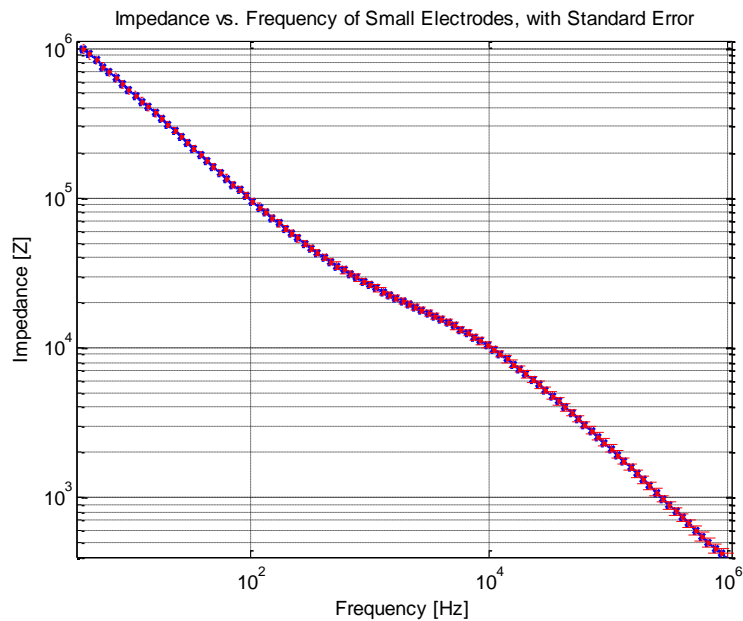


Fig. 23. Impedance vs. Frequency sweep for small FLEXcon electrodes.



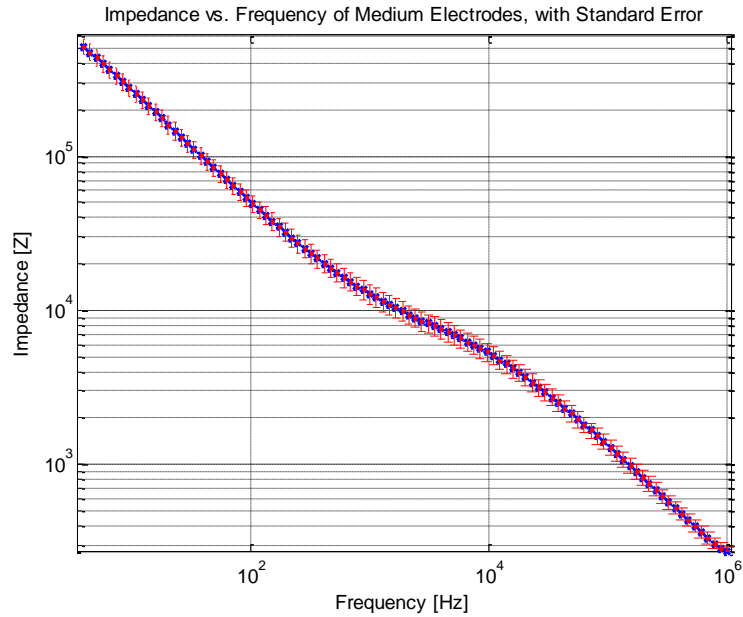


Fig. 24. Impedance vs. Frequency sweep for medium FLEXcon electrodes.

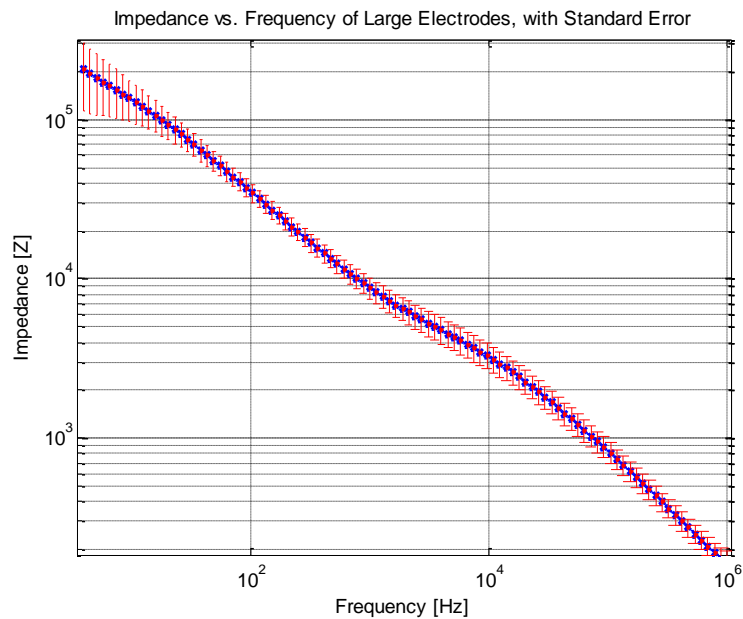


Fig. 25. Impedance vs. Frequency sweep for large FLEXcon electrodes.

Using the BioPac analog-to-digital signal converter (ADC), and the AcqKnowledge data acquisition and manipulation software, ECG waveforms were taken from a signal participant for all electrode types. The participant was asked to remain motionless for the control condition, and

movement was conducted for the second waveform recorded. Figure 26. depicts the Ag-AgCl electrode ECG waveform for a participant at rest.

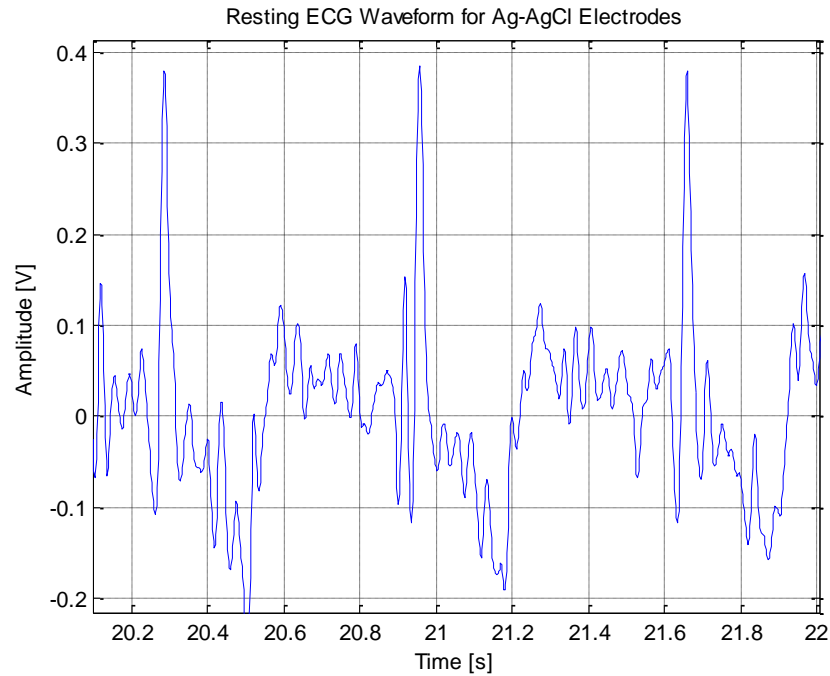


Fig. 26. Ag-AgCl resting ECG waveform for 2 second period.

The waveform shows a consistent signal-to-noise ratio (SNR), with baseline amplitude oscillations of noise present. The PQST waves are generally indiscernible due to the noise, yet the R wave is readily apparent. Figure 27. Depicts the Fast Fourier Transform of the resting Ag-AgCl waveform.

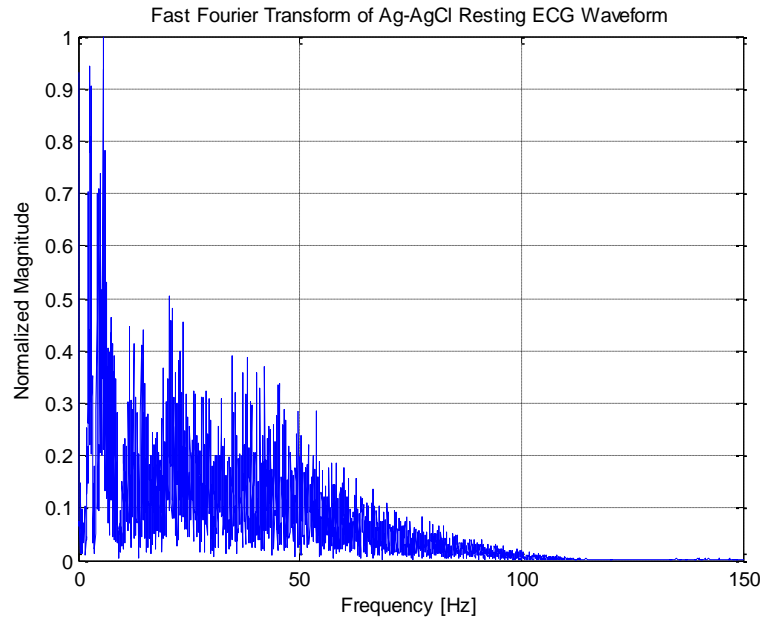


Fig. 27. FFT of resting Ag-AgCl ECG waveform.

Figures 28., and 29. Depict the ECG waveform and the FFT of the Ag-AgCl electrodes when movement occurs every ten seconds for the span of one minute. The movement shown on Fig. 28. Begins at the 20 s mark.

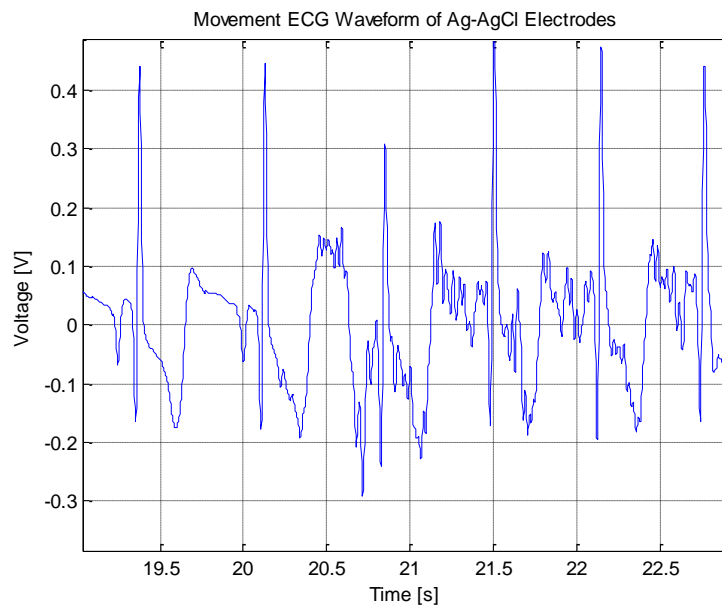


Fig. 28. Movement ECG waveform for Ag-AgCl electrodes.

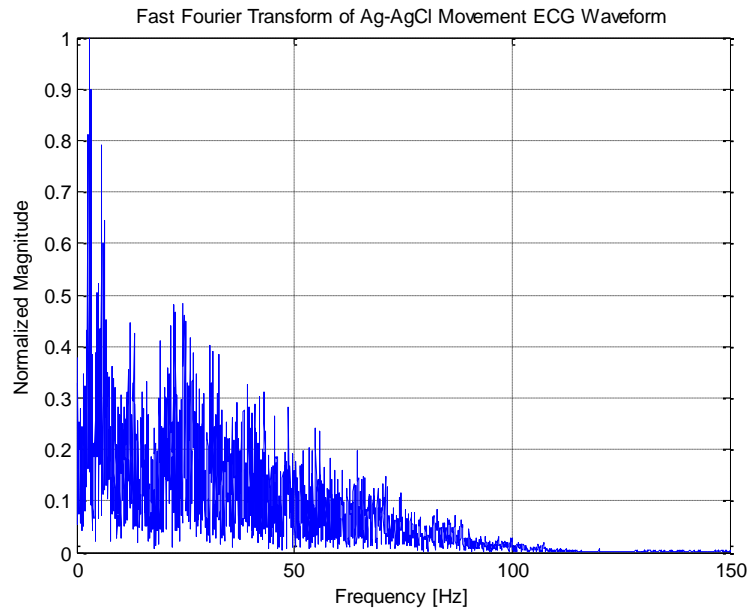


Fig. 29. FFT of movement Ag-AgCl ECG waveform.

Figures 30., and 31. depict the resting ECG waveform and FFT of the small FLEXcon electrodes. Figures 32., and 33. depict the movement ECG waveform and FFT of the small FLEXcon electrodes.

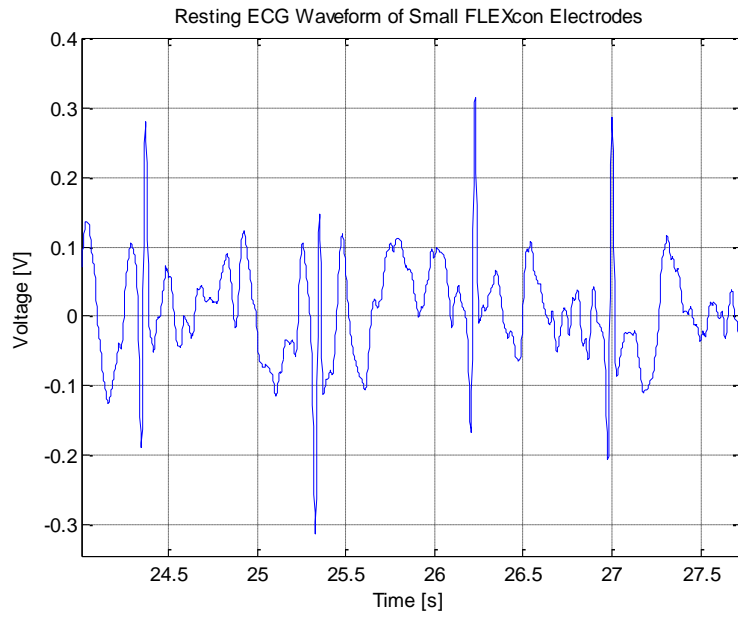


Fig. 30. Resting ECG waveform for small FLEXcon electrodes.

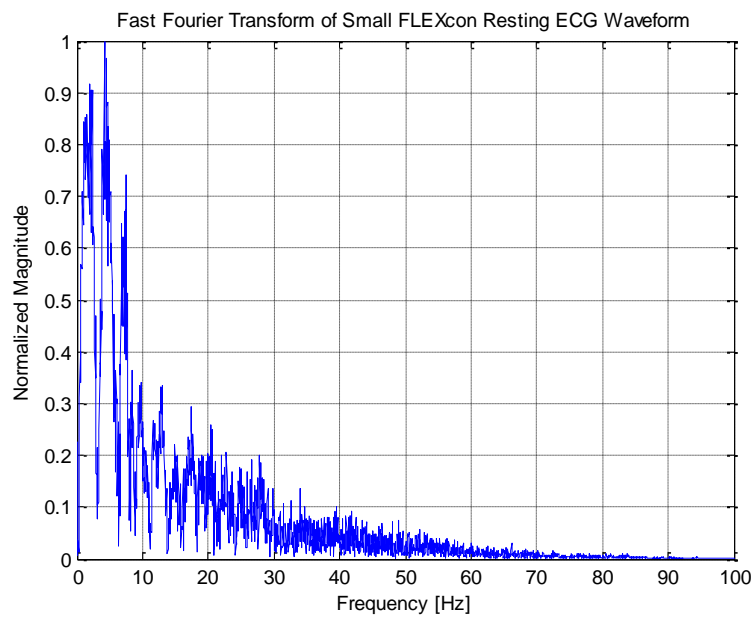


Fig. 31. FFT of resting small FLEXcon ECG waveform.

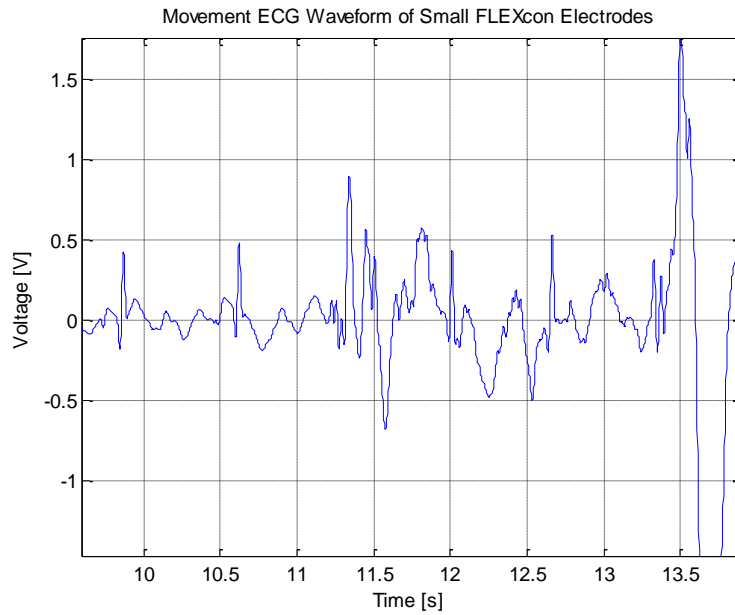


Fig. 32. Movement ECG waveform for small FLEXcon electrodes.

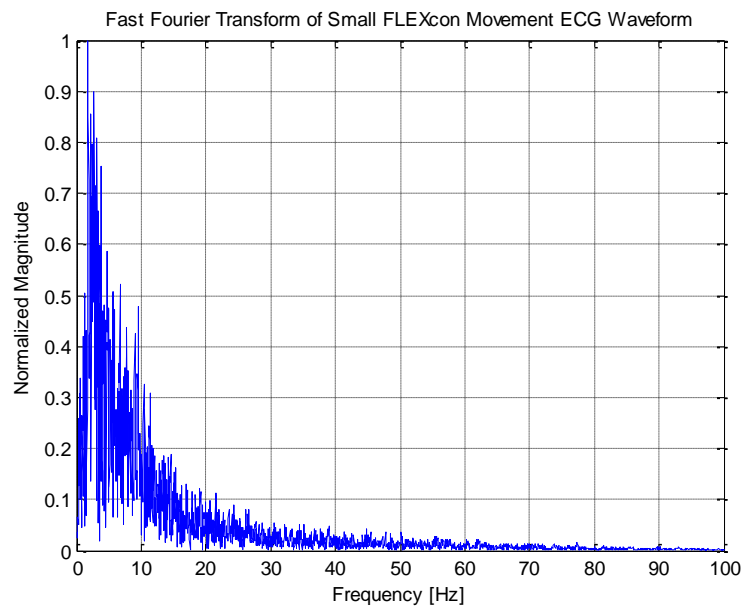


Fig. 33. FFT of movement small FLEXcon ECG waveform.

Figures 34., and 35. depict the resting ECG waveform and FFT of the medium FLEXcon electrodes. Figures 36., and 37. depict the movement ECG waveform and FFT of the medium FLEXcon electrodes.

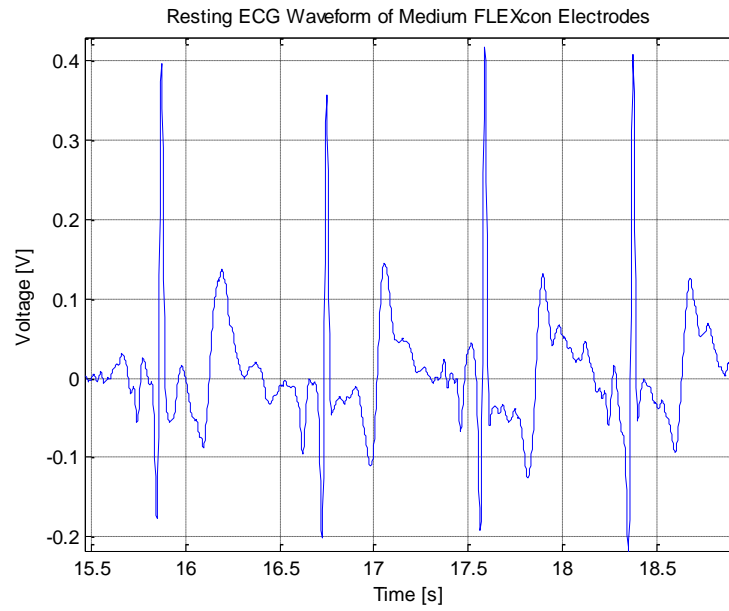


Fig. 34. Resting ECG waveform for medium FLEXcon electrodes.

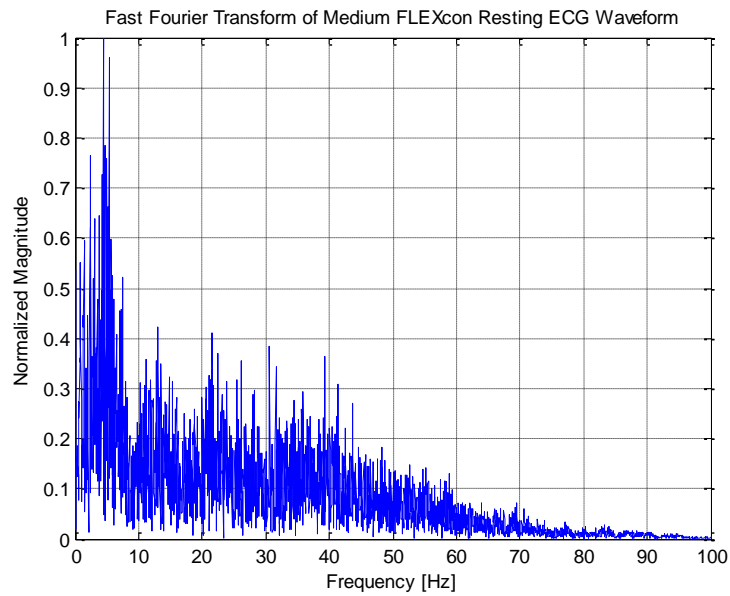


Fig. 35. FFT of resting medium FLEXcon ECG waveform.

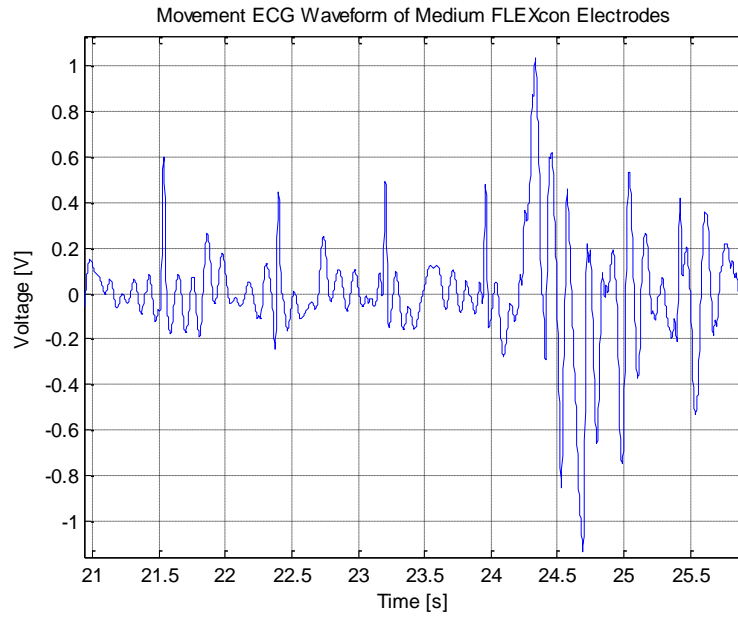


Fig. 36. Movement ECG waveform for medium FLEXcon electrodes.

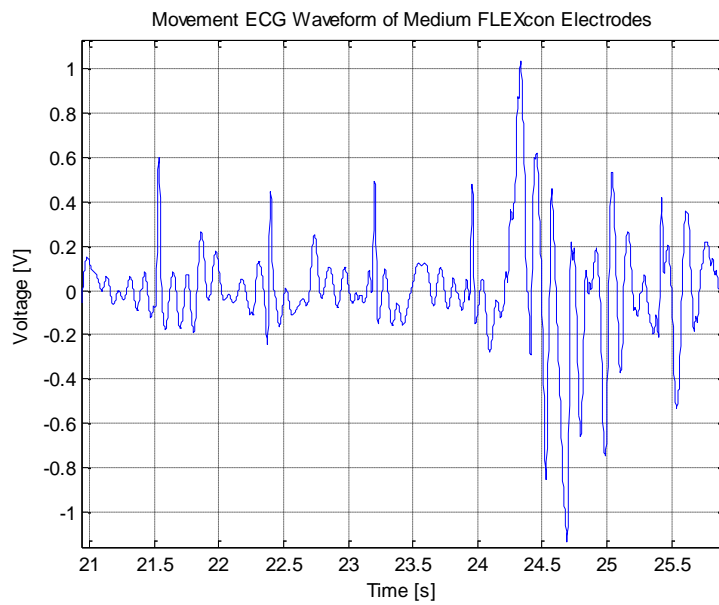


Fig. 37. FFT of movement medium FLEXcon ECG waveform.

Figures 38., and 39. depict the resting ECG waveform and FFT of the large FLEXcon electrodes. Figures 40., and 41. depict the movement ECG waveform and FFT of the large FLEXcon electrodes.



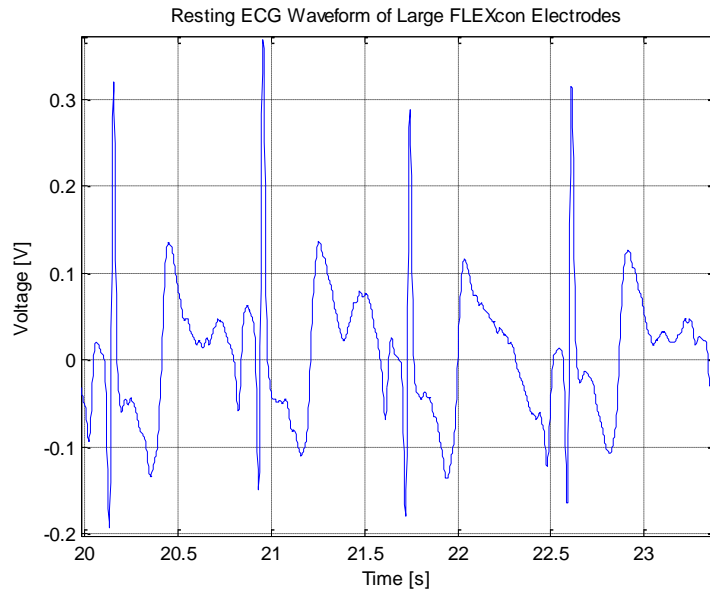


Fig. 38. Resting ECG waveform for large FLEXcon electrodes.

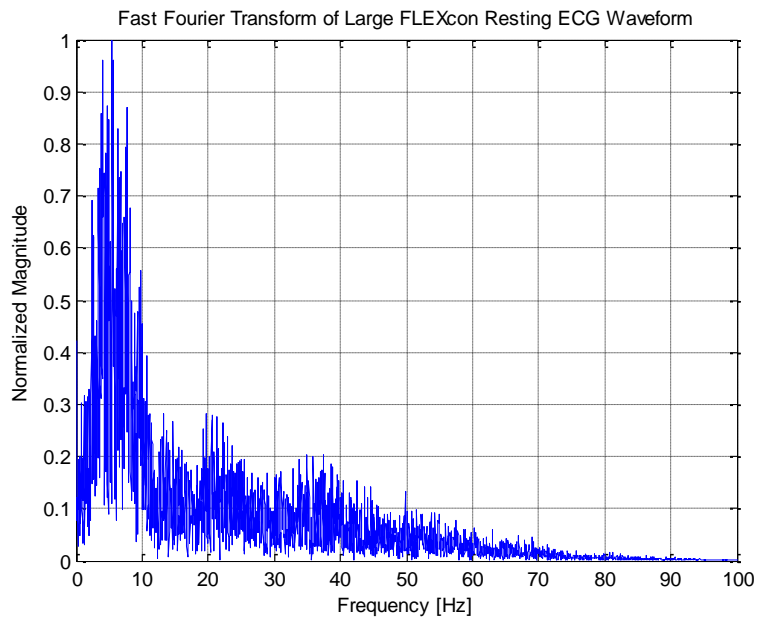


Fig. 39. FFT of resting large FLEXcon ECG waveform.

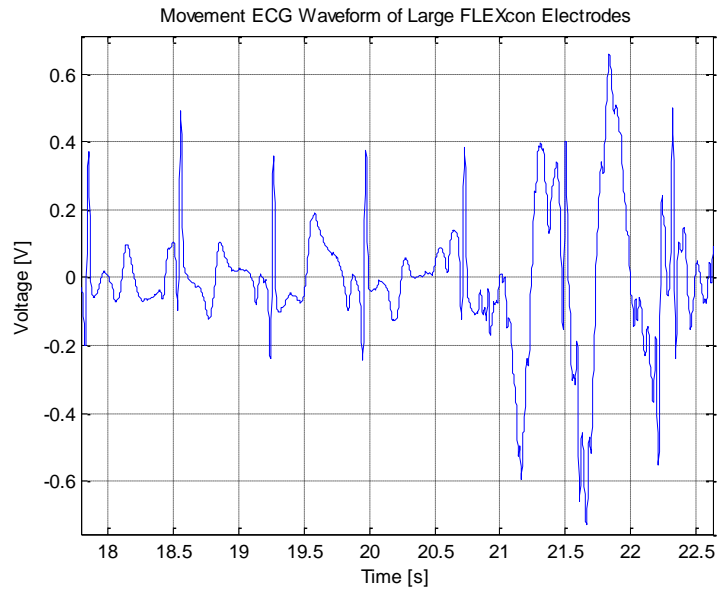


Fig. 40. Movement ECG waveform for large FLEXcon electrodes.

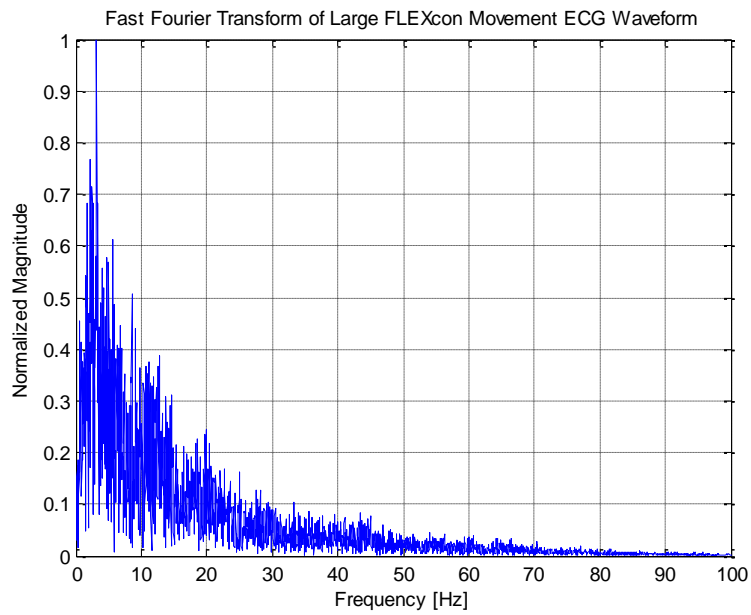


Fig. 41. FFT of movement large FLEXcon ECG waveform.

## Signal Processing and Peak Detection Algorithm

This section covers the signal processing steps that were taken to clean up the raw ECG data collected from the ten subjects using a Rozinn© holter monitor as part of this study. It also covers the method used to detect the QRS peak locations in the data. Peak detection is crucial for comparing the data gathered from silver/silver chloride electrodes against the novel ECG electrodes manufactured by FLEXcon. The team used the scripting language MATLAB to process the data and implement the peak detection algorithm.

### Import Raw Data, Sampling Frequency, time vector

The raw ECG data was collected using a Rozinn© holter monitor. This brand of holter monitors is capable of gathering ECG data from multiple channels simultaneously. As a result, ECG data was saved from silver/silver chloride electrodes and from FLEXcon electrodes at the same time in .csv files. The code used to import the data from both these channels has been provided below.

```
%% Read data
ecg= csvread('32223.csv');
ecg1= ecg(1:32400,3)./1000;    %FLEXcon electrode data, in Volts
ecg2= ecg(1:32400,2)./1000;    %silver chloride data, in Volts
% All flexcon variables end with 1, silver with 2 %
```

The MATLAB function *csvread* imports the data into a 3xN matrix, and individual channels are then extracted as shown above. All subsequent variables are named with a “1” at the end to indicate FLEXcon data and “2” to indicate silver/silver chloride data. Three minutes of resting ECG data was used for both channels.

Following this, the sampling frequency of 180 Hz was used to generate a time vector which was three minutes long. The variable duration stored the length of time in seconds of the ECG data. The time vector was transposed to a column vector to match the raw ECG data extracted previously.

```

%% Sampling frequency, time vector
Fs=180; %sampling frequency of Rozinn holter monitor
dt=1/Fs; %time increment
duration=length(ecg1)*dt; %length of data (180 seconds)
t=0:dt:duration-dt; %time vector
t=t'; %transpose time vector for detrending

```

### Detrending Solution, Correction for DC noise

One of the problems that are often encountered when analyzing ECG data is the presence of low frequency oscillations that occur as a consequence of breathing. Detrending the data involves the generation of a polynomial for each second of the data collected and subtracting it out of the raw signal. This is extremely important as the peak detection algorithm assumes that the amplitudes of the QRS complexes detected are on a comparable order of magnitude, and the presence of low frequency breathing artifacts may skew the analysis. Following this, the mean of the entire ECG signal was calculated for both channels and subtracted from the data to correct for DC offset. Figure 42. shows the resulting ECG waveform after these steps.

```

%% Detrending solution
N=180; %length for detrending solution, 1 second long
for i=1:N:length(ecg1)-N-1
    p1=polyfit(t(i:(i+N-1)),ecg1(i:(i+N-1)),1); %generate coefficients for polynomial for
    FLEXcon
    yfit1=polyval(p1,t(i:(i+N-1))); %create data set to be subtracted from raw ECG data,
    FLEXcon
    p2=polyfit(t(i:(i+N-1)),ecg2(i:(i+N-1)),1);%generate coefficients for polynomial for
    silver chloride
    yfit2=polyval(p2,t(i:(i+N-1)));%create data set to be subtracted from raw ECG data,
    silver chloride
    for j=1:N
        ecg1(i+j-1)=ecg1(i+j-1)-yfit1(j); %detrend the raw data, FLEXcon
        ecg2(i+j-1)=ecg2(i+j-1)-yfit2(j); %detrend the raw data, silver chloride
    end
end
%% Correction for DC noise level for threshold
ecg1=ecg1-mean(ecg1); %zeros the ECG essentially
ecg2=ecg2-mean(ecg2); %silver

```

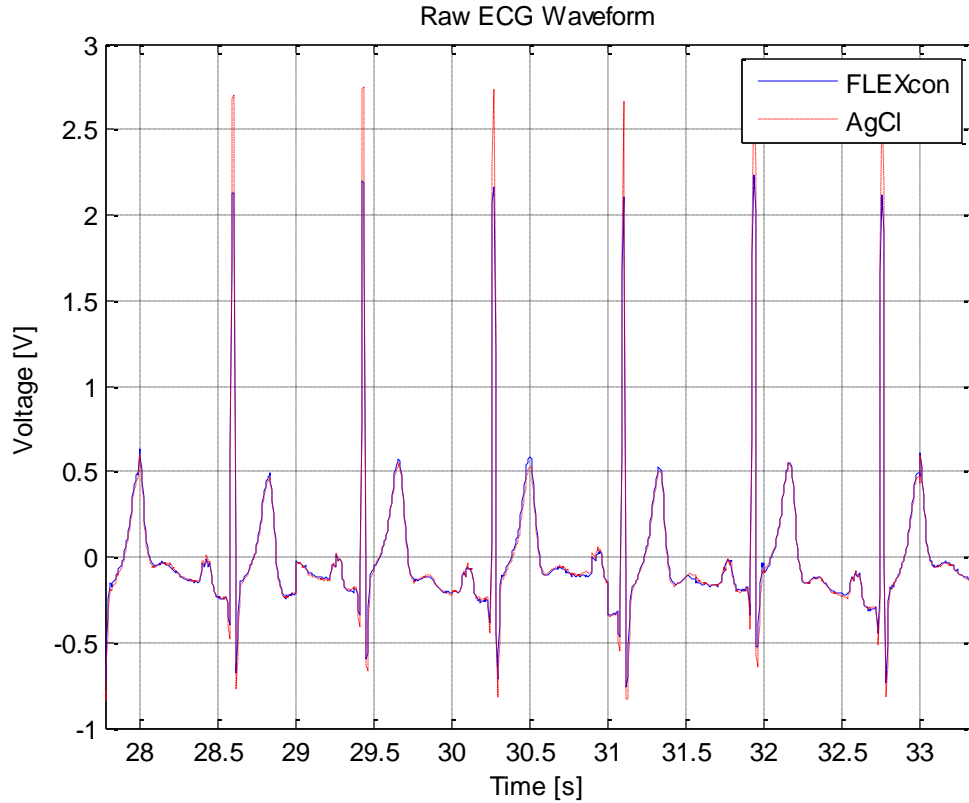


Fig. 42. Raw ECG after detrending and DC correction. FLEXcon data is shown in blue, whereas silver chloride data is in red.

### Bandpass Filtering

The relevant data in an ECG signal rests between 5 and 11 Hz. Power line interference occurring at multiples of 60 Hz and low frequency baseline drift noise could be minimized by this step. To attenuate signal components that occur at frequencies outside this range, the data was first lowpass filtered with a cutoff at 11 Hz and subsequently highpass filtered with a cutoff at 5 Hz. The code to perform this is shown below.

```
%% Lowpass filtering
bl=[1 0 0 0 0 0 -2 0 0 0 0 0 1];
al=[1 -2 1];
ecg_lp1=filter(bl,al,ecg1); % Lowpass filter FLEXcon data
ecg_lp2=filter(bl,al,ecg2); % LP filter silver data

%% Highpass filtering
bh=[-1 zeros(1,15) 32 zeros(1,15) 1];
ah=[1 1];
ecg_hp1=filter(bh,ah,ecg_lp1); %HP filter FLEXcon
ecg_hp2=filter(bh,ah,ecg_lp2); %HP filter AgCl
```

The second order lowpass filter implemented can be expressed by the following equation. This equation effectively retains all signal components that occur between 0 Hz and 11 Hz and attenuates higher frequencies by a factor of 36.

$$y(nT) = 2y(nT - T) - y(nT - 2T) + x(nT) - 2x(nT - 6T) + x(nT - 12T)$$

After lowpass filtering was done on the ECG data from both channels, it was passed through a highpass filter with a cutoff at 5 Hz expressed by the following difference equation. The peak detection algorithm uses this data set to express the peak locations.

$$y(nT) = 32x(nT - 16T) - y(nT - T) - x(nT) + x(nT - 32T)$$

#### Derivative Filtering, Squaring

After the raw ECG signal is filtered to retain the significant components, it was passed through a derivative filter for peak detection. A five point derivative filter accentuates the slope of the QRS complex significantly, making it easier for the peak detection algorithm to detect QRS complexes. Following the derivative filtering, the signal was squared to provide nonlinear amplification to the peaks. The difference equation for the five point derivative filter is provided as follows, along with the MATLAB implementation of this step.

$$y(nT) = \left(\frac{1}{8T}\right) [-x(nT - 2T) - 2x(nT - T) + 2x(nT + T) + x(nT + 2T)]$$

```

%% Derivative filtering, squaring
bd=(1/8)*[2 1 0 -1 -2];
ad=[1];
ecg_der1=filter(bd,ad, ecg_hp1);    %derivative filter FLEXcon
ecg_der2=filter(bd,ad, ecg_hp2);    %derivative filter AgCl

ecg_sq1=(ecg_der1).^2;
ecg_sq2=(ecg_der2).^2;

```

## Moving Average Filtering

This is a critical step in peak detection. The general idea is that by averaging signal amplitude for a certain predefined window length, the exact peak location can be picked out from the output of the squaring algorithm. For a sampling rate of 180 Hz, a window length of 30 is used to integrate the signal, as instructed in “A Real-Time QRS Detection Algorithm” by Pan and Tompkins. The difference equation for this step is provided below. ‘N’ stands for the window length, which has been selected to be 30 for this algorithm. Too large a moving window length can potentially result in peaks being missed, whereas too small a window length can give rise to multiple peaks in the integration waveform.

$$y(nT) = \left(\frac{1}{N}\right) [x(nT - (N - 1)T) + x(nT - (N - 2)T) + \dots + x(nT)]$$

```
%% Moving average filtering
N=30; %length of MA filter
bm=(1/N)*[ones(1,N)];
am=[1];
ecg_m1=filter(bm,am,ecg_sq1); %MA filter FLEXcon
ecg_m2=filter(bm,am,ecg_sq2); %MA filter AgCl
```

## Thresholding, peak indices search

After the signal has passed through a moving average filter, thresholds were set to be equal to the mean of the output of the moving average filters. Any data point that is detected to be higher than the threshold in amplitude is deemed to be roughly near a QRS peak. The

MATLAB function *find* was used to find these points and set them to be equal to 1.

```
%% Thresholds
thr1= mean(ecg_m1); % FLEXcon threshold
thr2= mean(ecg_m2); % AgCl threshold
ecg_p1=zeros(size(ecg_m1)); %vector to store peak approximation, ONLY CONTAINS 1s and 0s (FLEXcon)
ecg_p2=zeros(size(ecg_m2)); %vector to store peak approximation, ONLY CONTAINS 1s and 0s (AgCl)
ecg_p1(find(ecg_m1>=thr1))=1; %data > threshold --> 1, data < threshold --> 0
ecg_p2(find(ecg_m2>=thr2))=1;
```

After this step, the derivative of *ecg\_p1* and *ecg\_p2* were used to find the transitional points. The index locations of these transitional points were then stored in *upindex1*, *upindex2*,

*downindex1* and *downindex2*. *Upindex* contained the locations of the rising edges in the output of the moving average filter, whereas *downindex* contained the falling edge locations. By looking at the data that occurs between consecutive rising and falling edges, the peak locations could then be accurately determined.

```

%% search for peak indices
a1=diff(ecg_p1); %FLEXcon, derivative of square waveform
a2=diff(ecg_p2); %AgCl, derivative of square waveform

upindex1=find(a1==1); %find rising edges on square wave, FLEXcon
upindex2=find(a2==1); %find rising edges on square wave, AgCl

downindex1=find(a1==-1); %find falling edges on square wave, FLEXcon
downindex2=find(a2==-1); %find falling edges on square wave, FLEXcon

```

### Stage 3

To find the exact locations of the peaks, the maximum value between successive rising and falling edges were selected in a loop. The instantaneous time where the peak occurs was also stored in order to derive the subject's instantaneous heart rate, which was a crucial component in the data analysis. The code to perform this for both channels has been provided as follows.

Figures 43. & 44. demonstrates that the algorithm successfully picks out the QRS complex peaks for both channels.

```

%% peak detection, FLEXcon
prev_peak1=0;
for i=1:min(length(upindex1),length(downindex1))
    [amp1,indtemp1]=max(ecg_hp1(upindex1(i):downindex1(i)));
    indmax1(i)=indtemp1+upindex1(i)-1;
    rpeak1(i)=t(indmax1(i));
    bpm1(i)=60./(rpeak1(i)-prev_peak1);
    prev_peak1=rpeak1(i);
end

%% peak detection, AgCl
prev_peak2=0;
for i=1:min(length(upindex2),length(downindex2))
    [amp2,indtemp2]=max(ecg_hp2(upindex2(i):downindex2(i)));
    indmax2(i)=indtemp2+upindex2(i)-1;
    rpeak2(i)=t(indmax2(i));
    bpm2(i)=60./(rpeak2(i)-prev_peak2);
    prev_peak2=rpeak2(i);
end

```



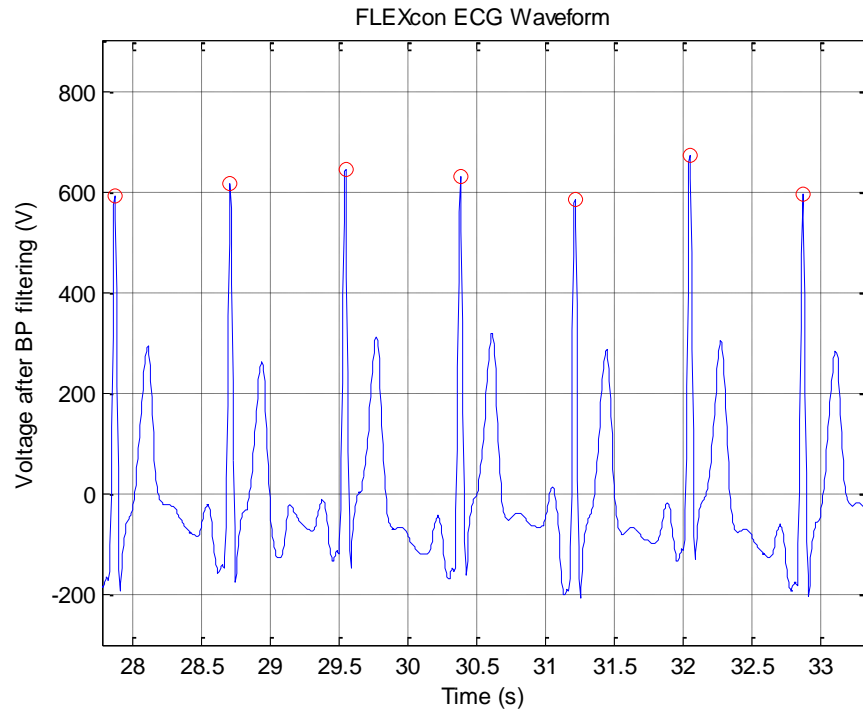


Fig. 43. Peak locations for FLEXcon electrodes superposed onto the bandpass filtered ECG

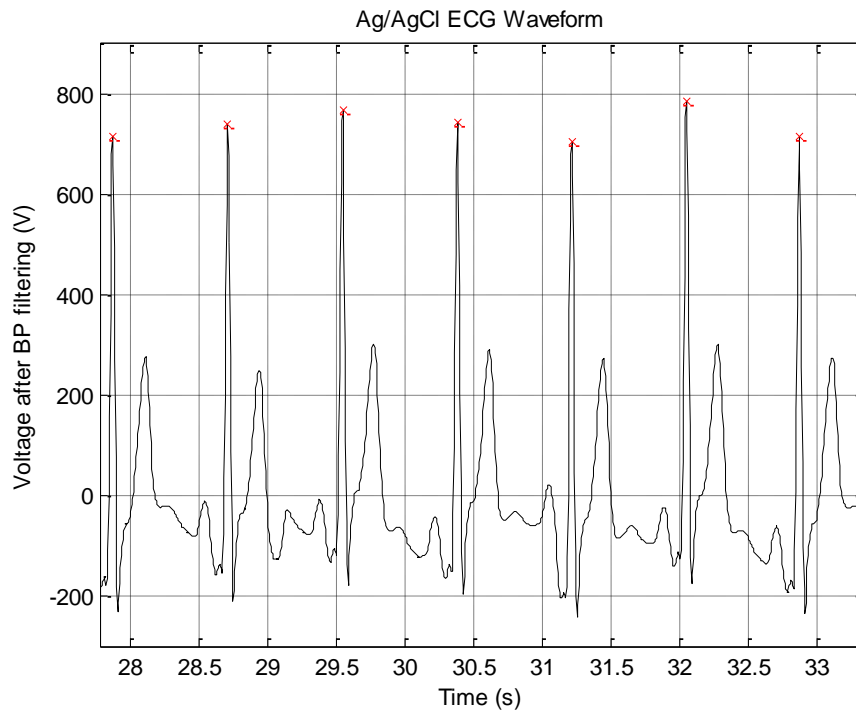


Fig. 44. Peak locations for silver/silver chloride electrodes superposed onto the bandpass filtered ECG

### FLEXcon and Ag/AgCl Comparison Metrics

To compare the FLEXcon electrodes to the Ag/AgCl electrodes, ECG waveforms from ten subjects were segmented into data sets that had no noticeable movement artifacts. The movement artifacts were found during the heart rate time interval series in where the magnitude of this data set would jump from roughly  $10^1$  to  $10^4$ . Considering that a living person with a heart rate over 10000 is impossible, these segments were discarded. After peak detection, each peak index corresponds to the same time index on a heart rate time interval series. The HR time series is computed first by taking the current peak index, and the previous peak index. These indices are in time, and taking 60 divided by the difference between these time indices gives the instantaneous heart rate in beats per minute. Plotting the magnitude of the heart rate versus time gives the representative heart rate time interval plot, shown in Fig. 45. for a 14 second period. In blue is the FLEXcon interpolated heart rate, and in red is the Ag/AgCl interpolated heart rate.

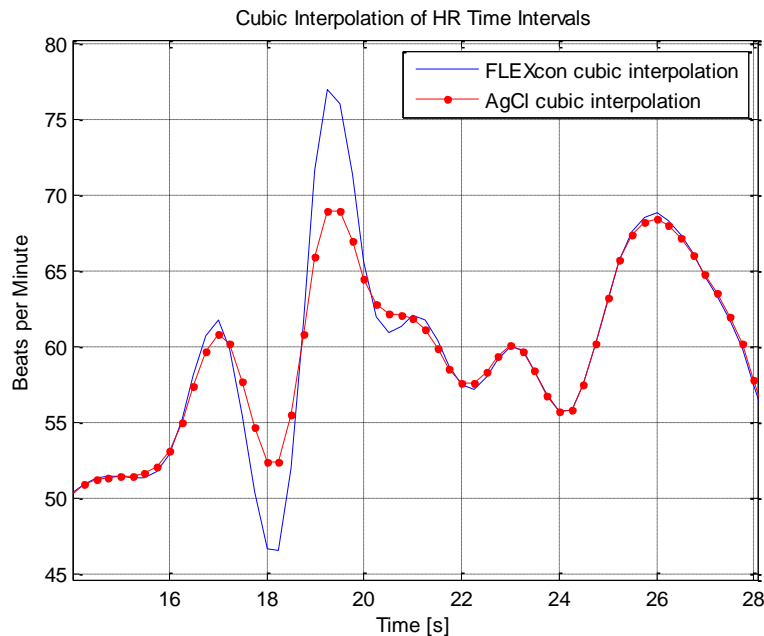


Fig. 45. Representative heart rate time interval series

Several statistical computations result from the heart rate time interval series. These metrics include the mean and standard deviation of the heart rate for each individual waveform. For all ten subjects there are group mean and standard deviations of the individual mean heart rates and individual standard deviations of heart rates. The root mean square of successive differences (RMSSD) allows the variation in heart rate for all individuals to be found, and the correlation coefficient between the FLEXcon and Ag/AgCl waveforms can be derived from the RMSSD calculations. The last analysis is of the frequency content in each heart rate interval time series. This is accomplished by using a normalized, and windowed, Fourier transform. The specific method is the Welch power spectral density algorithm. From this frequency function, the sympathetic versus parasympathetic power within the heart rate time interval series can be calculated using a composite trapezoidal integration algorithm. Figure 46. depicts the power spectral density for the same heart rate time interval series shown in Fig. 45. This plot has a normal frequency domain and a logarithmic power of the frequency content in the signal.

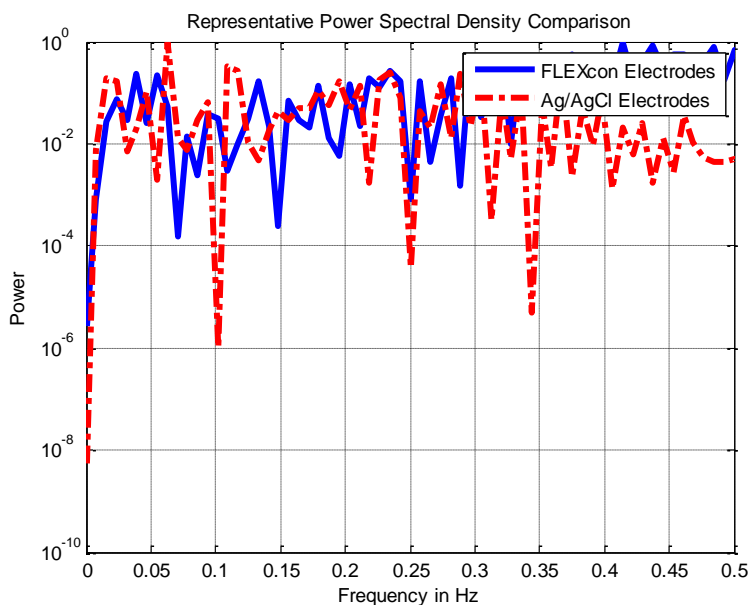


Fig. 46. Representation of the Welch power spectral density

Table 10 lists the mean heart rate, standard deviation of the heart rate, the low frequency versus high frequency mean ratio, and the low frequency versus high frequency standard deviation for each Ag/AgCl, small, medium, and large FLEXcon electrode.

Table 10 Mean and Standard Deviation of Heart Rate Interval Time Series

	Small 3.5 cm x 2.5 cm		Medium 4 cm x 3 cm		Large 5 cm x 4 cm	
	AgCl	Flexcon	AgCl	Flexcon	AgCl	Flexcon
<b>Mean Heart Rate (BPM)</b>	75.3	74.9	77.6	74.0	73.9	73.9
<b>Standard Deviation of Heart Rate (BPM)</b>	12.3	13.2	20.8	14.8	9.77	9.60
<b>Mean LF/HF Ratio</b>	5.06	6.61	8.96	8.73	16.3	16.5
<b>Standard Deviation of LF/HF Ratio</b>	6.55	9.14	16.7	17.4	26.4	27.4

Each data set corresponds to a three channel set up where one channel is the cumulative signal from Ag/AgCl and FLEXcon electrodes, the second channel is the Ag/AgCl electrode information, and the third channel is the FLEXcon electrode information. These three data sets were simultaneously collected from each subject, and each subject had three separate trials for each size of FLEXcon electrodes. Nine data sets were collected from each individual, with 90 total data sets. Sixty data sets, corresponding to the individual Ag/AgCl and FLEXcon electrode waveforms were analyzed, and the cumulative signal was ignored. The data was gathered over a six minute period, where the first three minutes are at rest and the second three minutes are with movement artifacts. Due to artifacts in the first three minutes, several segments were discarded. The total potential time of analysis is 180 minutes. Due to the segmentation of data, the total ECG time analyzed is 3991 seconds or 66.52 minutes. In total, only 37% of data was analyzed.

The RMSSD values have ten points per electrode size, giving three regression plots correlating the FLEXcon and Ag/AgCl RMSSD values between the two electrode types. Figure 47. depicts the RMSSD trend for the small FLEXcon electrode versus Ag/AgCl, Fig. 48. depicts

the RMSSD trend for the medium FLEXcon electrode versus Ag/AgCl, and Fig. 49. depicts the RMSSD trend for the large FLEXcon electrode versus Ag/AgCl.

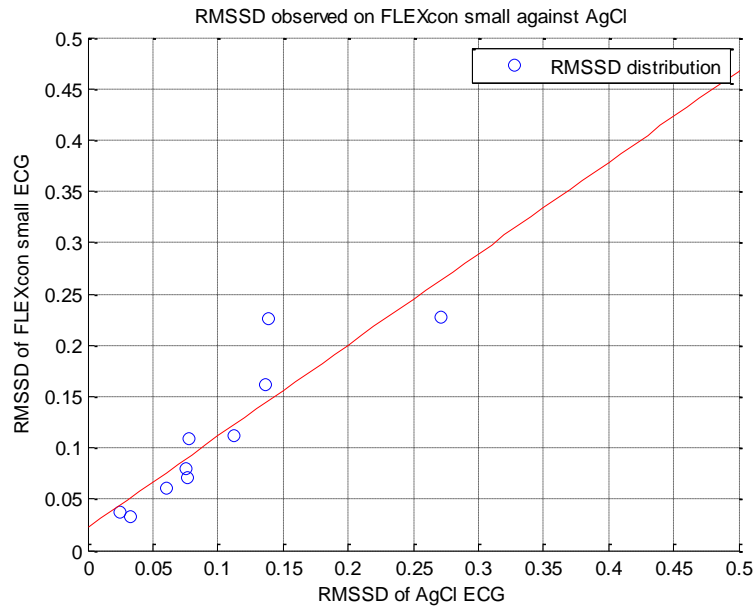


Fig. 47. RMSSD regression for small FLEXcon electrode and Ag/AgCl

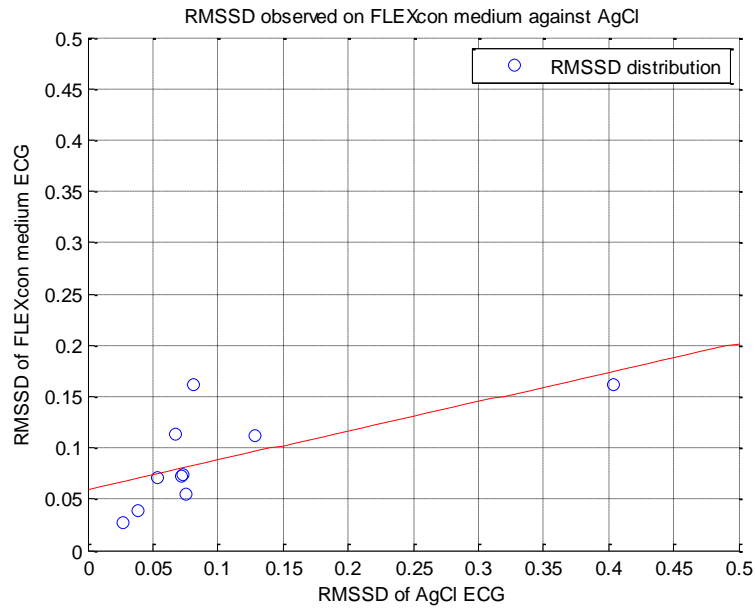


Fig. 48. RMSSD regression for medium FLEXcon electrode and Ag/AgCl

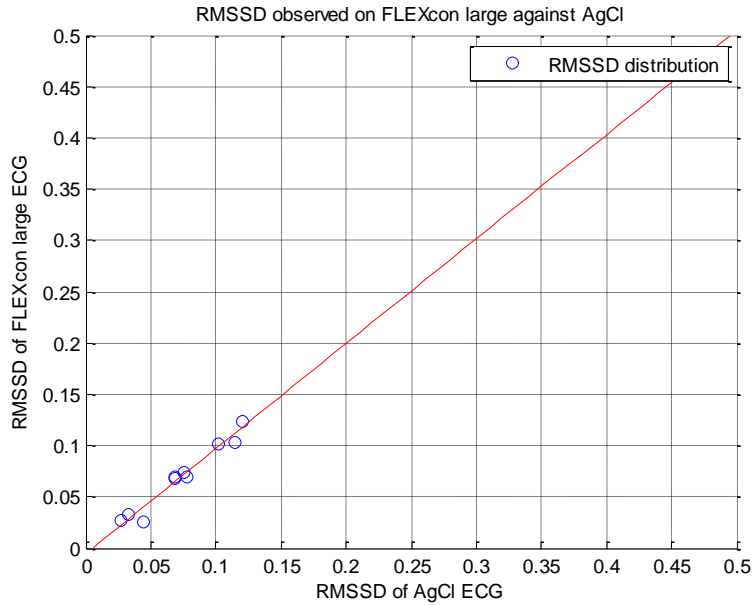


Figure 49. RMSSD regression for large FLEXcon electrode and Ag/AgCl

The correlation coefficient ( $R$ ) is a result from calculation of the similarities between the RMSSD values of each electrode group. These correlation coefficients are essentially computing how close the data points in the previous three figures deviate from the line of regression, with a range of values between zero and one - where one is an exact correlation. For the small FLEXcon electrode versus the Ag/AgCl electrode, the  $R$  value is 0.8887. For the medium FLEXcon electrode versus the Ag/AgCl electrode, the  $R$  value is 0.6583. For the large FLEXcon electrode versus the Ag/AgCl electrode, the  $R$  value is 0.9788. From these results, the large FLEXcon electrode is most significantly comparable to the industry standard Ag/AgCl hydrogel electrode.

## 6. Conclusion

FLEXcon's novel ECG electrodes were validated through this project. The dry electrodes are comparable to the industry gold standard Ag/AgCl electrodes. The optimal mixture to fabricate electrodes was determined to be 10% carbon combined with 90% PSA. This resulted in the lowest post-activation impedance. FLEXcon's electrodes are cost effective because they can be produced at a significantly cheaper cost than Ag/AgCl electrodes since carbon is cheaper than silver. These dry electrodes need to be activated prior to use in order to reduce the impedance. The team found the optimal activation parameters to be 200V, 100mA current and a 100ms discharge time. Further verification included testing the electrodes on human subjects using holter monitors, and comparing their performance to standard Ag/AgCl electrodes. Statistical analysis on the data collected proves that there is no statistical significant difference in signal quality between FLEXcon electrodes and Ag/AgCl electrodes. FLEXcon's electrodes address two of Ag/AgCl electrode's issues: dehydration and cost. They are cheaper, and are not dehydrated because they are dry electrodes. While addressing these problems, FLEXcon's novel electrodes produce ECG signal quality comparable to that of Ag/AgCl electrodes.

In the future, further comparisons can be made between FLEXcon's electrodes and Ag/AgCl electrodes. The electrodes should be tested on human subjects submerged in water to see if this affects the signal quality. A similar condition to be tested is perspiration. The electrodes could be applied to the skin while the subject is sweating, which will determine if perspiration causes any changes in signal quality.

### References

(n.d.). Retrieved from [http://www.hobbyprojects.com/general\\_theory/images/filter3.gif](http://www.hobbyprojects.com/general_theory/images/filter3.gif)

*Brief history of electrocardiography*. (2009, May 11). Retrieved September 3, 2012, from [www.ecglibrary.com](http://www.ecglibrary.com): <http://www.ecglibrary.com/ecghist.html>

3M. (2009). *Proper Skin Prep Helps Ensure ECG Trace Quality*. Retrieved September 3, 2012, from [3M.com/healthcare](http://3M.com/healthcare):



- [http://multimedia.3m.com/mws/mediawebserver?mwsId=SSSSSufSevTsZxtUm8\\_em8mvevUqe vTSevTSevTSeSSSSSS--&fn=70-2009-3356-5.pdf](http://multimedia.3m.com/mws/mediawebserver?mwsId=SSSSSufSevTsZxtUm8_em8mvevUqe vTSevTSevTSeSSSSSS--&fn=70-2009-3356-5.pdf)
- Ahn, N. T. (2007). *Frontier Orbitals*. Hoboken: John Wiley & Sons.
- Alcock, N. (2007, July 18). *Atomic Radii*. Retrieved September 4, 2012, from George Washington University: [http://home.gwu.edu/~xqiu/links\\_info/science/atom\\_radii.htm](http://home.gwu.edu/~xqiu/links_info/science/atom_radii.htm)
- Aston, R. (1990). *Principles of Biomedical Instrumentation and Measurement*. Merrill Publishing Company. .
- AUS-e-TUTE. (n.d.). *Chemistry Tutorial: Solubility Rules*. Retrieved September 4, 2012, from <http://www.usetute.com.au/solrules.html>
- Ball, C. W. (Mar 2010.). The electrocardiogram. . *Anesthesia and Intensive Care.*, 38(2): 231.
- Barany, S. (2009). Electrophoresis in strong electric fields. *Advances in Colloid and Interface Science*, 36-43.
- Berger, C. (2001). *Electrophoresis*. Retrieved September 3, 2012, from BioPharm: <http://ezproxy.wpi.edu/login?url=http://search.proquest.com/docview/195756687?accountid=29120>
- Britannica, E. (2012, September 4). *Carbon Black*. Retrieved September 4, 2012, from Encyclopaedia Britannica: <http://www.britannica.com/ezproxy.wpi.edu/EBchecked/topic/94868/carbon-black>
- Buendia, R. S.-P. (2010). A Novel Approach for Removing the Hook Effect Artefact from Electrical Bioimpedance Spectroscopy Measurements. *Journal of Physics: Conference Series 224*.
- Einthoven, W. (1893). Nieuwe methoden voor klinisch onderzoek [New methods for clinical investigation]. *Ned T Geneesk 29 II*, 263-286.
- Filter image*. (n.d.). Retrieved from [http://www.hobbyprojects.com/general\\_theory/images/filter3.gif](http://www.hobbyprojects.com/general_theory/images/filter3.gif)
- FLEXcon*. (n.d.). Retrieved September 3, 2012, from FLEXcon: <http://www.flexcon.com/Products-Solutions/Brands/Products/Item.aspx?id=154&BrandID=164>
- Gruetzmann, A. (2007). Novel dry electrodes for ECG monitoring. *Physiological Measurement*, 1375-1390.
- Hurst, J. W. (1998). Naming of the Waves in the ECG. *Circulation*, 1937-1942.
- Jenkins, D. (2009.). *History of the electrocardiogram*. Retrieved September 3, 2012, from ECG Timeline: [www.ecglibrary.com/ecghist.html](http://www.ecglibrary.com/ecghist.html)
- Johansson, L. (1966). Spectrum and Term System fo neutral Carbon Atom. *Ark. Fys.*, 201.
- Jung, H. M. (2012). CNT/PDMS Composite Flexible Dry Electrodes for Long-Term ECG Monitoring. *IEEE Transactions on Biomedical Engineering*, 59(5): 1472-1479.

- Kilpatrick, D. J. (1994). Origin of the Electrocardiogram. *IEEE Engineering in Medicine and Biology*, 479-486.
- Klabunde, R. E. (2007, April 6). *Electrocardiogram*. Retrieved October 9, 2012, from Cardiovascular Physiology Concepts: <http://www.cvphysiology.com/Arrhythmias/A009.htm>
- Krane, K. S. (1988). *Introductory Nuclear Physics*. New Jersey: John Wiley & Sons.
- Lerner, K. L. (2008). Electrophoresis. In K. L. Lerner, *The Gale Encyclopedia of Science* (pp. 1519-1521). Detroit: Gale.
- Luo, S. J. (2010.). A review of electrocardiogram filtering. *Journal of Electrocardiology*, 6(43): 486-496.
- Normal Vectors*. (n.d.). Retrieved from <https://lh3.googleusercontent.com/-p-igMwnR-3E/TWwxcYOBJQI/AAAAAAAAABu8/S-Kmrc1dLQM/normal-vectors.jpg>
- Pan, J. T. (1985, March). A Real-Time QRS Detection Algorithm. *IEEE Transactions on Biomedical Engineering*, Vol. BME-32, p. 1985.
- Philips. (2008, September). *Improving ECG Quality*. Retrieved September 3, 2012, from [http://incenter.medical.philips.com/doclib/enc/fetch/2000/4504/577242/577243/577245/577817/577869/Improving\\_ECG\\_Quality\\_Application\\_Note\\_%28ENG%29.pdf%3fnodeid%3d1557273%26vernum%3d3](http://incenter.medical.philips.com/doclib/enc/fetch/2000/4504/577242/577243/577245/577817/577869/Improving_ECG_Quality_Application_Note_%28ENG%29.pdf%3fnodeid%3d1557273%26vernum%3d3)
- Putz, M. V. (2011). *Carbon Bonding and Structures*. New York: Springer.
- Roberge, P. R. (2012). *Silver/Silver Chloride Reference Electrode*. Retrieved September 4, 2012, from Corrosion Doctors: <http://www.corrosion-doctors.org/Corrosion-Thermodynamics/Reference-Half-Cells-Silver.htm>
- Shifeng Huang, X. L. (2009). Effect of carbon black on properties of 0-3 piezoelectric ceramics/cement composites. *Current Applied Physics*, 9(6): 1191-1194.
- Sief Otten, M. L. (1998). *Patent No. 5833825*. USA.
- Townsend, N. (2001). *C3B Medical Electronics*. Retrieved September 4, 2012, from Robotics Research Group: [http://www.robots.ox.ac.uk/~neil/teaching/lectures/med\\_elec/notes2.pdf](http://www.robots.ox.ac.uk/~neil/teaching/lectures/med_elec/notes2.pdf)
- Webster, J. G. (1998). *The Measurement, Instrumentation and Sensors Handbook*. CRC Press.

## Appendix A

### THINflex® PP 075 H CLEAR A-208 TRACrite™ 100 Technical Data

Features & Benefits	Technical Data	Product Data Sheets	Pricing
<b>TECHNICAL DATA</b>			
<b>PRODUCT DATA</b>	<b>VALUE</b>	<b>DATA</b>	
<b>Physical Properties</b>			
Thickness (Mils[microns])		ASTM D 3652 (Modified for use with non-tape products)	
	Film 0.7 (18) +/- 10%		
	Adhesive 0.5-0.6 (13-15) +/- 0.1 (3)		
	Liner 1.0 (25) +/- 10%		
Dimensional Stability (%)		Applied Shrinkage: 24 hour dwell time on aluminum panel then 24 hours at 160°F (71°C)	
	No Shrinkage Observed		
<b>Adhesion Properties</b>			
Ultimate Peel from		ASTM D 903 (Modified for 72 hour dwell time)	
	Average		
	Oz/In (N/m)		
ABS	19 (209)		
Acrylic	27 (287)		
Corona Treated HDPE	14 (154)		
Glass	22 (242)		
HDPE	7 (77)		
Polycarbonate	26 (286)		
Polyester	19 (209)		
Polypropylene	7 (77)		
PVC	28 (308)		
Stainless Steel	24 (264)		
Styrene	20 (220)		
<b>Expected Shear</b>		ASTM D 3654 Method A a. 1 hr. dwell b. 1 sq. in. surface c. 4 lb. load	
Room Temp (hours)	75		
<b>Tack (gm/sq cm)</b>	200	ASTM D 2979	
<b>Expected Exterior Life</b>	Indoor use only		
<b>Service Temperature Range</b>	-40°F to 176°F (-40°C to 80°C)		
<b>Minimum Application Temperature</b>	50°F (10°C)		
<b>Storage Stability</b>	Two years when stored at 70°F (21°C) and 50% relative humidity		

Fig. 50. THINflex® PP 075 H CLEAR A-208 TRACrite™ 100 Table

## Appendix B


### Precision LC Meter 7600 Plus®, IET Labs Inc.™ Performance Sheet

Precision LCR Meter

7600 Plus Meter

Page 1 of 3

The 7600 Plus LCR meter performs precision impedance measurement over a frequency range of 10 Hz to 2 MHz. This instrument can measure 14 different impedance parameters with 0.05% accuracy, meeting today's requirements for component and material testing. User-friendly menu-driven programming makes the 7600 Plus ideal for applications in product development, incoming inspections, and production-line testing.



7600 Plus Precision LCR Meter

**Features:**

- Frequency range: 10 Hz to 2 MHz
- 0.05% basic measurement accuracy
- 7-digit measurement resolution
- Programmable test voltage and current
- Auto ranging
- Test setup and measurement data storage
- Four bnc terminal Kelvin connection
- Standard interfaces: USB host port, RS-232, Handler, Parallel printer port
- Optional interface: IEEE-488.2
- Graphical and tabular display of measurements: swept frequency, voltage, and current
- Sequence testing of up to 6 individual tests
- Load correction
- Binning (15)
- Built-in auto-calibration routine

**14 Different Impedance Parameters**  
Measure and display any two parameters simultaneously to achieve coverage and flexibility.

**Automated Test Sequencing**  
Run up to six different tests in sequence with a single push of the start button. Each test can have different conditions and limits.


**Swept Measurements**  
To test how components respond to changes in ac test frequency, voltage, or current, the 7600 Plus meter offers fast, accurate swept parameter measurements with results in graphical and tabular format. No complex programming or external control is required.

**Program and Data Storage**  
Test setups can be stored and recalled from either internal memory or from a standard USB flash drive. Measurement data can be stored on a USB flash drive in CSV format.


**Load Correction**  
Substantially improves instrument accuracy by measuring a known standard and applying correction to subsequent measurements. This is ideal for repetitive testing of identical devices under similar conditions.

**Automated Calibration Procedure**  
The 7600 Plus has a built-in calibration procedure, which can be performed using the SI traceable calibration kit (7000-09). The results and the date of the calibration are stored internally.

**Ease of Use**  
To ensure that the 7600 Plus is easy to operate, the unit offers a large LCD display and a user-friendly, menu-driven interface.



7600 Plus Rear Connectors



**IET LABS, INC.** in the **GenRad** Tradition  
534 Main Street, Westbury, NY 11590

www.letlabs.com  
TEL: (516) 334-5959 • (800) 899-8438 • FAX: (516) 334-5988  
7600 Plus DataSheet05-10-2012

Fig. 51. Precision LCR Meter 7600 Plus by IET Labs, Inc.

Appendix C

LCR measurement, DCR measurement, and Sweep measurement  
**Continuous Measurement and High-speed Testing Achieved with One Instrument**

**IMPEDANCE ANALYZER IM3570**



Measurements recommended with IMPEDANCE ANALYZER IM3570  
 1. Testing the resonance characteristics of piezoelectric elements

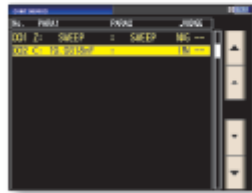


Frequency sweep measurement Z peak comparator screen  
 LCR mode Cs display screen (1 kHz measurement)

*Reduce Equipment Costs with Just 1 Device!*

Frequency sweep measurement can be used to measure the resonance frequency and its impedance, and then the peak comparator function can be used to make a pass/fail judgment on the resonance state.

In LCR mode, you can test capacitance by performing C measurement between 1 kHz and 120 Hz.



Continuous measurement screen



*High Speed and High Accuracy*

Frequency sweep measurement (impedance analyzer) and C measurement can be performed continuously with one instrument.

**Advantage #1 -- Measurement time shortened**

The measurement time has been shortened from previous models, achieving maximum speeds of 1.5ms\* (1 kHz) and 0.5ms\* (100kHz) in LCR mode. This is a significant increase in speed compared with previous Hioki products (3522-50 and 3532-50 with basic speed of 5ms). Faster speed contributes to an increase in test quantities. Furthermore, sweep measurement, which requires multiple points to be measured, realizes the quick speed of 0.3ms per point.

\* When the display is off (time increases by 0.3 ms when the display is on).

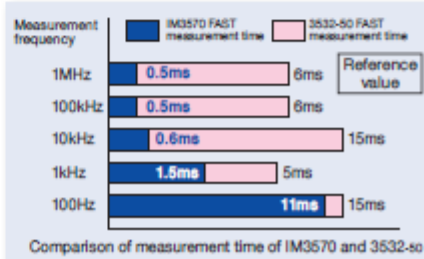


Fig. 52. Hioki IM 3570 Impedance Analyzer Data Sheet

## Appendix D

### MATLAB Statistical Analysis

The statistical results are generated by the following code listing in MATLAB2012A:

```
%MATLAB DATA ANALYSIS%
%%Function to calculate Gaussian Distribution%%

function f= Gaussian(x, mu, sigma)

exponent= -0.5*((x-mu)/sigma).^2;
denom= sigma*sqrt(2*pi);

f= exp(exponent)./denom;

%% OUTLIER REMOVAL
%%
%%Reading the data, calculation of total sum
pre_8= xlsread('Test_Results_8_10_12.xlsx', 1, 'C2:C31');
pre_10= xlsread('Test_Results_8_10_12.xlsx', 1, 'E2:E31');
pre_12= xlsread('Test_Results_8_10_12.xlsx', 1, 'G2:G31');
post_8= xlsread('Test_Results_8_10_12.xlsx', 1, 'D2:D31');
post_10= xlsread('Test_Results_8_10_12.xlsx', 1, 'F2:F31');
post_12= xlsread('Test_Results_8_10_12.xlsx', 1, 'H2:H31');

%% Find first and third quartiles, and Interquartile range

pre8_Q1= median(pre_8(find(pre_8<median(pre_8))));
pre8_Q3= median(pre_8(find(pre_8>median(pre_8))));
IQR_pre8= pre8_Q3 - pre8_Q1;

post8_Q1= median(post_8(find(post_8<median(post_8))));
post8_Q3= median(post_8(find(post_8>median(post_8))));
IQR_post8= post8_Q3 - post8_Q1;

pre10_Q1= median(pre_10(find(pre_10<median(pre_10))));
pre10_Q3= median(pre_10(find(pre_10>median(pre_10))));
IQR_pre10= pre10_Q3 - pre10_Q1;

post10_Q1= median(post_10(find(post_10<median(post_10))));
post10_Q3= median(post_10(find(post_10>median(post_10))));
IQR_post10= post10_Q3 - post10_Q1;

pre12_Q1= median(pre_12(find(pre_12<median(pre_12))));
pre12_Q3= median(pre_12(find(pre_12>median(pre_12))));
IQR_pre12= pre12_Q3 - pre12_Q1;

post12_Q1= median(post_12(find(post_12<median(post_12))));
post12_Q3= median(post_12(find(post_12>median(post_12))));
IQR_post12= post12_Q3 - post12_Q1;

%once we have the interquartile ranges, we need to multiply by 1.5 and
%subtract that from the lower quartile and add it to the upper quartile.
%Any data point outside this will be an outlier

%% OUTLIER REMOVAL FROM THE DATA

m=1.5;

%Pre 8
pre8_upper= IQR_pre8*(m)+pre8_Q3;
pre8_lower= pre8_Q1- IQR_pre8*(m);

count=30;

for i=1:27
```

```

    if pre_8(i)>pre8_upper
        pre_8(i)= [];
        count= count-1;
    elseif pre_8(i)<pre8_lower
        pre_8(i)= [];
        count= count-1;
    end
end

%Post 8
post8_upper= IQR_post8*(m)+ post8_Q3;
post8_lower= post8_Q1- IQR_post8*(m);

count=30;

for j=1:27

    if post_8(j)>post8_upper
        post_8(j)= [];
        count= count-1;
    elseif post_8(j)<post8_lower
        post_8(j)= [];
        count= count-1;
    end
end

%Pre 10
pre10_upper= IQR_pre10*(m)+pre10_Q3;
pre10_lower= pre10_Q1- IQR_pre10*(m);

count=30;

for k=1:27

    if pre_10(k)>pre10_upper
        pre_10(k)= [];
        count= count-1;
    elseif pre_10(k)<pre10_lower
        pre_10(k)= [];
        count= count-1;
    end
end

%Post 10
post10_upper= IQR_post10*(m)+ post10_Q3;
post10_lower= post10_Q1- IQR_post10*(m);

count=30;

for l=1:28

    if post_10(l)>post10_upper
        post_10(l)= [];
        count= count-1;
    elseif post_10(l)<post10_lower
        post_10(l)= [];
        count= count-1;
    end
end

%Pre 12
pre12_upper= IQR_pre12*(m)+pre12_Q3;
pre12_lower= pre12_Q1- IQR_pre12*(m);

count=30;

for k=1:count

    if pre_12(k)>pre12_upper
        pre_12(k)= [];
        count= count-1;
    end
end

```

```

elseif pre_12(k)<pre12_lower
    pre_12(k)= [];
    count= count-1;
end
end

end

%Post 12
post12_upper= IQR_post12*(m)+ post12_Q3;
post12_lower= post12_Q1- IQR_post12*(m);

count=30;

for l=1:28

    if post_12(l)>post12_upper
        post_12(l)= [];
        count= count-1;
    elseif post_12(l)<post12_lower
        post_12(l)= [];
        count= count-1;
    end
end

end

%% Calculate new averages, stdev and gaussian without outliers

%Pre 8
avg_8pre= mean(pre_8);
stdev_8pre= std(pre_8);
pre_8gauss = Gaussian(pre_8, avg_8pre, stdev_8pre);
figure(1);
subplot(2,1,1);
plot(pre_8, pre_8gauss, '.');
grid on;
title('Gaussian distribution for pre activation impedance, 8%');
xlabel('impedance/Mega Ohms');
ylabel('Gaussian distribution');

%post 8
avg_8post= mean(post_8);
stdev_8post= std(post_8);
post_8gauss = Gaussian(post_8, avg_8post, stdev_8post);
subplot(2,1,2);
plot(post_8, post_8gauss, '.');
grid on;
title('Gaussian distribution for post activation impedance, 8%');
xlabel('impedance/Ohms');
ylabel('Gaussian distribution');

%Pre 10
avg_10pre= mean(pre_10);
stdev_10pre= std(pre_10);
pre_10gauss = Gaussian(pre_10, avg_10pre, stdev_10pre);
figure(2)
subplot(2,1,1);
plot(pre_10, pre_10gauss, '.');
grid on;
title('Gaussian distribution for pre activation impedance, 10%');
xlabel('impedance/Mega Ohms');
ylabel('Gaussian distribution');

%post 10
avg_10post= mean(post_10);
stdev_10post= std(post_10);
post_10gauss = Gaussian(post_10, avg_10post, stdev_10post);
subplot(2,1,2);
plot(post_10, post_10gauss, '.');
grid on;
title('Gaussian distribution for post activation impedance, 10%');
xlabel('impedance/Ohms');
ylabel('Gaussian distribution');

```



```

%Pre 12
avg_12pre= mean(pre_12);
stdev_12pre= std(pre_12);
pre_12gauss = Gaussian(pre_12, avg_12pre, stdev_12pre);
figure(3)
subplot(2,1,1);
plot(pre_12, pre_12gauss, '.');
grid on;
title('Gaussian distribution for pre activation impedance, 12%');
xlabel('impedance/Mega Ohms');
ylabel('Gaussian distribution');

%post 12
avg_12post= mean(post_12);
stdev_12post= std(post_12);
post_12gauss = Gaussian(post_12, avg_12post, stdev_12post);
subplot(2,1,2);
plot(post_12, post_12gauss, '.');
grid on;
title('Gaussian distribution for post activation impedance, 12%');
xlabel('impedance/Ohms');
ylabel('Gaussian distribution');

%% T Tests for distributions without outliers

%Unpaired t tests

%8%
alpha=0.01;      % 95% significance level

[h_8pre,p_8pre]= ttest(pre_8, alpha);
[h_8post,p_8post]= ttest(post_8, alpha);

%10%
[h_10pre,p_10pre]= ttest(pre_10, alpha);
[h_10post,p_10post]= ttest(post_10, alpha);

%12%
[h_12pre,p_12pre]= ttest(pre_12, alpha);
[h_12post,p_12post]= ttest(post_12, alpha);

%paired t tests to pick between 8%, 10% and 12%
[h_10and12post, p_10and12post] = ttest2(post_10, post_12);
[h_10and8post, p_10and8post] = ttest2(post_10, post_8);
[h_12and8post, p_12and8post] = ttest2(post_12, post_8);

[h_10and12pre, p_10and12pre] = ttest2(pre_10, pre_12);
[h_10and8pre, p_10and8pre] = ttest2(pre_10, pre_8);
[h_12and8pre, p_12and8pre] = ttest2(pre_12, pre_8);

%we get an h value of 1 in the above lines, rejecting the null hypothesis
%that the two vectors have equal means. Since the sample average was the
%lowest for 10% and in theory it should stick to the patient skin better
%with 10%,we can select 10% as our preferred carbon level.

```

## MATLAB Mean Impedance vs. Power Plots

```

clc; clear all; close all;
data=xlsread('data.xlsx');

%.1uf
voltage=[200 120 75 45 20 5];
current=[1e-3 2e-3 5e-3 10e-3 20e-3 50e-3 100e-3];

figure(1)
grid on
hold on
xlabel('Power')
ylabel('Impedance')

```

```

title('0.1uF Activation Impedance')
n=1;
for j=1:1:7
    for i=1:1:6
        power(i,j)=voltage(i)*current(j);
        plot(power(i,j),data(n,3),'o');
        n=n+1;
    end
end

figure(2)
grid on
hold on
xlabel('Power')
ylabel('Impedance')
title('1.0uF Activation Impedance')
for j=1:1:7
    for i=1:1:6
        power(i,j)=voltage(i)*current(j);
        plot(power(i,j),data(n,3),'o');
        n=n+1;
    end
end

figure(3)
grid on
hold on
xlabel('Power')
ylabel('Impedance')
title('10.0uF Activation Impedance')
for j=1:1:6
    if i==6
        for i=1:1:3
            power(i,j)=voltage(i)*current(j);
            plot(power(i,j),data(n,3),'o');
            n=n+1;
        end
    else
        for i=1:1:6
            power(i,j)=voltage(i)*current(j);
            plot(power(i,j),data(n,3),'o');
            n=n+1;
        end
    end
end
end

```

## MATLAB ECG and FFT Waveform Plots

```

clc; clear all; close all;

agcl_rest=xlsread('agcl_electrode_rest.xls');
agcl_rest_fft=abs(fft(agcl_rest(:,2)));
agcl_rest_fft=agcl_rest_fft./max(max(agcl_rest_fft));

agcl_mov=xlsread('agcl_electrode_movement.xls');
agcl_mov_fft=abs(fft(agcl_mov(:,2)));
agcl_mov_fft=agcl_mov_fft./max(max(agcl_mov_fft));

small_rest=xlsread('carbon_electrode_small_rest.xls');
small_rest_fft=abs(fft(small_rest(:,2)));
small_rest_fft=small_rest_fft./max(max(small_rest_fft));

small_mov=xlsread('carbon_electrode_small_movement.xls');
small_mov_fft=abs(fft(small_mov(:,2)));
small_mov_fft=small_mov_fft./max(max(small_mov_fft));

medium_rest=xlsread('carbon_electrode_medium_rest.xls');
medium_rest_fft=abs(fft(medium_rest(:,2)));
medium_rest_fft=medium_rest_fft./max(max(medium_rest_fft));

```

```

medium_mov=xlsread('carbon_electrode_medium_movement.xls');
medium_mov_fft=abs(fft(medium_mov(:,2)));
medium_mov_fft=medium_mov_fft./max(max(medium_mov_fft));

large_rest=xlsread('carbon_electrode_large_rest.xls');
large_rest_fft=abs(fft(large_rest(:,2)));
large_rest_fft=large_rest_fft./max(max(large_rest_fft));

large_mov=xlsread('carbon_electrode_large_movement.xls');
large_mov_fft=abs(fft(large_mov(:,2)));
large_mov_fft=large_mov_fft./max(max(large_mov_fft));

f=0:1000/(length(agcl_rest_fft)-1):1000;

figure(1)
plot(large_mov(:,1),large_mov(:,2))
title('Movement ECG Waveform of Large FLEXcon Electrodes')
xlabel('Time [s]')
ylabel('Voltage [V]')
grid on

figure(2)
plot(f,large_mov_fft)
title('Fast Fourier Transform of Large FLEXcon Movement ECG Waveform')
xlabel('Frequency [Hz]')
ylabel('Normalized Magnitude')
axis([0 100 0 1])
grid on

```

## MATLAB Impedance vs. Frequency Sweep Plots

```

clc; clear all; close all;

csv_names={'130219105255.csv',
           '130219105447.csv',
           '130219105701.csv',
           '130219105913.csv',
           '130219110043.csv',
           '130219110222.csv',
           '130219110341.csv',
           '130219110500.csv',
           '130219110620.csv',
           '130219110744.csv'};

for i=1:length(csv_names)
    l_raw(:,i)=textread(csv_names{i},'%q');
    l_clean(:,i)=l_raw(36:434,i);
    lz_cell(:,i)=l_clean(3:4:399,i);
    lz_vec(:,i)=cellfun(@str2num,lz_cell(:,i));
end

f=l_clean(2:4:398,1);
f=cellfun(@str2num,f);

for i=1:length(lz_vec)
    m(i)=mean(lz_vec(i,1:1:2));
end

for i=1:length(lz_vec)
    eb(i)=std(lz_vec(i,1:1:length(csv_names)));
end

figure(1)
loglog(f,m,'x','LineWidth',2)
hold on
loglog(f,m,'-')

```

```

for i=1:length(lz_vec)
    errorbar(f(i),m(i),eb(i),'r')
end
xlabel('Frequency [Hz]')
ylabel('Impedance [Z]')
title('Impedance vs. Frequency of Large Electrodes, with Standard Error')
grid on
axis([min(f)*.90 max(f)*1.10 (min(eb)+min(m))*0.95 (max(eb)+max(m))*1.05]);

figure(2)
plot(f,m,'x','LineWidth',2)
hold on
plot(f,m,'-')

for i=1:length(lz_vec)
    errorbar(f(i),m(i),eb(i),'r')
end

xlabel('Frequency [Hz]')
ylabel('Impedance [Z]')
title('Impedance vs. Frequency of Large Electrodes, with Standard Error')
grid on
axis([min(f)*.90 max(f)*1.10 (min(eb)+min(m))*0.95 (max(eb)+max(m))*1.05]);

```

## Peak Detection Algorithm

```

clc; clear all; close all;

%% Read data
%ecg=dlmread('at_rest_1.txt');
ecg= csvread('32223.csv');
% ecg1= ecg(((15*180):(40*180)),3)./1000; %FLEXcon electrode data
% ecg2= ecg(((15*180):(40*180)),2)./1000; %silver chloride data
% ecg1 =[ecg1; (ecg((47*180):(172*180)),3)./1000];
% ecg2 =[ecg2; (ecg((47*180):(172*180)),2)./1000];
ecg1= ecg(1:32400,3)./1000; %FLEXcon electrode data
ecg2= ecg(1:32400,2)./1000; %silver chloride data
% All flexcon variables end with 1, silver with 2 %

%% Sampling frequency, time vector
Fs=180; %sampling frequency of Rozinn holter monitor
dt=1/Fs; %time increment
duration=length(ecg1)*dt; %length of data
t=0:dt:duration-dt; %time vector
t=t'; %transpose time vector for detrending

%% Detrending solution
N=180; %length for detrending solution, 1 second long
for i=1:N:length(ecg1)-N-1
    p1=polyfit(t(i:(i+N-1)),ecg1(i:(i+N-1)),1); %generate coefficients for
    polynomial for FLEXcon
    yfit1=polyval(p1,t(i:(i+N-1))); %create data set to be subtracted from raw ECG
    data, FLEXcon
    p2=polyfit(t(i:(i+N-1)),ecg2(i:(i+N-1)),1); %generate coefficients for
    polynomial for silver chloride
    yfit2=polyval(p2,t(i:(i+N-1))); %create data set to be subtracted from raw ECG
    data, silver chloride
    for j=1:N
        ecg1(i+j-1)=ecg1(i+j-1)-yfit1(j); %detrend the raw data, FLEXcon
        ecg2(i+j-1)=ecg2(i+j-1)-yfit2(j); %detrend the raw data, silver chloride
    end
end

%% Correction for DC noise level for threshold
ecg1=ecg1-mean(ecg1); %zeros the ECG essentially
ecg2=ecg2-mean(ecg2); %silver

```

```

%% Raw data
figure(1)
plot(t,ecg1);
%axis([5000/180 6000/180 -300 900])
grid on; hold on;
plot(t,ecg2, 'r-.');
axis([5000/180 6000/180 -1 3])
xlabel('Time [s]');
ylabel('Voltage [V]');
title('Raw ECG Waveform');
legend('FLEXcon','AgCl');

%% Lowpass filtering
bl=[1 0 0 0 0 0 -2 0 0 0 0 1];
al=[1 -2 1];
ecg_lp1=filter(bl,al,ecg1); % Lowpass filter FLEXcon data
ecg_lp2=filter(bl,al,ecg2); % LP filter silver data

%% Highpass filtering
bh=[-1 zeros(1,15) 32 zeros(1,15) 1];
ah=[1 1];
ecg_hp1=filter(bh,ah,ecg_lp1); %HP filter FLEXcon
ecg_hp2=filter(bh,ah,ecg_lp2); %HP filter AgCl

%% Derivative filtering, squaring
bd=(1/8)*[2 1 0 -1 -2];
ad=[1];
ecg_der1=filter(bd,ad, ecg_hp1); %derivative filter FLEXcon
ecg_der2=filter(bd,ad, ecg_hp2); %derivative filter AgCl

ecg_sq1=(ecg_der1).^2;
ecg_sq2=(ecg_der2).^2;

%% Moving average filtering
N=30; %length of MA filter
bm=(1/N)*[ones(1,N)];
am=[1];
ecg_m1=filter(bm,am,ecg_sq1); %MA filter FLEXcon
ecg_m2=filter(bm,am,ecg_sq2); %MA filter AgCl

figure(2)
plot(t,ecg_m1); %FLEXcon MA output for thresholding

figure(3)
plot(t,ecg_m2); %AgCl thresholding

%% Thresholds
%thr1=10; % FLEXcon threshold
%thr2=10; % AgCl threshold

thr1= mean(ecg_m1);
thr2= mean(ecg_m2);

ecg_p1=zeros(size(ecg_m1)); %vector to store peak approximation, ONLY CONTAINS 1s and 0s
(FLEXcon)
ecg_p2=zeros(size(ecg_m2)); %vector to store peak approximation, ONLY CONTAINS 1s and 0s
(AgCl)

ecg_p1(find(ecg_m1>=thr1))=1; %data > threshold --> 1, data < threshold --> 0
ecg_p2(find(ecg_m2>=thr2))=1;

figure(2)
plot(t,ecg_p1)
hold on; grid on;
plot(t,ecg_p2, 'r-.');
xlabel('Time [s]');
ylabel('Amplitude [filt V]');
title('Square ECG Peak Waveform');
legend('FLEXcon','AgCl');

%% search for peak indices

```

```

a1=diff(ecg_p1); %FLEXcon, derivative of square waveform
a2=diff(ecg_p2); %AgCl, derivative of square waveform

upindex1=find(a1==1); %find rising edges on square wave, FLEXcon
upindex2=find(a2==1); %find rising edges on square wave, AgCl

downindex1=find(a1==-1); %find falling edges on square wave, FLEXcon
downindex2=find(a2==-1); %find falling edges on square wave, FLEXcon

%% peak detection, FLEXcon
prev_peak1=0;
for i=1:min(length(upindex1),length(downindex1))
    [amp1,indtemp1]=max(ecg_hp1(upindex1(i):downindex1(i)));
    indmax1(i)=indtemp1+upindex1(i)-1;
    rpeak1(i)=t(indmax1(i));
    bpm1(i)=60./(rpeak1(i)-prev_peak1);
    prev_peak1=rpeak1(i);
end

%% peak detection, AgCl
prev_peak2=0;
for i=1:min(length(upindex2),length(downindex2))
    [amp2,indtemp2]=max(ecg_hp2(upindex2(i):downindex2(i)));
    indmax2(i)=indtemp2+upindex2(i)-1;
    rpeak2(i)=t(indmax2(i));
    bpm2(i)=60./(rpeak2(i)-prev_peak2);
    prev_peak2=rpeak2(i);
end

%% PD plots
figure(4)
plot(t, ecg_hp1)
hold on; grid on;
plot(rpeak1, ecg_hp1(indmax1),'or');
xlabel('Time (s)');ylabel('Voltage after BP filtering (V)');
title('FLEXcon ECG Waveform')
axis([5000/180 6000/180 -300 900])

figure(5)
plot(t, ecg_hp2,'k')
hold on; grid on;
plot(rpeak2, ecg_hp2(indmax2),'xr');
xlabel('Time (s)');ylabel('Voltage after BP filtering (V)');
title('Ag/AgCl ECG Waveform')
axis([5000/180 6000/180 -300 900])

%% R-R intervals, cubic interpolation
RR1=diff(rpeak1);
RR2=diff(rpeak2);

time_lr1=zeros(1,length(RR1));
time_lr2=zeros(1,length(RR2));

time_lr1(1)=0;
for i=2:length(RR1)
    time_lr1(i)=sum(RR1(1:i-1));
end

time_lr2(1)=0;
for i=2:length(RR2)
    time_lr2(i)=sum(RR2(1:i-1));
end

timeRR1=0:1/4:sum(RR1)-1/4;
timeRR2=0:1/4:sum(RR2)-1/4;

ys1=interp1(time_lr1,bpm1(1:length(time_lr1)),timeRR1,'spline');
ys2=interp1(time_lr2,bpm2(1:length(time_lr2)),timeRR2,'spline');

figure(6)
plot(timeRR1,ys1)

```

```

grid on; hold on;
plot(timeRR2,ys2,'r.-')
xlabel('Time [s]');
ylabel('Beats per Minute');
title('Cubic Interpolation of HR Time Intervals');
legend('FLEXcon cubic interpolation','AgCl cubic interpolation');

ys1= ys1-mean(ys1);
ys2= ys2-mean(ys2);

%% Power Spectral Density (PSD)
[psd_cubic1,f]=pwelch(ys1,length(ys1),[],512,4);
[psd_cubic2,f]=pwelch(ys2,length(ys2),[],512,4); %
%psd_linear=(abs(psd_linear)).^2;
psd_cubic1=(abs(psd_cubic1)).^2;
psd_cubic2=(abs(psd_cubic2)).^2;
%figure
%plot(f,psd_linear)
%xlim([0 0.5])
figure(7)
plot(f,psd_cubic1, 'LineWidth',3)
xlim([0 0.5])
grid on; hold on;
plot(f,psd_cubic2, 'r-','LineWidth',3)
xlabel('Frequency in Hz');
ylabel('Power');
title('Representative Power Spectral Density Comparison');
legend('FLEXcon Electrodes','Ag/AgCl Electrodes')

%% LF/HF

low_index=find(f>=0.04 & f<=0.15);
low_f=f(low_index);
low_psd_cubic1=psd_cubic1(low_index);
low_psd_cubic2=psd_cubic2(low_index);

high_index= find(f>=0.15 & f<=0.4);
high_f=f(high_index);
high_psd_cubic1=psd_cubic1(high_index);
high_psd_cubic2=psd_cubic2(high_index);

LF1= sum(low_psd_cubic1);
LF2= sum(low_psd_cubic2);

HF1= sum(high_psd_cubic1);
HF2= sum(high_psd_cubic2);

LFHF1= LF1/HF1
LFHF2= LF2/HF2

%% Mean, Standard Deviation, RMSSD, SDNN

mean_bpm1= mean(bpm1)
mean_bpm2= mean(bpm2)

std_bpm1= std(bpm1)
std_bpm2= std(bpm2)

sumSD1=0;
sumSD2=0;

for i=2:1:length(RR1)
    sumSD1= sumSD1+ ((RR1(i)-RR1(i-1))^2);
end

for i=2:1:length(RR2)
    sumSD2= sumSD2+ ((RR2(i)-RR2(i-1))^2);
end

RMSSD1= sqrt(sumSD1./(length(RR1)-1))

```

```

RMSSD2= sqrt(sumSD2./(length(RR2)-1))

SDNN1= std(RR1)
SDNN2= std(RR2)

temp=[LFHF1 mean_bpm1 std_bpm1 RMSSD1 SDNN1;
      LFHF2 mean_bpm2 std_bpm2 RMSSD2 SDNN2]

```

## RMSSD Analysis Algorithm

```

%% RMSSD DISTRIBUTION
clc; clear all; close all;
data=xlsread('electrode_comparison.xlsx');

smFL=data(1:6:60,5);
smAg=data(2:6:60,5);
rmssd_mean_smFL=mean(smFL);
rmssd_mean_smAg=mean(smAg);

figure(1)
scatter(smAg, smFL);
xlabel('RMSSD of AgCl ECG');
ylabel('RMSSD of FLEXcon small ECG');
title('RMSSD observed on FLEXcon small against AgCl');
grid on;
legend('RMSSD distribution');
axis([0 0.5 0 0.5])
hold on
p=polyfit(smAg,smFL,1);
yfit=polyval(p,0:0.01:1.5);
plot(0:0.01:1.5,yfit,'r')

medFL=data(3:6:60,5);
medAg=data(4:6:60,5);
rmssd_mean_medFL=mean(medFL);
rmssd_mean_medAg=mean(medAg);

figure(2)
scatter(medAg, medFL);
xlabel('RMSSD of AgCl ECG');
ylabel('RMSSD of FLEXcon medium ECG');
title('RMSSD observed on FLEXcon medium against AgCl');
grid on;
legend('RMSSD distribution');
axis([0 0.5 0 0.5])
hold on
p=polyfit(medAg,medFL,1);
yfit=polyval(p,0:0.01:1.5);
plot(0:0.01:1.5,yfit,'r')
active.BackgroundColor = [0 1 0];
active.Enable = 'on';

lFL=data(5:6:60,5);
lAg=data(6:6:60,5);
rmssd_mean_lFL=mean(lFL);
rmssd_mean_lAg=mean(lAg);

figure(3)
scatter(lAg, lFL);
xlabel('RMSSD of AgCl ECG');
ylabel('RMSSD of FLEXcon large ECG');
title('RMSSD observed on FLEXcon large against AgCl');
grid on;
legend('RMSSD distribution');
axis([0 0.5 0 0.5])
hold on
p=polyfit(lAg,lFL,1);
yfit=polyval(p,0:0.01:1.5);

```



```
plot(0:0.01:1.5,yfit,'r')

%% t test on RMSSD

[H_sm,P_sm,CI_sm]= ttest2(smFL,smAg,0.05,'both')

[H_med,P_med,CI_med]= ttest2(medFL,medAg,0.05,'both')

[H_lar,P_lar,CI_lar]= ttest2(lFL,lAg,0.05,'both')

mean_FLsm= mean(data(1:6:60,3));
std_FLsm= mean(data(1:6:60,4));

mean_FLmed= mean(data(3:6:60,3));
std_FLmed= mean(data(3:6:60,4));

mean_FLlar= mean(data(5:6:60,3));
std_FLlar= mean(data(5:6:60,4));

mean_Agsm= mean(data(2:6:60,3));
std_Agsm= mean(data(2:6:60,4));

mean_Agmed= mean(data(4:6:60,3));
std_Agmed= mean(data(4:6:60,4));

mean_Aglar= mean(data(6:6:60,3));
std_Aglar= mean(data(6:6:60,4));

temp=[mean_FLsm mean_Agsm mean_FLmed mean_Agmed mean_FLlar mean_Aglar;
      std_FLsm std_Agsm std_FLmed std_Agmed std_FLlar std_Aglar];

rsm= corrcoef(smFL,smAg);
```

## Appendix E

### Glossary of Statistical Terms and Tests

- **Population:** Every object in the data collected.
- **Sample:** A subset of the population.
- **Mean:** A measure of central tendency, the mean is the average value of a set of numbers. For the purposes of this project, the mean is used to refer to the *mean of the sample*, denoted by the symbol  $\bar{x}$ .
- **Median:** Another measure of central tendency, the median is the number separating the higher half of a dataset from the lower half of the dataset. It can be found by rearranging the sample from its lowest value to its highest value. By median, this project will refer to the *median of the sample*.
- **Standard Deviation:** It is a measure of the dispersion from the mean in the data and commonly denoted by the letter  $\sigma$ . In a normal (Gaussian) distribution, 68.2% of the data collected lies within the range of  $\bar{x} \pm \sigma$ . Therefore, a high standard deviation means that there exists high variability in the data.
- **Gaussian distribution:** It is a continuous probability distribution which has a characteristic bell-shaped probability density curve.
- **First Quartile (Q1):** Like the median, the first quartile separates the lowest 25% of the sample from the highest 75%.
- **Third Quartile (Q3):** The third quartile separates the highest 25% of the sample from the lowest 75%.
- **Interquartile Range (IQR):** The interquartile range is the difference between the third quartile and the first quartile.
- **Outlier:** An outlier is a single object/data point in the sample which is far removed from the mean of the sample. The outliers in a sample can be estimated using the first quartile, the third quartile and the interquartile range. No strict statistical definition exists for finding the outliers in a dataset. For the purposes of this project, any data point that was lower than  $Q1 - 1.5*(IQR)$  and higher than  $Q3 + 1.5*(IQR)$  were picked as outliers and removed from analysis.

## Appendix F

### Participant Consent Form

#### Study Protocol:

#### Non-Invasive Comparison of Novel FLEXcon Electrodes vs. Standard Ag-AgCl Electrodes.

#### Step 1: Give consent form to volunteer for reading and signature.

#### Step 2: Apply monitoring devices.

1. Wipe skin under left and right collar bone with alcohol swabs.
2. 3-lead Ag/AgCl ECG electrodes over the thorax and limbs.
  - a. White lead → Right collar bone
  - b. Black lead → Left collar bone
  - c. Red lead → Left lower abdomen
3. Connect leads to the Wireless Holter Monitor, worn via a strap around the waist.

#### Step 3: Turn on equipment and test all software.

1. Turn on Holter Monitor and make sure it is working properly.
2. Turn on PowerLab A/D converter and plug USB into computer.
3. Start LabChart Data Acquisition Software.
  - a. Set up ECG.
  - b. Set up sampling rate to 500 Hz.

#### Step 4: Experiments.

1. Relaxed Electrocardiogram.
  - a. Seat position.
    - i. Ask volunteer to take seat in a laboratory chair.
    - ii. Make sure volunteer is comfortable.
    - iii. Make sure all the sensors are placed in comfortable and secure positions.
    - iv. Begin waveform recording in LabChart.
    - v. Record ECG for 3 minutes.
    - vi. Save the recording using the file naming protocol explained below.

#### Step 5: Removing monitoring devices.

1. At the conclusion of the ECG measurement, remove ECG electrodes, and Holter Monitors. Help in the removing and cleaning process as needed.
2. Repeat Steps 1-5 using the small, medium, and large FLEXcon electrodes.

#### Step 6: Ensure subject safety.

1. Ask the subject if they are experiencing any allergic skin irritation due to the acrylic, and record their answer.

#### File naming protocol.

Save the corresponding record files according to the following formula:

'DATE\_ORDINAL\_ELECTRODE.extension'

DATE = MMDDYYYY in numbers.

ORDINAL = ordinal number of subject in that corresponding date.

ELECTRODE = 'FLEXcon' or 'Ag/AgCl'

## Appendix G

## Stage 1 Data Set

Table 11 Complete Mean &amp; STD Table for Stage 3 Impedance Data Set

Parameters			Pre-Activation [ $\Omega$ ]		Post-Activation [ $\Omega$ ]	
<i>Voltage</i>	<i>Capacitance</i>	<i>Current</i>	<i>MEAN</i>	<i>STD</i>	<i>MEAN</i>	<i>STD</i>
200V	.1 $\mu$ F	1mA	14636400	1520607	1653824	3407938
120V	.1 $\mu$ F	1mA	2198974	577531.6	1173874	1239023
75V	.1 $\mu$ F	1mA	2199626	237426.1	611177.8	997353.5
45V	.1 $\mu$ F	1mA	2443651	207027.3	1590801	1140364
20V	.1 $\mu$ F	1mA	2165919	786507.4	1633331	847051.9
5V	.1 $\mu$ F	1mA	6360598	8862035	1477895	1099961
200V	.1 $\mu$ F	2mA	20423840	4184816	47500.61	49270.68
120V	.1 $\mu$ F	2mA	18319196	10762102	5567859	12322094
75V	.1 $\mu$ F	2mA	21228380	3771418	10665030	14057955
45V	.1 $\mu$ F	2mA	16198315	9971588	16397071	9744139
20V	.1 $\mu$ F	2mA	21755020	4128219	22370860	5039054
5V	.1 $\mu$ F	2mA	23073880	6988715	13413121	12437663
200V	.1 $\mu$ F	5mA	16443560	6663539	12217.84	7905.9
120V	.1 $\mu$ F	5mA	17338540	9042852	10639719	14614636
75V	.1 $\mu$ F	5mA	21273900	4090344	13936858	12792668
45V	.1 $\mu$ F	5mA	18160430	9691436	18471767	10901223
20V	.1 $\mu$ F	5mA	22170840	732922.3	22989980	1083008
5V	.1 $\mu$ F	5mA	21270080	2059371	17620112	9963031
200V	.1 $\mu$ F	10mA	25713840	5408599	12215105	16639228
120V	.1 $\mu$ F	10mA	23572240	2186583	18866309	10797970
75V	.1 $\mu$ F	10mA	20302260	3092992	9574641	13082697
45V	.1 $\mu$ F	10mA	18186320	1638069	8201691	11225125
20V	.1 $\mu$ F	10mA	21989540	3009596	22968180	3418870
5V	.1 $\mu$ F	10mA	21648500	3514644	18094921	10158022
200V	.1 $\mu$ F	20mA	18835105	3706363	3678.83	1875.343
120V	.1 $\mu$ F	20mA	21513340	3324093	5310927	11869314
75V	.1 $\mu$ F	20mA	21073900	3458819	18358739	10300525
45V	.1 $\mu$ F	20mA	22893120	3298875	23050260	3183548
20V	.1 $\mu$ F	20mA	23185740	3126309	22940080	3150006
5V	.1 $\mu$ F	20mA	21284980	584814.2	12902898	9761501
200V	.1 $\mu$ F	50mA	20234640	1898718	4729812	10568322
120V	.1 $\mu$ F	50mA	19016740	2901618	8169034	11203827
75V	.1 $\mu$ F	50mA	21290060	3779017	17936729	10597021
45V	.1 $\mu$ F	50mA	24101740	2521022	24797640	4169780
20V	.1 $\mu$ F	50mA	22368240	1857666	22963560	1679374
5V	.1 $\mu$ F	50mA	19207160	2866172	11794877	10741855
200V	.1 $\mu$ F	100mA	17177040	8404301	6040.96	6671.187
120V	.1 $\mu$ F	100mA	19619920	4020815	5132837	11457930
75V	.1 $\mu$ F	100mA	22298540	6076935	8631424	11815131
45V	.1 $\mu$ F	100mA	24044000	3329040	24083820	3580727

20V	.1 $\mu$ F	100mA	21073680	2847513	18316350	10348991
5V	.1 $\mu$ F	100mA	23102640	2970523	18766881	10319693
200V	1 $\mu$ F	1mA	18793092	10943162	6147310	12173124
120V	1 $\mu$ F	1mA	23432200	2652928	8358164	11538802
75V	1 $\mu$ F	1mA	24290700	2792264	13317231	12837114
45V	1 $\mu$ F	1mA	25280940	2453704	20649991	11823469
20V	1 $\mu$ F	1mA	23658000	1836036	23617220	2092379
5V	1 $\mu$ F	1mA	22144520	1718994	18899720	9660354
200V	1 $\mu$ F	2mA	20699980	3898524	4334663	9468002
120V	1 $\mu$ F	2mA	20230880	3632078	13919999	12742644
75V	1 $\mu$ F	2mA	18737640	3382171	8694742	12006978
45V	1 $\mu$ F	2mA	22628000	2846161	12724938	11509633
20V	1 $\mu$ F	2mA	19111600	1203094	15811693	8909142
5V	1 $\mu$ F	2mA	19410980	420248.6	15200367	8516893
200V	1 $\mu$ F	5mA	21580720	4707117	4966122	11093513
120V	1 $\mu$ F	5mA	22167280	1746724	9295118	12729316
75V	1 $\mu$ F	5mA	22242800	1914323	13531420	12436992
45V	1 $\mu$ F	5mA	21287740	2183627	17813827	10096481
20V	1 $\mu$ F	5mA	15547958	8614955	19870820	1965733
5V	1 $\mu$ F	5mA	22983620	5708802	19283805	11611022
200V	1 $\mu$ F	10mA	20869620	2340181	2412.112	1342.27
120V	1 $\mu$ F	10mA	7827510	9834031	1247.771	262.3298
75V	1 $\mu$ F	10mA	22572700	3568272	19743351	11496051
45V	1 $\mu$ F	10mA	20972300	2493912	13190207	12057603
20V	1 $\mu$ F	10mA	20448820	2940829	12162801	11234977
5V	1 $\mu$ F	10mA	22473160	935866.1	18616556	10524174
200V	1 $\mu$ F	20mA	22890720	4372069	5774326	12910818
120V	1 $\mu$ F	20mA	22976160	3246869	4392982	9820261
75V	1 $\mu$ F	20mA	18405219	10726063	10867875	14930243
45V	1 $\mu$ F	20mA	19654500	1225567	16366135	9233106
20V	1 $\mu$ F	20mA	15923529	8910025	15881104	8939320
5V	1 $\mu$ F	20mA	19807080	5811174	15393918	10093846
200V	1 $\mu$ F	50mA	20295500	1768892	4416104	9873691
120V	1 $\mu$ F	50mA	20354280	7460542	5754493	12865892
75V	1 $\mu$ F	50mA	20490820	3413482	7261.704	8166.807
45V	1 $\mu$ F	50mA	22140700	5309857	16249662	9917794
20V	1 $\mu$ F	50mA	21320500	3895169	18388141	11025947
5V	1 $\mu$ F	50mA	21304600	1206842	17332062	9761126
200V	1 $\mu$ F	100mA	20716840	2772424	443.5232	189.509
120V	1 $\mu$ F	100mA	20636080	3326407	829.6632	296.6535
75V	1 $\mu$ F	100mA	20179500	5748409	4143076	9255993
45V	1 $\mu$ F	100mA	17188472	7976142	10109178	10241248
20V	1 $\mu$ F	100mA	20964280	1801548	21157280	1002969
5V	1 $\mu$ F	100mA	16308773	9255497	14969605	9723512
200V	10 $\mu$ F	1mA	14944124	9253258	5638675	10263417
120V	10 $\mu$ F	1mA	21608900	4040027	9844898	13395137
75V	10 $\mu$ F	1mA	18792560	1268525	8198809	10251290
45V	10 $\mu$ F	1mA	21263780	5967698	16599475	14357906
20V	10 $\mu$ F	1mA	18214520	1933357	18768060	1119792
5V	10 $\mu$ F	1mA	19803160	1819918	17743200	6443152

200V	10 $\mu$ F	2mA	20910080	6311669	1153687	2129351
120V	10 $\mu$ F	2mA	19246560	1891773	4930991	8691508
75V	10 $\mu$ F	2mA	18346738	10448299	10155861	13901490
45V	10 $\mu$ F	2mA	20344900	7395168	15745965	13434574
20V	10 $\mu$ F	2mA	12181010	11305004	11443064	11400528
5V	10 $\mu$ F	2mA	20641720	2156390	17128759	10127915
200V	10 $\mu$ F	5mA	20221480	1411898	8318.874	5921.798
120V	10 $\mu$ F	5mA	15521296	8670207	4183166	9298040
75V	10 $\mu$ F	5mA	11962006	11118744	4207201	8806525
45V	10 $\mu$ F	5mA	24470380	4953512	10329505	14028392
20V	10 $\mu$ F	5mA	18009200	10583935	18886723	11141835
5V	10 $\mu$ F	5mA	21774100	2329822	17881612	10072890
200V	10 $\mu$ F	10mA	21570320	3224722	1673.75	494.7733
120V	10 $\mu$ F	10mA	14716858	8453589	2856.382	3497.503
75V	10 $\mu$ F	10mA	15136414	8486168	7641584	10393145
45V	10 $\mu$ F	10mA	18913400	2012246	8706605	11952138
20V	10 $\mu$ F	10mA	20153360	1528876	16450396	9288995
5V	10 $\mu$ F	10mA	16017733	9096929	11508679	10580860
200V	10 $\mu$ F	20mA	15640541	8898123	1195.448	2161.881
120V	10 $\mu$ F	20mA	21097100	1966878	1048.699	1506.763
75V	10 $\mu$ F	20mA	15446566	5454359	3722.766	3905.171
45V	10 $\mu$ F	20mA	12862048	11816030	10805362	10894943
20V	10 $\mu$ F	20mA	17988250	9176021	18106621	10282063
5V	10 $\mu$ F	20mA	14609116	8816261	15527111	9127104
200V	10 $\mu$ F	50mA	19232240	1254804	469.6034	376.6848
120V	10 $\mu$ F	50mA	16755040	5501363	4638054	10360401
75V	10 $\mu$ F	50mA	11046087	8934252	15917699	10755606
45V	10 $\mu$ F	50mA	23052000	2143055	13813665	12665530
20V	10 $\mu$ F	50mA	22912620	4981176	16397966	9438271
5V	10 $\mu$ F	50mA	18814307	10422068	18137149	10305116
200V	10 $\mu$ F	100mA	16047945	9270757	9106.96	14457.08
120V	10 $\mu$ F	100mA	20734580	1757133	2350.79	1696.166
75V	10 $\mu$ F	100mA	13366263	10538992	4101699	9168941
45V	10 $\mu$ F	100mA	20616240	1989455	546190.3	1209246
20V	10 $\mu$ F	100mA	15899312	8810599	11665750	10730465
5V	10 $\mu$ F	100mA	20054360	1125106	15596078	8548419
200V	100 $\mu$ F	1mA	16045962	8876481	8595199	11391617
120V	100 $\mu$ F	1mA	20031940	2840451	8459899	11460684
75V	100 $\mu$ F	1mA	19953580	1496006	5009177	8345154
45V	100 $\mu$ F	1mA	16203496	9108246	7010131	8870964
20V	100 $\mu$ F	1mA	19433200	2599805	15733947	8928791
5V	100 $\mu$ F	1mA	18960660	626938.8	14827644	8308685
200V	100 $\mu$ F	2mA	21936080	1937055	11605860	10784904
120V	100 $\mu$ F	2mA	21258440	1462071	20001.44	9669.189
75V	100 $\mu$ F	2mA	19974200	2519972	26776.3	21029.48
45V	100 $\mu$ F	2mA	21485000	3167253	10578221	10541473

20V	100 $\mu$ F	2mA	16743861	9471049	12086950	11071474
5V	100 $\mu$ F	2mA	20047980	1808046	15355890	8692896
200V	100 $\mu$ F	5mA	17908480	6455690	8369.32	9591.658
120V	100 $\mu$ F	5mA	16651305	9418118	50816.65	105591
75V	100 $\mu$ F	5mA	16212119	8947458	3852534	8608340
45V	100 $\mu$ F	5mA	23027200	1830998	13407318	12250681
20V	100 $\mu$ F	5mA	19048638	10564758	13856438	12816752
5V	100 $\mu$ F	5mA	22465100	1005901	17976309	10176629
200V	100 $\mu$ F	10mA	16725935	9339428	1351.688	617.5122
120V	100 $\mu$ F	10mA	19293880	1741075	3567.102	2878.392
75V	100 $\mu$ F	10mA	20158660	2246016	4840462	10810685
45V	100 $\mu$ F	10mA	19967840	651318.5	10971675	10046403
20V	100 $\mu$ F	10mA	19034940	1913898	16044595	9289515
5V	100 $\mu$ F	10mA	17391259	9567888	16590098	9430666
200V	100 $\mu$ F	20mA	20002280	1909702	1453.359	1592.998
120V	100 $\mu$ F	20mA	20420100	1856389	11453.01	16447.72
75V	100 $\mu$ F	20mA	21135140	878139.8	3882518	8675599
45V	100 $\mu$ F	20mA	14914416	8247230	14454434	8418662
20V	100 $\mu$ F	20mA	18914140	1620190	19083624	11419250
5V	100 $\mu$ F	20mA	11259021	9783383	16165991	9267639
200V	100 $\mu$ F	50mA	12347102	10866349	1573.935	836.9623
120V	100 $\mu$ F	50mA	20619500	2753699	8404.433	10905.42
75V	100 $\mu$ F	50mA	19121880	1846886	4615.146	4661.464
45V	100 $\mu$ F	50mA	21032040	1132806	5515172	9029777
20V	100 $\mu$ F	50mA	21928220	1081908	23113100	1006921
5V	100 $\mu$ F	50mA	17397921	10045793	15917788	8956765
200V	100 $\mu$ F	100mA	24456900	3695032	15879.99	10940.56
120V	100 $\mu$ F	100mA	19739148	11206031	79145.03	153743
75V	100 $\mu$ F	100mA	24158680	6739214	20566975	13311476
45V	100 $\mu$ F	100mA	18929040	1974391	11774871	10799984
20V	100 $\mu$ F	100mA	21178480	1223216	22027560	858598
5V	100 $\mu$ F	100mA	21251200	2039318	21459100	1942155



## Stage 3 Data Set

Table 12 ECG Statistical Data from Holter Monitor Study

	Data Set	LFHF1/LFHF2	mean_bpm	stdev	RMSSD	SDNN
FLEXsm	32200	0.115478	60.7939	20.2264	0.162078	0.145045
AgAgClsm	32200	0.732602	60.17384	15.81995	0.136034	0.134312
FLEXmed	32201	0.02405	56.70799	26.93959	0.162123	0.143802
AgAgClmed	32201	1.977593	54.22242	23.63568	0.081215	0.081143
FLEXlrg	32202	0.755144	54.79061	4.986064	0.069372	0.089745
AgAgClrg	32202	0.837004	54.79103	4.989303	0.069013	0.089793
FLEXsm	32203	1.864379	90.67573	15.78291	0.226128	0.165255
AgAgClsm	32203	2.120368	94.58032	25.55936	0.139057	0.116364
FLEXmed	32204	1.233448	87.23204	14.89159	0.055505	0.047154
AgAgClmed	32204	1.217927	89.0053	19.43673	0.075415	0.070167
FLEXlrg	32205	1.422611	84.44314	9.290831	0.102009	0.083592
AgAgClrg	32205	1.298235	84.43318	9.262671	0.102067	0.083582
FLEXsm	32206	0.795306	74.94703	7.540951	0.060891	0.081442
AgAgClsm	32206	0.85582	74.94663	7.540027	0.060889	0.081415
FLEXmed	32207	2.032206	74.10102	15.7365	0.070487	0.09281
AgAgClmed	32207	2.554229	73.32206	13.66124	0.054126	0.078721
FLEXlrg	32208	8.427059	73.72798	7.42193	0.068656	0.081444
AgAgClrg	32208	8.389069	73.72535	7.41006	0.068171	0.081272
FLEXsm	32209	3.482458	82.23354	10.6115	0.070798	0.076561
AgAgClsm	32209	3.546698	82.25557	10.67431	0.076084	0.078068
FLEXmed	32210	9.733993	87.03194	29.32527	0.112407	0.083469
AgAgClmed	32210	2.778694	91.04032	33.76334	0.127903	0.10866
FLEXlrg	32211	3.15332	85.19336	17.7208	0.103152	0.105677
AgAgClrg	32211	3.067877	85.43892	18.81765	0.114578	0.11104
FLEXsm	32212	0.240154	70.9016	14.33862	0.112198	0.103586
AgAgClsm	32212	0.239874	70.90352	14.34177	0.112709	0.103739
FLEXmed	32213	0.779402	68.30566	18.78853	0.113253	0.106384
AgAgClmed	32213	0.793778	67.28251	15.17159	0.067039	0.062204
FLEXlrg	32214	8.600545	68.11892	10.77145	0.12346	0.116721
AgAgClrg	32214	8.788925	67.45588	9.663989	0.120315	0.110542
FLEXsm	32215	2.144912	79.00958	3.310359	0.0334	0.032013
AgAgClsm	32215	2.281293	79.00843	3.297644	0.03319	0.031873
FLEXmed	32216	0.32633	80.50483	3.405304	0.039327	0.030462
AgAgClmed	32216	0.284591	80.50256	3.373997	0.038583	0.030217
FLEXlrg	32217	3.70249	82.18458	3.840546	0.02525	0.03367
AgAgClrg	32217	3.364493	82.28119	5.207108	0.044282	0.039505

<b>FLEXsm</b>	32218	9.272487	82.15149	9.838289	0.037748	0.044353
<b>AgAgClsm</b>	32218	9.972932	82.1104	9.636913	0.024489	0.041495
<b>FLEXmed</b>	32219	21.43511	83.04281	4.283717	0.026555	0.036878
<b>AgAgClmed</b>	32219	22.01814	83.04332	4.291414	0.026565	0.0369
<b>FLEXlrg</b>	32220	69.68619	82.51175	5.756404	0.027176	0.049969
<b>AgAgClrg</b>	32220	74.80441	82.51198	5.756223	0.027367	0.05
<b>FLEXsm</b>	32221	12.09203	75.52643	7.266304	0.109071	0.079121
<b>AgAgClsm</b>	32221	25.20104	75.36104	6.602555	0.077836	0.063401
<b>FLEXmed</b>	32222	1.08093	74.85776	11.97772	0.072124	0.063968
<b>AgAgClmed</b>	32222	1.106051	74.85727	11.97643	0.072036	0.063928
<b>FLEXlrg</b>	32223	62.27231	80.63327	8.819586	0.032638	0.075572
<b>AgAgClrg</b>	32223	61.01428	80.6342	8.824895	0.032913	0.075604
<b>FLEXsm</b>	32224	0.851092	63.71633	34.75368	0.226807	0.204128
<b>AgAgClsm</b>	32224	0.420575	64.84749	21.66034	0.271167	0.221883
<b>FLEXmed</b>	32225	0.507751	58.69086	14.6728	0.161173	0.146154
<b>AgAgClmed</b>	32225	0.03221	93.53589	74.85961	0.403599	0.332405
<b>FLEXlrg</b>	32226	1.851071	59.17038	19.22364	0.074436	0.065634
<b>AgAgClrg</b>	32226	1.660257	59.17349	19.22796	0.075955	0.066121
<b>FLEXsm</b>	32901	19.69471	68.87823	7.96708	0.080339	0.095823
<b>AgAgClsm</b>	32901	20.74458	68.86074	7.914424	0.075709	0.094686
<b>FLEXmed</b>	32902	52.42554	69.16672	8.327496	0.073486	0.103235
<b>AgAgClmed</b>	32902	54.51254	69.16144	8.307076	0.073582	0.103228
<b>FLEXlrg</b>	32903	2.926673	68.47285	8.211589	0.069475	0.079338
<b>AgAgClrg</b>	32903	2.134821	68.52478	8.539375	0.077264	0.082245